

St. John's University

St. John's Scholar

Theses and Dissertations

2024

**EXPOSURE TO DITHIOCARBAMATE FUNGICIDE ZIRAM RESULTS
IN HEPATIC AND RENAL TOXICITY IN LONG-EVAN RATS**

Jeffrey Chen

Follow this and additional works at: https://scholar.stjohns.edu/theses_dissertations



Part of the **Toxicology Commons**

EXPOSURE TO DITHIOCARBAMATE FUNGICIDE ZIRAM RESULTS IN
HEPATIC AND RENAL TOXICITY IN LONG-EVAN RATS

A dissertation submitted in partial fulfillment
of the requirements for the degree of

DOCTOR OF PHILOSOPHY

to the faculty of the

DEPARTMENT OF PHARMACEUTICAL SCIENCES

of

COLLEGE OF PHARMACY AND HEALTH SCIENCES

at

ST. JOHN'S UNIVERSITY

New York

by

Jeffrey Chen

Date Submitted: 4/10/2023

Date Approved: 4/24/2023

Jeffrey Chen

Diane Hardej, Ph.D.

© Copyright by Jeffrey Chen 2024

All Rights Reserved

ABSTRACT

EXPOSURE TO DITHIOCARBAMATE FUNGICIDE ZIRAM RESULTS IN HEPATIC AND RENAL TOXICITY IN LONG-EVAN RATS

Jeffrey Chen

Ziram is a broad spectrum fungicide that is used on a variety of crops. It has been shown to display a wide array of toxicological effects, however, there is still a scarcity of mechanistic data regarding how it facilitates those effects. One of its presumed mechanisms of toxicity is due to the production of oxidative stress. However, whether the production of oxidative stress is due to its dimethyldithiocarbamate backbone, its metal moiety, or a combination of both, is still unknown. Contributing to the production of oxidative stress is ziram's ability to alter essential metal homeostasis through transchelation of other essential metals. To study the individual effects of the backbone structure and the metal moiety, sodium-dimethyldithiocarbamate and zinc chloride were used in conjunction with Ziram. This study sought to investigate the effects of ziram and its individual components with regards to altered metal homeostasis, and the downstream effects of this disturbance on the antioxidant defense system, along with the physiological parameters of the kidney and liver of exposed rats.

Rats were orally dosed for 6-weeks with either PEG-400 (vehicle), ziram, sodium-dimethyldithiocarbamate, or zinc chloride. Metal analysis demonstrated increases in zinc and copper levels in the liver along with increases in zinc in the kidneys of animals treated

with ziram only. Analysis of antioxidant parameters demonstrated increases in the glutathione defense system and total antioxidant levels in the liver and kidney of animals treated with ziram. Histopathological evaluation of ziram and sodium-dimethyldithiocarbamate treated tissue showed vacuolization and lipid deposition in the liver. In renal tissue, thickening of the basement membrane and vacuolization of tubular cells accompanied by increases in kidney injury marker-1 were seen in animals treated with ziram and sodium-dimethyldithiocarbamate.

The kidneys of ziram and sodium-dimethyldithiocarbamate exposed animals demonstrated deleterious effects which is a novel finding, as kidney has not previously been shown to be a target organ of toxicity with these agents. It is concluded that the overall toxicological profile of ziram is mediated by an intrinsic property of the compound itself, rather than being attributed solely to any individual structural component.

DEDICATION

Dedicated to my parents, Zhi Cheng Chen, and Hui Ling Chen

ACKNOWLEDGEMENTS

Success is not just the result of your own efforts, it also depends on the support and encouragement of others. I am forever grateful and acknowledge the following:

My committee members Dr. Trombetta, Dr. Cerreta, Dr. Cheng, and Dr. Mantell for their guidance in this project.

My mentor Dr. Hardej, for taking me under her wing and allowing me to grow not only as a scientist, but as an individual. You have been a wonderful mentor and words cannot explain my gratitude towards you.

The PHS department and the department Chair, Dr. Korlipara for financial support through funding of the lab and the Teaching Fellowship.

The Science Supply team, Animal Care team, and Environmental Health and Safety team for all the support that they have provided me throughout my research.

The PHS Teaching Lab team: Dr. Carvalho, Joyce, Susana, Velda, and Pratibha. Thank you for aiding in my professional development.

My past lab mates, Ben and Amanda, for showing me the ropes of being a graduate student and for always being a source of support and encouragement.

A special acknowledgement for Ben, for if it wasn't for you, I would not have found my place in Hardej Lab, and for pushing me to do the PepsiCo internship. You laid the ground work for my project and was an incredible role model as a scientist to me. I am grateful to have lab senior and a friend like you in my life.

My close friend, Randy Liang, for being with me throughout the entire process. Through the lowest of times and the highest of times. There was not one moment during this process where you were not there.

Mumtaz, for teaching me all sorts of research techniques and for being a great friend.

Olivia, Ali, and Belkys, for great friends and always being there when I needed help.

All of my friends outside of St. John's for always being understand and patient.

My partner, Ashley Tan, for your constant patience, support and belief in me. This would not be possible without you at my side.

My brothers, Mark and Mike, for always supporting me.

My parents to whom I dedicate this thesis to, Zhi Cheng Chen, and Hui Ling Chen. There was not one moment in my life where I did not feel supported and loved from you two. Just knowing that you two have your utmost faith in me have kept me going through it

all. This thesis is a testament to the love and support you have given me throughout my entire life and without it, this would not have been possible.

TABLE OF CONTENTS

DEDICATION ii

ACKNOWLEDGEMENTS iii

LIST OF TABLES x

LIST OF FIGURES xi

CHAPTER 1. INTRODUCTION 1

 1.1 Pesticides 1

 1.2 Ziram 2

 1.3 Essential Metals 7

 1.3.1 *Zinc* 7

 1.3.2 *Copper* 8

 1.3.3 *Iron* 8

 1.4 Oxidative Stress and free radicals 9

 1.5 Antioxidants 11

 1.5.1 *Glutathione Defense System* 11

 1.6 Pilot Study: The hepatic and renal effects of Ziram on Long-Evan Rats 12

 1.7 Purpose of the Study 14

 1.8 Hypotheses 15

 1.9 Specific Aims 16

CHAPTER 2. MATERIAL AND METHODS 17

 2.1 Animal care 17

 2.2 Dose Preparation 17

 2.3 Dose Calculation 18

 2.4 Animal Dosing and Fasting 18

2.5 Animal Sacrifice and Sample Collection	19
2.6 Serum Chemistry Analysis.....	19
2.7 Inductively Coupled Plasma-Optical Emission Spectroscopy (ICP-OES)	20
2.8 Tissue Homogenates and Protein Determination	21
2.9 Determination of Total Glutathione and Glutathione to Glutathione disulfide ratio (GSH/GSSG).....	22
2.10 Determination of Glutathione Reductase and Peroxidase Activity.....	23
2.11 Measurement of Total Antioxidant Capacity	24
2.12 Measurement of 4-Hydroxynonenol (4-HNE) ELISA.....	25
2.13 Measurement of Protein Oxidation	25
2.14 Measurement of Serum Creatinine.....	27
2.15 Measurement of Urine Creatinine	27
2.16 Calculation of Urine Flow Rate and Creatinine Clearance	28
2.17 Immunohistochemistry Staining for KIM-1.....	28
2.18 Immunohistochemistry Staining for NGAL.....	29
2.19 Light Microscopy Tissue Preparation	31
2.19.1 <i>Hematoxylin and Eosin Staining</i>	31
2.19.2 <i>Masson's Trichrome Staining</i>	32
2.19.3 <i>Periodic Acid-Schiff Staining with and without Diastase Digestion</i>	32
2.20 Transmission Electron Microscopy.....	34
2.21 Statistical Analysis	35
CHAPTER 3. RESULTS	36
3.1 Animal Weight and Weight Gain.....	36
3.2 Serum Chemistry Analysis.....	36
3.2.1 <i>Vetscan Preventive Care Profile Plus</i>	36

3.2.2 <i>Vetscan T4/Cholesterol Profile</i>	37
3.3 Inductively Coupled Plasma-Optical Emission Spectroscopy (ICP-OES)	37
3.3.1 <i>Zinc</i>	38
3.3.2 <i>Copper</i>	39
3.3.3 <i>Iron</i>	39
3.4 Determination of Total Glutathione and Glutathione to Glutathione disulfide ratio (GSH/GSSG).....	40
3.4.1 <i>Total Glutathione Levels</i>	40
3.4.2 <i>GSH/GSSG Ratio</i>	40
3.4.3 <i>GSH Levels</i>	41
3.4.4 <i>GSSG Levels</i>	41
3.5 Determination of Glutathione Reductase and Peroxidase Activity.....	41
3.5.1 <i>Glutathione Reductase</i>	42
3.5.2 <i>Glutathione Peroxidase</i>	42
3.6 Total Antioxidant Levels.....	42
3.7 Measurement of 4-Hydroxynonenol (4-HNE) ELISA.....	43
3.8 Measurement of Protein Oxidation	43
3.9 Measurement of Creatinine Clearance and Associated Parameters	43
3.9.1 <i>Urine Creatinine</i>	44
3.9.2 <i>Serum Creatinine</i>	44
3.9.3 <i>Urine Flow Rate</i>	44
3.9.4 <i>Total Water Consumption</i>	45
3.9.5 <i>Total Urine Production</i>	45
3.9.6 <i>Creatinine Clearance</i>	45
3.10 Immunohistochemical Detection of KIM-1 and NGAL	45

3.10.1 <i>KIM-1</i>	46
3.10.2 <i>NGAL</i>	46
3.11 Light Microscopy – Hematoxylin and Eosin Staining.....	47
3.11.1 <i>Liver – H&E</i>	47
3.11.2 <i>Kidney – H&E</i>	48
3.12 Light Microscopy – Masson’s Trichrome Staining.....	49
3.12.1 <i>Liver – Masson’s Trichrome Staining</i>	49
3.12.2 <i>Kidney – Masson’s Trichrome Staining</i>	50
3.13 Light Microscopy – Periodic Acid-Schiff Staining with and without Diastase Digestion.....	50
3.13.1 <i>Liver – P.A.S Staining with Diastase Digestion</i>	51
3.13.2 <i>Kidney – P.A.S Staining without Diastase Digestion</i>	51
3.14 Transmission Electron Microscopy.....	52
3.14.1 <i>Liver – TEM</i>	53
3.14.2 <i>Kidney – TEM of Glomeruli</i>	53
3.14.3 <i>Kidney – TEM of Tubular Cells</i>	54
CHAPTER 4. DISCUSSION.....	96
CHAPTER 5. CONCLUSION.....	110
REFERENCES.....	111

LIST OF TABLES

Table 1. ICP-OES Wavelengths and Detection Limits.....	21
Table 2. Serum Parameters: Preventive Care Profile Plus and T4 Rotor	57
Table 3. ICP-OES Elemental Analysis: Zinc (ppm)/Dry Weight (g)	58
Table 4. ICP-OES Elemental Analysis: Copper (ppm)/Dry Weight (g).....	59
Table 5. ICP-OES Elemental Analysis: Iron (ppm)/Dry Weight (g).....	60

LIST OF FIGURES

Figure 1. Chemical Structure of Ziram	2
Figure 2. Animal Weights (g)	55
Figure 3. Animal Weight Gain (g)	56
Figure 4. Total Glutathione Levels (nmol)/Tissue Weight (g)	61
Figure 5. [GSH]/[GSSG]	62
Figure 6. Reduced Glutathione (GSH) (μM)/Tissue Weight (g)	63
Figure 7. Oxidized Glutathione (GSSG) (μM)/Tissue Weight (g)	64
Figure 8. Glutathione Reductase Activity (nmol/min/mL)/Protein (mg)	65
Figure 9. Glutathione Peroxidase Activity (nmol/min/mL)/Protein (mg)	66
Figure 10. Total Antioxidant Levels (mM)/Protein (mg)	67
Figure 11. 4-Hydroxynonenol (4-HNE) (μg)/Protein (mg)	68
Figure 12. Protein Carbonyls (nmol)/Protein (mg)	69
Figure 13. Urine Creatinine (mg/dL)	70
Figure 14. Serum Creatinine (mg/dL)	71
Figure 15. Urine Flow Rate (mL/min)	72
Figure 16. Total Water Consumption in 14 Hours (mL)	73
Figure 17. Urine Volume Production in 14 Hours	74
Figure 18. Creatinine Clearance (mL/min)	75
Figure 19. Immunohistochemical Staining for KIM-1, Objective x40	76
Figure 20. Immunohistochemical Staining for NGAL, Objective x40	77
Figure 21. Liver Histology: Hematoxylin and Eosin Staining	78
Figure 22. Kidney Histology: Hematoxylin and Eosin Staining	79
Figure 23. Liver Histology: Masson's Trichrome Staining	80

Figure 24. Kidney Histology: Masson’s Trichrome Staining.....	81
Figure 25. Liver Histology: P.A.S Staining with Diastase Digestion.....	82
Figure 26. Kidney Histology: P.A.S Staining without Diastase Digestion	83
Figure 27. Liver TEM – Control.....	84
Figure 28. Liver TEM – ZM.....	85
Figure 29. Liver TEM – Na-DMDTC.....	86
Figure 30. Liver TEM – ZnCl ₂	87
Figure 31. Kidney TEM - Glomerulus - Control	88
Figure 32. Kidney TEM - Glomerulus - ZM	89
Figure 33. Kidney TEM - Glomerulus – Na-DMDTC	90
Figure 34. Kidney TEM - Glomerulus – ZnCl ₂	91
Figure 35. Kidney TEM – Tubular Cells – Control.....	92
Figure 36. Kidney TEM – Tubular Cells – ZM.....	93
Figure 37. Kidney TEM – Tubular Cells – Na-DMDTC.....	94
Figure 38. Kidney TEM – Tubular Cells – ZnCl ₂	95

CHAPTER 1. INTRODUCTION

1.1 Pesticides

A pesticide is a substance or mixture of substances designed to prevent, destroy, repel, or mitigate certain animal species or plants that are characterized as pests. Pesticides are classified based on the target organism that they act on. These categories include, but are not limited to, insecticides for controlling insects, herbicides for destroying weeds and unwanted vegetation, fungicides for the prevention of growth of mold and fungi, and rodenticides for controlling rodents. Pesticides are extensively used due to their utility on global scale, both for human health and for the global economy. For example, pesticides play a crucial role in the control of vector-borne diseases, such as malaria and yellow fever, that are a threat to the health of large populations (Costa and Aschner, 2014). Pesticides are also used in modern agriculture, due to their effectiveness and low cost, to enhance the quality and quantity of crop yields. Global pesticide expenditures at the producer level totaled \$56 billion in 2012, with herbicides accounting for the largest portion of the total followed by insecticides, fungicides, and other pesticides. In 2012, the U.S. spent \$9 billion on pesticide expenditures, accounting for 16% of the total world expenditures. On a by-product level, the U.S. expenditures account for 21% of world expenditures on herbicides, 14% on insecticides, 10% on fungicides and 23% on fumigants in 2012 (Atwood and Paisley-Jones, 2017).

In both 2011 and 2012, U.S. pesticide usage totaled over 1.1 billion pounds. Between the years of 2008 to 2012, U.S. pesticide use was responsible for 23% of the total pounds of pesticide applied, 25% of total pounds of herbicide applied, 43% of total pounds of fumigants applied, 12% of fungicides applied, and 6% of insecticides applied worldwide

(Atwood and Paisley-Jones, 2017). Ideally, the deleterious effects of pesticides would be specific for its intended target organism, however, the effects of pesticides can have species cross-over, leading to unforeseen consequences to the environment and to human health. Occupational human exposure poses the highest risk of toxicity and can occur during the production and application of pesticides. Non-occupational toxicity can occur during domestic use, consumption of contaminated food and water and run-off from farms. Due to this lack of specificity, it is paramount to extensively evaluate the safety of these compounds.

1.2 Ziram

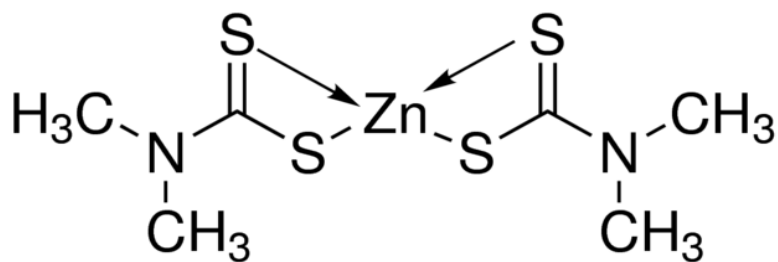


Figure 1. Chemical Structure of Ziram

Dithiocarbamates (DTC) are a family of chemicals used primarily as fungicides. They were first established in the 1940s, and since, have been used throughout the world to control over 400 fungal pathogens on more than 100 crops. These crops include grapes, citrus, fruits, potatoes, tomatoes, melons, and bananas (Janz, 2014). Dithiocarbamates are classified according to their chemical structure. The subclasses include methyldithiocarbamate, dimethyldithiocarbamates, diethyldithiocarbamates, and ethylene-bis-dithiocarbamates. Complexed to their molecular structure are metal atoms which are generally used to determine their name. For example, Maneb is attached to manganese

(Mn), Zineb is attached to zinc, and Mancozeb is attached to both manganese and zinc (Costa and Aschner, 2014).

Ziram (ZM) (Figure 1) is a dimethyldithiocarbamate that is complexed to the metal zinc. Ziram is an agricultural fungicide that was first registered in the U.S. in the 1960s. It is a multi-site fungicide with a wide spectrum of activity and plays an integral role in resistance management. Upon first being registered, its intended uses include the control of scab in apples and pears, leaf curl in peaches, anthracnose, and early blight in tomatoes. In 1981, its use broadened into controlling leaf blight, scab, shot-hole, brown rot, leaf spot, rust, and powdery mildew in a variety of fruits and vegetables such as apricot, cherries and almonds. In addition, it is used as a rabbit repellent for outdoor foliar applications and ornamentals and as an additive in industrial adhesives, caulking, and latex paints (EPA RED, 2003).

In 2014, the total annual domestic use of ZM was estimated to be 1.9 million pounds of active ingredient and in the latest available data from the USGS in 2018, approximately 1.25 million pounds of ZM was used (EPA OPP, 2014; USGS, 2018). Every fifteen (15) years, the U.S. EPA reevaluates the safety data of pesticides for reregistration and issues a new docket outlining recent toxicity data used in their risk assessment. The last Reregistration Eligibility Decision (RED) for ZM was released in 2003 and on October 2nd, 2015, the agency formally initiated a registration review for ZM. At the time of writing this dissertation, a formal public RED docket for ZM has not been released, however, in December 2021, a Proposed Interim Registration Review Decision had been released. In the Proposed Interim Registration Review document, the EPA identified risks associated with dermal and inhalation exposure to occupational workers, bystander risk to adults and

children, along with ecological risk. All of these risks are involved in the registered conventional uses of ZM. The document includes a benefit assessment which deemed ZM to be high value in peaches and apricots as the alternatives will lead to yield and/or quality loss. However, when weighing the benefits of ZM versus the risks identified, the Agency could not find that the benefits outweigh the significant risk to occupational handlers. Therefore, the agency has issued a cancellation of all conventional uses of ZM as it is necessary to protect human health and the environment (EPA OPP, 2021).

Metabolism and pharmacokinetic studies of ZM have been conducted and the results demonstrate that ZM is rapidly absorbed and excreted via the urine, expired air, and in the feces (EPA RED, 2003). Following oral administration of radiolabeled ZM, water-soluble metabolites, were found in the blood, kidneys, liver, ovaries, spleen, and thyroid of female rats after 24 hours (IARC, 1991). Rat metabolism data suggest that upon exposure, ZM is metabolized into three active ingredients, which either dissociate or reduce into dimethyldithiocarbamate anions and are then subsequently metabolized to carbon disulfide and dimethylamine (EPA OPP, 2021). Of these two metabolites, carbon disulfide is a well-studied and known toxicant. Inhalation studies conducted on mice demonstrated a significant increase in lipid peroxidation in the liver, along with nephropathy (Jarvisalo et al, 1977; ATSDR, 1996). Altered lipid metabolism effects, such as elevated levels of serum cholesterol, phospholipids and triglyceride levels were also seen after exposure to carbon disulfide in rats (Wronska-Nofer 1972). Rabbits, intermittently, over a period of 38 weeks, revealed an increase in chronic interstitial nephritis (ATSDR, 1996).

Ziram has been shown to display a wide array of toxicological effects and its primary target organs are believed to be the nervous system, thyroid, and liver (EPA RED,

2003). Ziram exposure has been linked to an increased risk in Parkinson's disease. Ziram exposure to primary ventral mesencephalic cultures and neuroblastoma SK-N-MC cells demonstrated preferential damage to tyrosine hydroxylase positive neurons along with dysfunction of the ubiquitin proteasome system, a biological pathway implicated in the etiology of PD (Chou et al., 2008). An epidemiology study conducted in California's heavily agricultural valleys at workplaces and residences from 1974 to 1999, demonstrated that at workplaces, combined exposure to ZM, maneb, and paraquat increased risk of PD by three-fold and combined exposure to ZM and paraquat, increased PD risk by 80% (Wang et al., 2011). Single oral dose exposure causes neurological impairments while multiple, repeated dosing results in inhibition of brain cholinesterase and brain neurotoxic esterase in rats (EPA RED, 2003).

In addition to the nervous system, the liver and the thyroid are also target organs for ZM. Various doses in subchronic and chronic rat studies, along with mouse carcinogenicity studies, have demonstrated liver histopathology accompanied with increases in hepatic serum enzyme levels (EPA RED, 2003). A 90-day oral toxicity study of ZM showed increased thyroid:body weight ratio and reduced activity of thyroid I¹²⁵ uptake (Pandey and Dikshith, 1990). Ziram is currently classified as "suggestive of carcinogenicity" to humans due to its association with increased incidents of thyroid C-cell hyperplasia and tumor formation in rats after long-term dietary exposure (EPA RED, 2003).

Numerous studies in the literature have implicated that the generation of oxidative stress is a main mechanism of toxicity of ZM and other DTCs. In the study of Matei and Trombetta (2013), rat hippocampal astrocytes treated with ZM exhibited lipid

peroxidation, increases in heat shock and heme oxygenase I stress proteins, accompanied with decreases in GSH/GSSG ratio. HEK293 cells treated with ZM exhibited elevated levels of protein carbonyls and heme oxygenase I (Dennis and Valentine, 2015). Following treatment of ZM, increased cellular superoxide anion content and decreased GSH levels were seen in rat thymic lymphocytes (Kanemoto-Kataoka et al., 2017). Reduction of cellular glutathione accompanied with an increase in protein carbonyl and hydrogen peroxide levels were seen in the intestines of rats after treatment with thiram, a dimethyldithiocarbamate similar to ZM (Salam et al., 2021). Human erythrocytes treated with thiram demonstrated increases in protein and lipid oxidation along with increased hydrogen peroxide levels (Salam et al., 2020).

The generation of oxidative stress is facilitated, at least in part, by the metal moiety present in the specific DTC structure. However, in addition to the metal complexed to its chemical structure, DTC compounds possess the ability to chelate metals, further disrupting metal homeostasis and fueling production of reactive oxygen species (ROS). Mancozeb exposure caused decreases in copper levels in the liver but increases in copper levels in the kidneys of Sprague-Dawley rats (Kistingner and Hardej, 2022). Long-Evan rats treated with disulfiram exhibited increased copper levels in the heart whereas in another study, disulfiram exposure to Sprague-Dawley rats cause copper accumulation in the cerebellum and hippocampus (Delmaestro and Trombetta, 1995; Stephenson and Trombetta, 2020). Ziram has also been shown to participate in the chelation of other metals. My master's research showed that rat hippocampal astrocytes treated with ZM demonstrated significant increases in copper accumulation (unpublished data). This finding

is confirmed in the study of Dennis and Valentine (2015), which showed that ZM treatment caused increases in copper levels in HEK293 cells.

1.3 Essential Metals

Essential metals are metals that are considered to be essential for normal biological functioning. Currently, there are 10 metals that are classified as essential metals: sodium (Na), potassium (K), magnesium (Mg), calcium (Ca), manganese (Mn), iron (Fe), cobalt (Co), copper (Cu), zinc (Zn), and molybdenum (Mo) (Jomova et al., 2022). The levels of essential metals in the body are kept in a delicate equilibrium as their deficiency will lead to disease states, but in excess, will lead to toxicity. Compounds, such as dithiocarbamates, can alter essential metal homeostasis, therefore the study of metals is integral to human health.

1.3.1 Zinc

Zinc is the second most abundant essential metal and exists as Zn^{2+} . Zinc plays crucial roles with various ligands and as a cofactor for more than 300 proteins. This allows Zn to participate in numerous biochemical activities, the most important being a participant in signaling pathways involved in the physiological processes of the neuronal, immune, and reproduction system. Furthermore, zinc is an integral structural element in zinc finger motifs which occur in numerous RNA and DNA binding proteins (Jomova et al., 2022). According to the WHO, zinc deficiency is one of the top 10 risk factors leading to higher burden of disease and has been associated with retarded growth and development, impaired function of reproductive organs, and immune disorders (WHO, 2002; Jomova et al., 2022). Elevated levels of zinc have been associated with gastrointestinal distress, alteration of

levels of other essential metals such as copper and iron, and inhibition of components in the immune system (EPA, 2005; Jomova et al., 2022)

1.3.2 Copper

Copper is pivotal to numerous biological processes and exists in biological systems in oxidation states of +1 (cuprous) and +2 (cupric). In the body, copper is responsible for transfer of electrons within biological molecules, iron metabolism, scavenging of free radicals, and various neurological functions (Jomova et al., 2022). It plays crucial roles in numerous proteins such as Cu/Zn superoxide dismutase (SOD), cytochrome *c* oxidase, mitogen-activated protein kinase MEK1, and cAMP-degrading phosphodiesterase PDE3B. In these proteins, copper ions participate by donating or accepting electrons, aiding in the protein's biochemical reactions (Chen et al., 2020). Copper homeostasis is tightly controlled, as excess copper can lead to the generation of ROS via Fenton reactions causing damage to all biomolecules, such as DNA, lipids, and proteins. Altered copper homeostasis is also associated with a host of neurodegenerative diseases such as Menkes disease, Wilson's disease, Alzheimer's disease, Parkinson's disease, and Huntington's disease.

1.3.3 Iron

Iron is utilized in over a hundred enzymatic reactions ranging from oxygen transport, DNA synthesis, and electron transport. Iron can exist in various valence states, however, the biologically relevant valence states are Fe^{+2} and Fe^{+3} . More than 95% of the functional iron in the human body is in the form of porphyrin rings, known as heme. About 80% of heme iron is found in circulating hemoglobin and myoglobin where they function to deliver oxygen to the entire body. The rest of the iron is found in storage proteins such as ferritin and hemosiderin, circulating in the plasma bound to transferrin or used in

enzymatic processes (Zoroddu et al., 2019). Similar to copper, the homeostasis of iron is tightly regulated as alterations in iron levels can affect human health. In its deficit, formation of erythrocytes is impaired leading to anemia. Although generally not a life-threatening disease, anemia can lead to a significant impact on human health and can manifest itself by fatigue and decreases in physical activity. In excess, iron is able to redox cycle between Fe^{3+} and Fe^{2+} generating ROS leading to damage to biomolecules.

1.4 Oxidative Stress and free radicals

The term “oxidative stress” refers to the imbalance between the generation of ROS and the counteractive functions of cellular antioxidant defense systems. In a state of oxidative stress, the cell’s defense systems become overwhelmed, leading to cellular damage and death (Aruoma, 1998). Oxidative stress has been implicated as a cause of numerous ailments such as cancer, arthritis, autoimmune disorders, cardiovascular, and neurodegenerative diseases (Pham-Huy et al., 2008). ROS and reactive nitrogen species (RNS) refer to free radicals and other non-radical reactive derivatives. A free radical is a molecule with one or more unpaired electrons in its outer shell. Examples of free radicals include hydroxyl radical ($\text{HO}\bullet$), superoxide ($\text{O}_2^{\bullet-}$), nitric oxide ($\text{NO}\bullet$), nitrogen dioxide ($\text{NO}_2\bullet$), peroxy ($\text{ROO}\bullet$), and lipid peroxy ($\text{LOO}\bullet$). Molecules that are not free radicals but can result in the formation of free radicals in living organism include: hydrogen peroxide (H_2O_2), peroxynitrate (ONOO^-), ozone (O_3), singlet oxygen ($^1\text{O}_2$), hypochlorous acid (HOCl), dinitrogen trioxide (N_2O_3), and lipid peroxide (LOOH) (Aruoma, 1998; Pham-Huy et al., 2008).

Free radicals can be created through breakage of chemical bonds resulting in each fragment keeping an electron, by cleavage of a radical to give another radical, or through

redox reactions (Pham-Huy et al., 2008). Two reactions that are responsible for the formation of free radicals include the Haber-Weiss reaction and the Fenton reaction. In the Haber-Weiss reaction, the interaction between the less reactive superoxide radical and hydrogen peroxide, generates the extremely reactive hydroxyl radical (Kehrer, 2000). The Fenton reaction describes the reaction of hydrogen peroxide and transition metals. In the Fenton reaction, ferrous iron (Fe^{+2}) reacts with hydrogen peroxide to form a hydroxyl radical, hydroxide ion, and ferric iron (Fe^{+3}). In addition to iron, copper ions can also participate in this reaction thus forming hydroxyl radicals in a Fenton-like reaction.

In a state of oxidative stress, the production of free radicals and oxidants are in excess, thus leading to alterations in cellular membranes, proteins, lipids, and DNA. Two common occurrences in a state of oxidative stress are lipid peroxidation and oxidation of proteins. Lipid peroxidation is a process in which free radicals attack lipids, especially polyunsaturated fatty acids, containing a carbon-carbon double bond. In this process, a free radical such as a hydroxyl radical reacts with the allylic hydrogen of a lipid forming a carbon-centered lipid radical ($\text{L}\cdot$). The lipid radical subsequently reacts with oxygen forming a lipid peroxy radical ($\text{LOO}\cdot$) and this newly formed radical will react with a nearby lipid molecule generating a new $\text{L}\cdot$ and lipid hydroperoxide (LOOH). This cycle continues and propagates until an antioxidant donates a hydrogen atom to the $\text{LOO}\cdot$ radical to terminate the reaction. The end products of lipid peroxidation include lipid hydroperoxides and toxic aldehydes such as malondialdehyde (MDA) and 4-hydroxynonenol (4-HNE) (Ayala et al., 2014). Protein oxidation can occur via oxidative modification of specific amino acid, free radical mediated peptide cleavage, or formation of protein cross-links due to lipid peroxidation products. Oxidation of proteins can disturb

enzymatic activity, receptors, and/or membrane transport. Oxidized proteins may also become reactive, further contributing to oxidative damage through lipid peroxidation and disrupting cellular functions. The products of protein oxidation include protein carbonyls and amino acid modifications such as methionine sulfoxide and protein peroxide (Lobo et al., 2010).

1.5 Antioxidants

In order to counterbalance the effects of oxidants and free radicals, the human body is equipped with various protective measures, known as antioxidants. Antioxidants are molecules that are stable enough to donate electrons to a free radical, thus neutralizing it. Antioxidants can act as radical scavengers, hydrogen donors, electron donors, peroxide decomposers, singlet oxygen quenchers, and metal-chelating agents (Lobo et al., 2010). Antioxidants are generally divided into two categories: enzymatic and nonenzymatic antioxidants. Examples of these antioxidants include SOD, catalase, thioredoxin, α -tocopherol, ascorbic acid, and glutathione.

1.5.1 *Glutathione Defense System*

Glutathione (GSH) is a tripeptide consisting of cysteine, glycine, and glutamic acid and is considered one of the most important low molecular weight antioxidants in the cell. Glutathione is found in the cytosol of cells, with most cells containing GSH concentrations of roughly 1- 2 mM, while in hepatocytes, the concentrations can reach up to 10 mM. Glutathione plays a crucial role in detoxification of many reactive species, and it is able to partake in this role through reduction, conjugation, and interaction with other non-enzymatic antioxidants. Glutathione is utilized in the reduction of H_2O_2 catalyzed by members of the glutathione peroxidase (GPx) family. In this reaction, H_2O_2 is reduced by

GSH into H₂O and GSSG, thus preventing the formation of hydroxyl radicals. The GSSG molecule is then subsequently recycled back to GSH by the enzyme glutathione reductase using NADPH as a cofactor. Glutathione is also able to eliminate many xenobiotic compounds by conjugating with these compounds followed by secretion of the glutathione adduct out of the cell. Conjugation is catalyzed by the enzyme, glutathione-S transferase (GST) (Forman et al., 2009). In addition, GSH is able to aid other antioxidants in the detoxification of free radicals. An example of this involves the recycling of oxidized vitamin C, back to its reduced form in an enzymatic reaction using GSH as a substrate. The start of this reaction involves the antioxidant, vitamin E, which can aid in reducing lipid hydroxyl radicals and lipid peroxides formed from polyunsaturated fatty acids. Oxidized vitamin E is then reduced by vitamin C. Lastly, oxidized vitamin C is restored back to its reduced form by an enzymatic reaction catalyzed by glutaredoxin or protein disulfide isomerases, using GSH as a cofactor (May et al., 2003; Forman et al., 2009)

1.6 Pilot Study: The hepatic and renal effects of Ziram on Long-Evan Rats

The foundation of this dissertation project is based upon the results found in the initial pilot study. In the pilot study, Long-Evan rats were dosed orally every day, for 28 days with either 50% (v/v) PEG400 as a vehicle control, 50 mg/kg ZM, or 100 mg/kg ZM. Significant differences in weight were seen starting on day 21 in animals treated with 50 mg/kg ZM and significant differences were seen starting on day 6 in animals treated with 100 mg/kg ZM, as compared to the control. Serum chemistry analysis demonstrated significant decreases in alkaline phosphatase, blood urea nitrogen, amylase, albumin, and total protein in animals treated with 100 mg/kg ZM as compared to the control. Metal analysis utilizing Inductively Coupled Plasma – Optical Emission Spectroscopy

demonstrated significant increases in zinc and copper levels in the liver of animals treated with ZM. Significant increases in zinc levels, accompanied by significant decreases in copper and iron levels, were seen in the kidneys of animals treated with ZM. In the serum, significant increases in zinc levels were seen in animals treated with ZM. Histopathological examination of ZM treated animal tissue stained with hematoxylin and eosin demonstrated the presence of vacuolization and infiltration in the liver, and the presence of cast formation in the tubules of the kidneys. Biochemical analysis of liver tissue showed significant decreases in total glutathione levels in animals treated with ZM as compared to the control.

1.7 Purpose of the Study

The results of the pilot study demonstrated that ZM was able to disrupt metal homeostasis, alter glutathione levels, and cause hepatic and renal toxicity. However, the underlying mechanism of how ZM facilitates these effects remain unknown. The purpose of this study was to elucidate what roles the organic dimethyldithiocarbamate (DMDTC) backbone or the metal moiety played in the toxicity of ZM. In order to conduct this study, a sodium dimethyldithiocarbamate (Na-DMDTC) treatment group and a ZnCl_2 treatment group were included to identify effects associated with either the backbone structure or the metal moiety, respectively. The original pilot study was also extended by two weeks for a final study length of 6 weeks as suggested by the committee. Ultimately, the purpose of this study was to investigate the effects of ZM and its individual components, the backbone and its metal moiety, with regard to metal homeostasis and oxidative stress, and the downstream effects of this disturbance on the antioxidant defense systems along with physiological parameters of the kidney and the liver of exposed rats.

1.8 Hypotheses

The hypotheses of this dissertation project are as follows:

- Ziram exposure alters essential metal homeostasis in the liver and kidneys.
- Ziram exposure alters the antioxidant status of hepatic and renal tissues, resulting in toxicity.
- Ziram exposure results in renal toxicity, altering creatinine clearance.
- Ziram exposures alters cellular morphology of hepatic and renal tissues.

1.9 Specific Aims

- Measurement of zinc, copper and iron levels in the liver, kidney, serum, urine and feces of rats using Inductively Coupled Plasma – Optical Emission Spectroscopy.
- Measurement of total glutathione, reduced to oxidized glutathione ratio, glutathione reductase activity, glutathione peroxidase activity and total antioxidant capacity in the liver and kidneys of rats.
- Measurement of lipid peroxidation and protein oxidation markers, 4-hydroxynonenol and protein carbonyls, using ELISA and colorimetric assays in liver and kidneys of rats.
- Measurement of urine creatinine, serum creatinine and urine flow rate to calculate creatinine clearance of rats.
- Detection of renal specific injury markers, kidney injury marker-1 (KIM-1) and neutrophil gelatinase-associated lipocalin (NGAL) using immunohistochemical staining.
- Investigation of gross morphological changes in liver and kidney via light microscopy using hematoxylin and eosin, periodic acid - Schiff, and Masson's trichrome staining.
- Investigation of ultrastructural changes in liver and kidney using transmission electron microscopy.

CHAPTER 2. MATERIAL AND METHODS

2.1 Animal care

Long-Evan rats between the weights of 225 to 250g were purchased from Charles River Laboratories (Wilmington, MA, USA), and used for this study. Rats were housed two per cage and were acclimatized before dosing. Animals were kept on a twelve-hour light/dark cycle and had free access to water and food (Purina Rodent Laboratory Chow 5001; Metal content: Zn 79 ppm; Cu 13 ppm; Fe 270 ppm). This study was approved under protocol #1941 by the St. John's University Institutional Animal Care and Use Committee.

2.2 Dose Preparation

Ziram and Na-DMDTC were purchased from Santa Cruz Biotechnology (Dallas, TX, USA). Ultrapure ZnCl_2 (anhydrous, ampuled under argon, 99.999% trace metals basis) was purchased from BeanTown Chemical (Hudson, NH, USA). Ultrapure water was obtained from Arium Pro Ultrapure Water System (Sartorius, Göttingen, Germany). Polyethylene glycol 400 (Carbowax PEG 400; Fisher Scientific, Ottawa, Ontario, Canada) was used as the vehicle control and a 50% (v/v) PEG400 was prepared using ultrapure water. Vehicle control and all treatments were made fresh daily in 50% (v/v) PEG400 and stored in 15 mL tubes and protected from light. Ziram dose of 100 mg/kg was used to determine the doses of Na-DMDTC and ZnCl_2 . The dose of 100 mg/kg ZM chosen for this study was modeled based off other studies published in the literature (Giavini et., 1983; Enomoto et al. 1989). Dose concentrations were made to be administered as 1 mL/kg, resulting in 100 mg/mL of ZM, 94 mg/mL Na-DMDTC, and 45 mg/mL ZnCl_2 . The dose of 94 mg/kg Na-DMDTC and 45 mg/kg ZnCl_2 give the equivalent molar dose of the

backbone and the zinc metal, respectively, found in a 100 mg/kg dose of ZM. The dose calculations can be found in section 2.3.

2.3 Dose Calculation

ZM Molecular Weight = 305.84 g/mol; Concentration = 100 mg/mL

$$\text{Molarity (M)} = \frac{\text{moles of solute}}{\text{liters of solution}}$$

$$M \text{ of ZM} = \left(\frac{0.1 \text{ g of ZM}}{305.84 \frac{\text{g}}{\text{mol}}} \right) / 0.01 \text{ L} = 0.327 \text{ M of ZM}$$

Na-DMDTC Molecular Weight = 143.21 g/mol

$$0.327 \text{ M} = \left(\frac{X \text{ g of Na-DMDTC}}{143.21 \frac{\text{g}}{\text{mol}}} \right) / 0.01 \text{ L}$$

$$X = 46.83 \text{ mg of Na-DMDTC}$$

According to the chemical structure, there are two moles of backbone to 1 mole of ZM, therefore a total of 94 mg (46.83×2) of Na-DMDTC was used, leading to a final concentration of 94 mg/mL.

ZnCl₂ Molecular Weight = 136.3 g/mol

$$0.327 \text{ M} = \left(\frac{X \text{ g of ZnCl}_2}{136.3 \frac{\text{g}}{\text{mol}}} \right) / 0.01 \text{ L}$$

$$X = 44.57 \text{ mg of ZnCl}_2$$

2.4 Animal Dosing and Fasting

Once acclimatized, animals were divided into four dosing groups: 1 mL/kg of 50% (v/v) PEG400 (vehicle control); 100 mg/kg ZM; 94 mg/kg Na-DMDTC; 45 mg/kg ZnCl₂.

The dose was given via oral gavage once daily for forty-two days (6 weeks). All doses were created to administer a 1 mL/kg treatment volume. Before administration of each treatment, animals were weighed and examined. Immediately after the last treatment dose, animals were fasted overnight for 14 hours in metabolism cages with free access to water.

2.5 Animal Sacrifice and Sample Collection

While fasting, urine and feces were collected in pre-weighed 50 mL tubes connected to metabolism cages. After fasting, rats were anesthetized using 5% isoflurane for 20 minutes and blood was collected via open-cardiac puncture. Animals were then euthanized by severing of the abdominal aorta. Urine samples were aliquoted and stored at -80° C for biochemical analysis or stored in glass snap-cap vials at -20 ° C for metal analysis. Blood samples were transferred into serum separator tubes (Z-serum clot activator tube, Greiner Bio-One, Monroe, NC, USA), allowed to clot for 30 minutes at room temperature, and then centrifuged for 10 minutes at 1800 *x g* at 4° C to complete serum separation. An aliquot of serum was immediately taken and used for serum chemistry analysis and the remainder was aliquoted and stored at -80° C for biochemical analysis or stored in glass snap-cap vials at -20° C for metal analysis. After euthanasia, liver and kidneys were removed, rinsed in cold pH 7.4 phosphate buffer, and stored in either snap-cap vials at -20° C for metal analysis or liquid nitrogen for biochemical analysis.

2.6 Serum Chemistry Analysis

Serum chemistry parameters were measured using the Vetscan Preventive Care Profile Plus and the VetScan Thyroxine (T4) / Cholesterol Profile (Zoetis, Parsipanny, NJ, USA). Serum aliquots were immediately analyzed on their respective rotors after serum

separation, using the Vetscan VS2 Chemistry Analyzer (Zoetis, Parsipanny, NJ, USA). The rotors were filled with 100 μ L of serum and placed in the machine. Once analysis was finished, the machine provided a printout of the parameters analyzed and the results of each analyte. The parameters examined include aspartate aminotransferase (AST), alanine aminotransferase (ALT), alkaline phosphatase (ALP), albumin (ALB), total protein (TP), blood-urea-nitrogen (BUN), total bilirubin (TBIL), glucose (GLUC), sodium (Na^+), potassium (K^+), Calcium (Ca^{2+}), globulin (GLOB), thyroxine (T4), and total cholesterol.

2.7 Inductively Coupled Plasma-Optical Emission Spectroscopy (ICP-OES)

Elemental analysis of zinc (Zn), copper (Cu) and iron (Fe) were carried out using inductively coupled plasma-optical emission spectroscopy (ICP-OES; Perkin Elmer Optima 2100 DV, Waltham, MA, USA), according to the method of Kistinger and Hardej (2022). Prior to analysis, samples were lyophilized for 48 hours using FreeZone 4.5 Liter Benchtop Freeze Dry System (Labconco, Kansas City, MO, USA), weighed in acid-washed beakers, and digested slowly in ultrapure nitric acid (J.T. Baker through VWR, Radnor, PA, USA) on hotplates. After complete evaporation, the residual residue was reconstituted in 4 to 5 mL of 2% (v/v) nitric acid and filtered using 0.2 μ m PTFE syringe filters (VWR, Radnor, PA, USA) into 15 mL conical tubes to remove any insoluble debris. Concentrations of zinc, copper, and iron were determined by using standard curves generated with commercial zinc, copper, and iron standards (1000 ppm stock; Perkin Elmer, Waltham, MA). Results were expressed as ppm of metal per gram of dry weight of the sample (in g) before digestion occurred. The wavelengths and analytical detection limits for each metal are listed in Table 1.

Table 1. ICP-OES Wavelengths and Detection Limits

Metal	Detection Limit	Wavelength
Zinc (Zn)	206.200 nm	0.0059 mg/L
Copper (Cu)	327.393 nm	0.0097 mg/L
Iron (Fe)	206.200 nm	0.0059 mg/L

2.8 Tissue Homogenates and Protein Determination

For biochemical analysis, 100-200 mg of frozen tissue were homogenized on ice using a pestle and microtube (Argos; Elign, IL, USA) in 0.5 mL of ice-cold homogenization buffer (0.1M phosphate buffer, pH 7.4, containing 1 mM EDTA, and mammalian protease inhibitor cocktail (G-Biosciences, St. Louis, MO, USA). Tissue homogenates were then centrifuged at 10,000 x g at 4° C for 15 minutes and supernatants were aliquoted and stored at -80° C. Protein determination of supernatants was carried out using the Amresco® Bradford protocol. Tissue supernatant was incubated with Bradford reagent (VWR, Radnor, PA, USA), absorbance read at 595 nm and then compared to a protein standard curve made from bovine serum albumin (Thermo Fisher Scientific, Rockford, IL, USA).

For the Antioxidant Assay, tissue homogenization and protein determination occurred exactly as the protocol states in the previous paragraph with the exception of EDTA being omitted from the homogenization buffer and the concentration of the buffer being 0.01M instead of 0.1M. This is due to EDTA and a high concentration of phosphate buffer resulting in interference in the assay.

For the Protein Carbonyl Assay, tissue homogenization and protein determination occurred exactly as the protocol states in the previous paragraph with the exception of the homogenization buffer being a pH of 6.7 as recommended by the assay protocol.

For the Glutathione Assay, 100-200 mg of frozen tissue were homogenized in 0.5 mL of 5% (w/v) metaphosphoric acid (Millipore Sigma, St. Louis, MO, USA), and then centrifuged at $10,000 \times g$ at 4°C for 15 minutes. Supernatants were aliquoted and stored at -20°C .

2.9 Determination of Total Glutathione and Glutathione to Glutathione disulfide ratio (GSH/GSSG)

A modified method in the Glutathione Assay Kit from Cayman Chemical (Ann Arbor, MI, USA) was used to establish total glutathione levels and the ratio of glutathione (GSH) to glutathione disulfide (GSSG). In this assay, the rate of yellow product formation, TNB (5-thio-2-(nitrobenzoic acid)), was directly proportional to the concentration of GSH in the sample. TNB formation was created with the addition of DTNB (Ellman's reagent; 5-5'-dithio-bis-2- (nitrobenzoic acid)) into the sample to form the mixed disulfide, GSTNB (GSH and TNB). GSTNB was subsequently reduced by glutathione reductase to recycle GSH and produce more TNB. The modification of this method was the direct homogenization of tissue samples in 5% (v/v) metaphosphoric acid (MPA; Millipore Sigma, St. Louis, MO, USA) (Kisting and Hardej, 2022).

Determination of total glutathione and GSSG levels were done in parallel on the same plate. Samples were diluted and separated for either total glutathione or GSSG analysis. GSSG samples were incubated with 2-vinylpyridine (2-VP; Millipore Sigma, St. Louis, MO, USA) for 1 hour at room temperature. 2-VP acts as a derivatizing agent for

GSH in the assay as it alkylates GSH and thus masks GSH leaving only GSSG in the sample. After incubation, all samples were treated with triethanolamine (TEAM; Millipore Sigma, St. Louis, MO) and transferred to a 96-well plate. Two standard curves were generated with the provided assay standards for total glutathione and for GSSG determination. The assay standards were prepared identically as compared to their respective samples. Assay Cocktail was added to each well and the plate was read on an iMark microplate reader (Bio-Rad; Hercules, CA, USA), at 415 nm, every 5 minutes for a total of 30 minutes. The results were normalized to weight of tissue sample before homogenization in 5% (w/v) MPA. Reduced glutathione (GSH) levels were calculated using the following formula: $GSH = \text{Total GSH } (\mu\text{M}) - (2 \times \text{GSSG } (\mu\text{M}))$. The ratio of GSH to GSSG was then calculated by dividing GSH with GSSG values.

2.10 Determination of Glutathione Reductase and Peroxidase Activity

Glutathione reductase (GR) activity was determined in tissue homogenates with the use of the Glutathione Reductase Assay kit from Cayman Chemical (Ann Arbor, MI, USA). In this method, GR activity is measured by the rate of NADPH oxidation. The oxidation of NADPH to NADP⁺ caused a decrease in absorbance at 340 nm which is directly proportional to the GR activity in the sample. Samples and positive control (Baker's yeast; supplied in the kit) were diluted, mixed with the kit-supplied reaction cocktail, and read at 340 nm every minute for five minutes in an Infinite M Plex plate reader (Tecan, Männedor, Switzerland). GR activity was normalized to the protein content obtained in the Bradford assay.

Glutathione peroxidase (GPx) was determined in tissue homogenates using the Glutathione Peroxidase Assay kit from Cayman Chemical (Ann Arbor, MI, USA). In this

method, GPx activity was measured using a rate limiting reaction with cumene hydroperoxide, causing the conversion of GSH to GSSG. GSSG was then reduced by GR with the oxidation of NADPH to NADP⁺. Oxidation is accompanied with a decrease in absorbance at 340 nm, and in conditions where GPx activity is rate limiting, this decrease is directly proportional to the GPx activity in the sample. Samples and positive control (bovine erythrocytes) were diluted, mixed with the kit-supplied reaction cocktail, and read at 340 nm every minute for five minutes in an Infinite M Plex plate reader (Tecan, Männedor, Switzerland). GPx activity was normalized to the protein content found in the Bradford assay.

2.11 Measurement of Total Antioxidant Capacity

The total antioxidant capacity of tissue homogenates was measured using the Antioxidant Assay kit from Cayman Chemical (Ann Arbor, MI, USA). This assay is based upon the potential of antioxidants in the sample to inhibit the oxidation of ABTS[®] (2,2'-Azino-di-[3-ethylbenzthiazoline sulphonate]) to ABTS^{®•+} by metmyoglobin. In this reaction, the antioxidants in the sample causes suppression of ABTS^{®•+} formation, thus a suppression of absorbance at 405 nm is proportional to the concentration of antioxidants in the sample. Standards and samples were diluted and pipetted into a 96-well plate that was provided by the manufacturer. In each well, metmyoglobin and chromogen (ABTS[®]) were added and then the reaction was initiated by the addition of Hydrogen Peroxide Working Solution. The plate was then incubated at room temperature, on an orbital shaker for five minutes. Absorbance was measured at 405 nm in an iMark microplate reader (Bio-Rad; Hercules, CA). Total antioxidant capacity is expressed as mM of Trolox (standard provided by the kit) and was normalized to the protein content of the sample.

2.12 Measurement of 4-Hydroxynonenol (4-HNE) ELISA

4-HNE was measured using the Lipid Peroxidation 4-HNE ELISA Assay Kit from Abcam (Cambridge, MA, USA) according to the manufacturer's instructions. Prior to starting the assay, well strips were coated with 4-HNE conjugate provided in the kit and incubated overnight at 4°C. The next day, 4-HNE standards and samples were diluted and pipetted into duplicate wells and incubated for 10 minutes at room temperature, on an orbital shaker. Following incubation, anti-4-HNE antibody was added into the wells and incubated at room temperature for 1 hour, on an orbital shaker. After incubation, wells were thoroughly washed, and secondary antibody conjugated to HRP was added. Well strips were then incubated at room temperature for 1 hour, on an orbital shaker. Well strips were washed again followed by the addition of Substrate Solution. Well strips were incubated at room temperature for 20 minutes on an orbital shaker for the development of color. Following incubation, Stop Solution was added, and the well strips were read. Absorbance was measured at 450 nm in an iMark microplate reader (Bio-Rad; Hercules, CA). Samples absorbances were compared to the 4-HNE standard curve. Results were expressed as μg of 4-HNE per mg of protein.

2.13 Measurement of Protein Oxidation

Protein oxidation in tissue homogenates was measured using the Protein Carbonyl Colorimetric Assay Kit from Cayman Chemical (Ann Arbor, MI, USA). As per assay kit instructions, nucleic acids were removed from tissue homogenates prior to the start of the assay to avoid interferences. Nucleic acid removal was carried out by incubating all samples with streptomycin sulfate at a final concentration of 1% in the sample. The samples were incubated at room temperature for 15 minutes and then centrifuged at 6000 x g for 10

minutes at 4°C. The supernatant was then divided into sample tubes and control tubes. In each control tube, 2.5M HCl was added and in each sample tube, 2,4-dinitrophenylhydrazine (DNPH) dissolved in 2.5M HCl was added. All tubes were then incubated in the dark at room temperature for one hour. All tubes were vortexed every 15 minutes during the one-hour incubation. Following incubation, samples were deproteinated with 20% trichloroacetic acid (TCA) and incubated on ice for five minutes. Samples were then centrifuged at 10,000 x g for 10 minutes at 4°C. The supernatant was removed by vacuum suctioning and then discarded. The pellet was kept and resuspended in 1 mL of 10% TCA and incubated on ice for five minutes. Following incubation, the supernatant was discarded, and the pellet was manually resuspended in 1 mL of a 1:1 mixture of ethanol and ethyl acetate using wooden applicator sticks. This step was repeated for a total of three times to remove excess DNPH. After the final wash, the pellet was resuspended in guanidine hydrochloride by vortexing and centrifuged at 10,000 x g for 10 minutes at 4°C. The supernatant was then pipetted into duplicate wells of the 96 well plate provided by the manufacture and read at 370 nm in a Tecan Infinite 200 PRO microplate reader (Tecan, Männedorf Switzerland). Protein carbonyl content was calculated by subtracting the sample absorbance by the control tube absorbance that it was paired with. This value was divided by the molar extinction coefficient of DNPH followed by an adjustment for the solution pathlength in the well. The value for the adjustment was provided by the kit manufacturer. Protein carbonyl content was normalized to the protein content of the sample.

2.14 Measurement of Serum Creatinine

Serum creatinine was measured using the Creatinine Serum Colorimetric Assay Kit from Cayman Chemical (Ann Arbor, MI, USA). This method utilizes the Jaffe's reaction where creatinine treated with alkaline picrate produces a yellow/orange color that can be measured quantitatively. The color development was directly proportional to the concentration of creatinine. Standard and samples were diluted and pipetted in duplicate wells in a 96-well plate provided by the kit. Creatinine Reaction Buffer was then added to all wells followed by Creatinine Serum Color Reagent. Sample absorbances were measured at an absorbance of 490 nm using the iMark microplate reader (Bio-Rad; Hercules, CA, USA). Afterwards, the samples were incubated at room temperature for 7 minutes and the absorbances were measured again at 490 nm using the iMark microplate reader (Bio-Rad; Hercules, CA, USA). The adjusted optical density of standards and samples were calculated by subtracting the initial absorbance reading from the final (7 minute) absorbance reading. The concentration of creatinine in the samples was calculated using a standard curve plotted from the adjusted optical density of standards. The results were expressed as mg/dl of creatinine.

2.15 Measurement of Urine Creatinine

Urine creatinine was measured using the Creatinine Urinary Colorimetric Assay kit from Cayman Chemical (Ann Arbor, MI, USA). This method utilizes the Jaffe's reaction where creatinine treated with alkaline picrate produces a yellow/orange color that can be measured quantitatively. The color created from creatinine is then destroyed at acidic pH. After acidification, the difference in color intensity was measured and was proportional to the creatinine concentration. Standard and samples were diluted and pipetted in duplicate

wells in a 96-well plate provided by the kit. The reaction was then initiated by the addition of Alkaline Picrate Solution to all wells. The plate was incubated on a shaker for 10 minutes at room temperature. Following incubation, absorbances of samples were measured at an absorbance of 490 nm using the iMark microplate reader (Bio-Rad; Hercules, CA, USA) for an initial reading. Acid solution was added to all wells to dissipate the color formed from the reaction. The plate was then incubated on an orbital shaker for 20 minutes at room temperature. After incubation, sample absorbances were measured at an absorbance of 490 nm using the iMark microplate reader (Bio-Rad; Hercules, CA, USA) for a final absorbance reading. The average final absorbance of each standard and sample were subtracted from the initial absorbance, yielding the corrected absorbance. The concentration of creatinine in the samples was calculated using a standard curve plotted from the corrected absorbances. The results are expressed as mg/dl of creatinine.

2.16 Calculation of Urine Flow Rate and Creatinine Clearance

Creatinine clearance is calculated using the formula: $Clcr = \text{urine creatinine (mg/dL)} \times \text{urine flow rate (mL/min)} / \text{serum creatinine (mg/dL)}$, provided by Bazzano *et al.* (2015). Urine flow rate was calculated by dividing the 14 hours of urine volume by 840, which equates to the number of minutes in 14 hours (14 hours x 60 min = 840): $\text{urine flow (mL/min)} = \text{value of urine volume (mL in 24h)} / 840$.

2.17 Immunohistochemistry Staining for KIM-1

Immunohistochemistry was performed on kidney tissues using a batch processing method. Formalin-fixed paraffin sections (3 – 5 μm thickness) were de-paraffinized and serially rehydrated in decreasing concentrations of ethanol (100%, 95%, 70%, and 30%), followed by full hydration in water. Heat-activated antigen retrieval was performed in

citrate buffer pH 6.0 (1:100 diluted in dH₂O, catalog number: H-3300, Vector Laboratories Inc., CA, USA) using semi-automated Retriever (Electron Microscopy Sciences; Pennsylvania, USA). Sections were allowed to equilibrate to room temperature followed by 2 washes in PBS (0.1 M, pH 7.4). Endogenous peroxidases were removed by incubating with ready-to-use Bloxall® blocking solution (catalog number: SP-6000-100, Vector Laboratories Inc., CA, USA) for 10 min followed by 5 minutes wash in PBS. The sections were incubated with blocking buffer (10% normal horse serum + 0.3% triton-X-100 diluted in PBS1) for 1 hour at room temperature followed by incubation with goat anti-KIM-1 primary antibody (10 µg/mL, catalog number: AF3689, R&D Systems, MN, USA) overnight at 4°C. Thereafter, sections were washed three times in PBS for 5 minutes each followed by incubation with ImmPRESS® horse anti-goat IgG (catalog number: MP-7405, Vector Laboratories Inc., CA, USA) horseradish peroxidase labeled secondary antibody for 1 hour at room temperature. The sections were washed three times in PBS for 5 minutes each and developed with ImmPACT® 3,3'-diaminobenzidine (DAB) (catalog number: SK-4105, Vector Laboratories Inc., CA, USA). The sections were counterstained with hematoxylin followed by serial ethanol dehydration, clearing with xylene and permanently mounted in permount. Tissue sections were visualized using Nikon Eclipse Ts2R microscope system equipped with Imaging Source camera and NIS Elements Basic Research software (version 5.11.03) was used to obtain high (objective magnification, 40x) light micrographs.

2.18 Immunohistochemistry Staining for NGAL

Immunohistochemistry was performed on kidney tissues using batch processing method. Formalin-fixed paraffin sections (3 – 5 µm thickness) were de-paraffinized and

serially rehydrated in decreasing concentrations of ethanol (100%, 95%, 70%, and 30%), followed by full hydration in water. Heat-activated antigen retrieval was performed in citrate buffer pH 6.0 (1:100 diluted in dH₂O, catalog number: H-3300, Vector Laboratories Inc., CA, USA) using semi-automated Retriever (Electron Microscopy Sciences; Pennsylvania, USA). Sections were allowed to equilibrate to room temperature followed by 2 washes in PBS (0.1 M, pH 7.4). Endogenous peroxidases were removed by incubating with ready-to-use Bloxall® blocking solution (catalog number: SP-6000-100, Vector Laboratories Inc., CA, USA) for 10 min followed by 5 minutes wash in PBS. The sections were incubated with blocking buffer (10% normal horse serum + 0.3% triton-X-100 diluted in PBS1) for 1 hour at room temperature followed by incubation with goat anti-NGAL primary antibody (10 µg/mL, catalog number: AF1757, R&D Systems, MN, USA) overnight at 4°C. Thereafter, sections were washed three times in PBS for 5 minutes each followed by incubation with ImmPRESS® horse anti-goat IgG (catalog number: MP-7405, Vector Laboratories Inc., CA, USA) horseradish peroxidase labeled secondary antibody for 1 hour at room temperature. The sections were washed three times in PBS for 5 minutes each and developed with ImmPACT® 3,3'-diaminobenzidine (DAB) (catalog number: SK-4105, Vector Laboratories Inc., CA, USA). The sections were counterstained with hematoxylin followed by serial ethanol dehydration, clearing with xylene and permanently mounted in permount. Tissue sections were visualized using Nikon Eclipse Ts2R microscope system equipped with Imaging Source camera and NIS Elements Basic Research software (version 5.11.03) was used to obtain high (objective magnification, 40x) light micrographs.

2.19 Light Microscopy Tissue Preparation

Tissues were fixed in 10% neutral buffered formalin (VWR, Radnor, PA, USA) and were serially dehydrated to 100% ethanol, cleared in xylene, and infiltrated with paraffin using a Microm STP 120 tissue processor (Thermo Fisher Scientific, Waltham, MA, USA). Tissue was embedded into paraffin blocks and sectioned at 5 μ M thickness using an American Optical Model 820 Spencer microtome (American Optical, Buffalo, NY, USA). Sections were visualized using Nikon Eclipse Ts2R microscope system equipped with Imaging Source camera and NIS Elements Basic Research software (version 5.11.03) was used to obtain high (objective magnification, 40x) light micrographs.

2.19.1 Hematoxylin and Eosin Staining

Hematoxylin and eosin staining is a basic screening technique used for histopathology. Slides prepared as described in section 2.19, were deparaffinized in 3 changes of xylene (5 minutes each). The sections were serially rehydrated in decreasing concentrations of ethanol (100%, 95%, 70%, and 30%) for 2 minutes each. The slides were washed in distilled water for 1 minute. Next, the slides were stained with hematoxylin for 10 minutes, followed by two washes in distilled water for 1 minute each. Afterwards, the slides were placed in 1% ammonium hydroxide solution, made in 70% ethanol, for 1 minute. The sections were washed with tap water for 1 minute, followed by distilled water for 1 minute. After washing, the slides were placed in a 70% ethanol solution for 2 minutes followed by staining with eosin for 30 seconds. The slides were serially dehydrated by increasing concentrations of ethanol (95% and 3 changes of 100%) for 2 minutes each. Lastly, slides were cleared with 3 changes of xylene for 2 minutes each and permanently mounted in permount.

2.19.2 *Masson's Trichrome Staining*

Masson's trichrome staining is a technique used for detection of extracellular matrix deposition. Slides prepared as described in section 2.19 were deparaffinized in 3 changes of xylene (5 minutes each). The sections were serially rehydrated in decreasing concentrations of ethanol (100%, 95%, 70%, and 30%) for 2 minutes each. The slides were washed in distilled water for 1 minute. Following that, the slides were placed in Bouin's fixative and incubated at room temperature overnight. Slides were washed in running tap water until the disappearance of a yellow color from the picric acid was seen. Next, slides were washed in distilled water and stained in Weigert's iron hematoxylin for 10 minutes. Slides were washed in running tap water for 10 minutes followed by a 1-minute rinse in distilled water. Next, the slides were stained with Biebric Scarlet-Acid Fuchsin for 2 minutes, washed with distilled water, and stained with Phosphomolybdic-Phosphotungstic acid for 15 minutes. The slides were stained with Aniline blue for 5 minutes, washed in distilled water and incubated with 1% acetic acid solution for 1 minute. Lastly, slides were serially dehydrated by increasing concentrations of ethanol (2 changes of 95%, followed by 2 changes of 100%) for 2 minutes and cleared with 2 changes of xylene for 2 minutes. Slides were permanently mounted in permount.

2.19.3 *Periodic Acid-Schiff Staining with and without Diastase Digestion*

Periodic acid-Schiff staining is a technique used to detect the presence of carbohydrates such as polysaccharides, mucin, and glycogen. Diastase (α -amylase) digestion was used in the diagnosis of glycogen storage diseases and in this study, diastase digestion was used on liver sections to identify if the accumulation of vacuoles seen in the H&E liver sections were due to increased glycogen deposition.

For liver sections, slides were prepared as described in section 2.19 and were deparaffinized in 3 changes of xylene (5 minutes each). The sections were serially rehydrated in decreasing concentrations of ethanol (100%, 95%, 70%, and 30%) for 2 minutes each. The slides were washed in distilled water for 1 minute. Following that, slides were placed in preheated, 1% diastase solution at 37°C for 1 hour. Slides were washed in running tap water for 5 minutes and incubated in a 0.5% periodic acid solution for 5 minutes. Next, the slides were rinsed in 4 changes of distilled water and stained with Schiff reagent for 15 minutes. The slides were washed in running tap water for 10 minutes for the development of a pink color. Lastly, slides were serially dehydrated by increasing concentrations of ethanol (2 changes of 95%, followed by 2 changes of 100%) for 2 minutes and cleared with 2 changes of xylene for 2 minutes. Slides were permanently mounted in permount.

For kidney sections, slides were prepared as described in section 2.19 and were deparaffinized in 3 changes of xylene (5 minutes each). The sections were serially rehydrated in decreasing concentrations of ethanol (100%, 95%, 70%, and 30%) for 2 minutes each. The slides were washed in distilled water for 1 minute and incubated in a 0.5% periodic acid solution for 5 minutes. Next, the slides were rinsed in 4 changes of distilled water and stained with Schiff reagent for 15 minutes. Afterwards, slides were washed in running tap water for 10 minutes for the development of a pink color and stained with Harris hematoxylin for 5 minutes. Slides were washed in running tap water for 5 minutes and then quickly dipped, five times, in 1% HCl acid alcohol solution to differentiate. The slides were washed again in running tap water for 30 seconds and then dipped twice in ammonia water to blue the sections. Next, the slides were washed in

running tap water for 10 minutes, followed by serial dehydration by increasing concentrations of ethanol (2 changes of 95%, followed by 2 changes of 100%) for 2 minutes. Lastly, slides were cleared in 2 changes of xylene for 2 minutes each and permanently mounted in permount.

2.20 Transmission Electron Microscopy

Transmission electron microscopy is a technique used to investigate ultrastructural changes in the tissue of treated animals. Both liver and kidney tissue were minced into small pieces in a glass petri dish, filled with ice cold Sorensen's phosphate buffer (pH 7.4). The minced tissue was then fixed for 3 hours at 4°C in 3.0% glutaraldehyde made in Sorensen's phosphate buffer. After fixation, the tissue was washed with Sorensen's buffer overnight at 4°C. Next, the tissue was post-fixed in 1.0% osmium tetroxide solution made in Sorensen's phosphate buffer for 1 hour, on constant rotation. The tissue was washed with Sorensen's phosphate buffer for 1 hour at 4°C and serially dehydrated with acetone (30%, 60% and 90% for 10 minutes each and then 3 changes of 100% acetone for 5 minutes each). Afterwards, the tissue was infiltrated with increasing concentrations of LX112-Araldite plastic and acetone mixture until fully infiltrated with just LX112-Araldite. The tissue was embedded into BEEM[®] capsules and placed in a heated oven overnight at 45°C. Next, the capsules were transferred to a 60°C oven for a week for polymerization. Ultra-thin sections were cut using a DiATOME Ultra45° (DiATOME, Hatfield, PA, USA) on a Leica EM UC6 (Leica, Hernalser Hauptstrasse, Austria) and were collected on copper grids. Copper grids containing ultra-thin sections were then stained with uranyl acetate followed by lead citrate. Grids were viewed using a JEOL JEM-1200EX TEM (JOEL, Peabody, MA, USA).

2.21 Statistical Analysis

Statistical analysis was carried out using GraphPad Prism ® version 5 (Graphpad Software, Inc., La Jolla, CA). The significances of the results were determined by using a one-way ANOVA followed by Tukey's multiple comparisons post-hoc test. The results were expressed as the mean \pm standard error of the mean (SEM). $P < 0.05$ is the minimum acceptable level of significance. Grubbs' Outlier test was used to analyze the metal data for outliers and those that were deemed outliers were removed from the analysis.

CHAPTER 3. RESULTS

3.1 Animal Weight and Weight Gain

Animal weights were measured every day before dosing (n = 33; n = 8 for control, Na-DMDTC, and ZnCl₂; n = 9 for ZM). Animal weights were plotted over the 6-week dosing period. A significant decrease in total raw weight (Figure 2) was seen in the ZM treatment group as compared to the ZnCl₂ treatment group in week 4 and remained significant for the remainder of the study. A significant decrease in total raw weight (Figure 2) was seen in the ZM treatment group as compared to the control in week 5 and remained significant for the remainder of the study. A significant decrease in weight gain was seen in the ZM treatment group as compared to all other groups starting at week 1 and remained significant for the entire duration of the study (Figure 3).

3.2 Serum Chemistry Analysis

3.2.1 *Vetscan Preventive Care Profile Plus*

Serum chemistry analysis was conducted using the Vetscan Preventive Care Profile Plus rotor on the VetScan V2 instrument. Fresh serum was used for serum chemistry analysis directly after euthanasia (n = 33; n = 8 for control, Na-DMDTC, and ZnCl₂; n = 9 for ZM). The Vetscan Preventive Care Profile Plus rotor analyzed the following parameters: aspartate aminotransferase, alanine aminotransferase, alkaline phosphatase, albumin, total protein, blood-urea-nitrogen, total bilirubin, glucose, sodium, potassium, calcium, and globulin.

A summary of the data is found in Table 2. There were no significant changes between any treatment group for the following parameters: aspartate aminotransferase, alkaline phosphatase, albumin, total protein, blood-urea-nitrogen, total bilirubin, sodium,

potassium, calcium, and globulin. A significant decrease in the levels of alanine aminotransferase were seen in animals treated with ZM (25.1 U/L, SEM: 1.09) when compared to the control (32.6 U/L, SEM: 1.64). A significant decrease in the levels of glucose were seen in animals treated with ZM (170 mg/dL, SEM: 7.42) when compared to control (203 mg/dL, SEM: 8.13).

3.2.2 Vetscan T4/Cholesterol Profile

Following the same guidelines as the previous section (3.2.1), fresh serum was used for serum chemistry analysis directly after euthanasia (n = 33; n = 8 for control, Na-DMDTC, and ZnCl₂; n = 9 for ZM) with the Vetscan T4/Cholesterol Profile rotors for the parameters: thyroxine and cholesterol. A summary of the data is found in Table 2. No significant changes across the groups were seen for either parameter.

3.3 Inductively Coupled Plasma-Optical Emission Spectroscopy (ICP-OES)

The liver, kidney, serum, urine, and feces were lyophilized, digested in ultra-pure nitric acid, and subjected to metal analysis using Inductively Coupled Plasma-Optical Emission Spectroscopy (ICP-OES). The levels of zinc, copper, and iron were measured in all of the aforementioned samples.

For the liver, n = 33; n = 8 for control, Na-DMDTC, and ZnCl₂; n = 9 for ZM. For the kidney, n = 24; n = 6 for all groups. The variation in the n numbers for the kidney was due to sample allocation. The kidneys of two animals per group were used for light/electron microscopy and biochemical analysis whereas the kidneys of the other animals were used for metal analysis and biochemical analysis. For the serum, n = 32; n = 7 for control; n = 8 for Na-DMDTC, and ZnCl₂; n = 9 for ZM. The lower n number for control was due to an issue in sample preparation. For the urine, n = 19; n = 6 for control; n = 3 for Na-DMDTC,

and ZnCl₂; n = 7 for ZM. The large variation in n number is due to an issue in sample preparation. For the feces, n = 31; n = 7 for control; n = 8 for ZM, Na-DMDTC, and ZnCl₂. The lower n number for control and ZM was due to an issue in sample preparation. All the sample preparation issues were due to samples being lost during lyophilization, resulting in lower n-numbers.

The results from this experiment are grouped by metal analyte and are summarized in Figures 4, 5, and 6.

3.3.1 Zinc

A summary of the ICP-OES results for zinc is found in Table 3. A significant increase in zinc levels were seen in livers of animals treated with ZM (64.03 ppm Zn/g tissue, SEM: 3.166) as compared to control (26.33 ppm Zn/g tissue, SEM: 0.60), Na-DMDTC (26.86 ppm Zn/g tissue, SEM: 0.94), and ZnCl₂ (ppm Zn/g tissue 29.22, SEM: 1.29) treated animals.

For the kidneys, a significant increase in zinc levels were seen in the animals treated with ZM (41.37 ppm Zn/g tissue, SEM: 2.37) as compared to control (22.10 ppm Zn/g tissue, SEM: 0.84), Na-DMDTC (21.56 ppm Zn/g tissue, SEM: 0.33), and ZnCl₂ (24.91 ppm Zn/g tissue, SEM: 0.89) treated animals.

For the serum, a significant increase in zinc levels were seen in animals treated with ZM (11.91 ppm Zn/g tissue, SEM: 1.11) as compared to control (2.46 ppm Zn/g tissue, SEM: 0.19), Na-DMDTC (2.42 ppm Zn/g tissue, SEM: 0.22), and ZnCl₂ (3.59 ppm Zn/g tissue, SEM: 0.32) treated animals.

For the urine, a significant increase in zinc levels were seen in animals treated with ZM (14.12 ppm Zn/g tissue, SEM: 3.58) as compared to control (1.59 ppm Zn/g tissue,

SEM: 0.33), Na-DMDTC (1.34 ppm Zn/g tissue, SEM: 0.42), and ZnCl₂ (4.08 ppm Zn/g tissue, SEM: 0.86) treated animals.

For the feces, a significant increase in zinc levels were seen in animals treated with ZM (264.80 ppm Zn/g tissue, SEM: 28.09) and ZnCl₂ (258.60 ppm Zn/g tissue, SEM: 25.80) as compared to control (31.93 ppm Zn/g tissue, SEM: 2.54), and Na-DMDTC (30.75 ppm Zn/g tissue, SEM: 2.19) treated animals.

3.3.2 Copper

A summary of the ICP-OES results for copper is found in Table 4. There were no significant differences between all of the treatment groups in copper levels in kidney, urine, and feces.

For the liver, a significant increase in copper levels were seen in the animals treated with ZM (5.22 ppm Cu/g tissue, SEM: 0.16) as compared to control (3.85 ppm Cu/g tissue, SEM: 0.06), Na-DMDTC (4.013 ppm Cu/g tissue, SEM: 0.07), and ZnCl₂ (3.84 ppm Cu/g tissue, SEM: 0.03) treated animals.

For the serum, a significant decrease in copper levels were seen in the animals treated with ZM (4.461 ppm Cu/g tissue, SEM: 0.08) as compared to control (4.95 ppm Cu/g tissue, SEM: 0.07) animals.

3.3.3 Iron

A summary of the ICP-OES results for iron is found in Table 5. There were no significant differences between all of the treatment groups in iron levels in kidney, serum, urine, and feces as compared to the control.

For the liver, a significant decrease in iron levels were seen in the animals treated with ZnCl₂ (62.13 ppm Fe/g tissue, SEM: 5.32) as compared to control (93.09 ppm Fe/g tissue, SEM: 4.90) animals.

3.4 Determination of Total Glutathione and Glutathione to Glutathione disulfide ratio (GSH/GSSG)

Total glutathione levels and the ratio of reduced to oxidized glutathione were measured using the Glutathione Assay Kit from Cayman Chemical (Ann Arbor, MI, USA). Both parameters were measured in the liver and kidney of treated (ZM, Na-DMDTC, and ZnCl₂) and control animals (for liver, n = 20, n = 5 per treatment group; for kidney, n = 32, n = 8 per treatment group). The results of the total glutathione assay were normalized to the weight of the tissue prior to homogenization in metaphosphoric acid. Each experiment was conducted twice to ensure consistency.

Due to significant changes in the GSH/GSSG ratio, separate figures showing the levels of GSH and GSSG individually are found in Figure 6 and 7, respectively.

3.4.1 Total Glutathione Levels

The result of this assay is summarized in Figure 4. There were no significant differences in total glutathione levels in the liver of animals across all the groups.

For the kidney, total glutathione levels were significantly increased in ZM treated group (1983 nmol/g tissue, SEM: 304.7) when compared to the control (845.70 nmol/g tissue, SEM: 151.7)

3.4.2 GSH/GSSG Ratio

The result of this assay is summarized in Figure 5. For the liver, the GSH/GSSG ratios were significantly increased in ZM treated group (12, SEM: 1.739) when compared

to the control (5.39, SEM: 0.35), Na-DMDTC (7.22, SEM: 0.53) and ZnCl₂ (6.37, SEM: 0.51) treated animals.

There were no significant differences in the GSH/GSSG ratio in the kidney of animals across all the groups.

3.4.3 GSH Levels

The result of this assay is summarized in Figure 6. There were no significant differences in the levels of GSH in the liver of animals across all the groups.

For the kidney, a significant increase in GSH levels were seen in animals treated with ZM (1571 nmol/g of tissue, SEM: 200.7) when compared to the control (567.5 nmol/g of tissue, SEM: 96.99).

3.4.4 GSSG Levels

The result of this assay is summarized in Figure 7. There were no significant differences in the levels of GSSG in the kidneys of animals across all the groups.

For the liver, a significant decrease in GSSG levels were seen in animals treated with ZM (857.1 nmol/g of tissue, SEM: 159.90) when compared to control (1548 nmol/g of tissue, SEM: 117.60).

3.5 Determination of Glutathione Reductase and Peroxidase Activity

The Glutathione Reductase Assay Kit and the Glutathione Peroxidase Assay Kit from Cayman Chemical (Ann Arbor, MI, USA) were used to measure the activity of both enzymes. The activities of glutathione reductase and peroxidase were assessed in both the liver and kidney of treated (ZM, Na-DMDTC, and ZnCl₂) and control animals (n = 24, n = 6 per treatment group). Each experiment was conducted twice to ensure consistency.

3.5.1 *Glutathione Reductase*

The result of this assay is summarized in Figure 8. There were no significant differences in the activity of glutathione reductase in the liver or kidneys of animals across all the groups.

3.5.2 *Glutathione Peroxidase*

The result of this assay is summarized in Figure 9. There were no significant differences in the activity of glutathione peroxidase in the liver or kidneys of animals across all the groups.

3.6 Total Antioxidant Levels

Total antioxidant levels were measured using the Total Antioxidant Assay Kit from Cayman Chemical (Ann Arbor, MI, USA). The antioxidant levels were assessed in both the liver and kidney of treated (ZM, Na-DMDTC, and ZnCl₂) and control animals (n = 24, n = 6 per treatment group). The control and treated samples were compared to a standard curve of Trolox and the results were expressed as millimolar Trolox equivalents, normalized to protein content. Each experiment was conducted twice to ensure consistency. The result of this assay is summarized in Figure 10.

For the liver, a significant increase in the total antioxidant levels were seen in animals treated with ZM (2.51 mmol of Trolox/mg of protein, SEM: 0.05) when compared to control (2.11 mmol of Trolox/mg of protein, SEM: 0.09).

For the kidney, a significant increase in the total antioxidant levels were seen in animals treated with ZM (1.05 mmol of Trolox/mg of protein, SEM: 0.05) when compared to control (0.86 mmol of Trolox/mg of protein, SEM: 0.02).

3.7 Measurement of 4-Hydroxynonenol (4-HNE) ELISA

The lipid peroxidation marker, 4-HNE, was measured using the Lipid Peroxidation (4-HNE) Competitive ELISA Assay Kit from Abcam (Cambridge, MA, USA). The 4-HNE levels were assessed in both the liver and kidney of treated (ZM, Na-DMDTC, and ZnCl₂) and control animals (n = 24, n = 6 per treatment group). The controls and treated samples were compared to a standard curve of 4-HNE BSA. Each experiment was conducted twice to ensure consistency. The results of this assay are summarized in Figure 11.

There were no significant differences in levels of 4-HNE in the liver or kidneys of animals across all the groups.

3.8 Measurement of Protein Oxidation

The Protein Carbonyl Assay Kit from Cayman Chemical (Ann Arbor, MI, USA) was used to measure protein oxidation in both liver and kidney of control and treated (ZM, Na-DMDTC, and ZnCl₂) animals (n = 24, n = 6 per treatment group). The levels of protein carbonyls were assessed between a sample incubated and derivatized with DNPH and its own control, which did not undergo derivatization with DNPH. Each experiment was conducted twice to ensure consistency. The result of this assay is summarized in Figure 12.

There were no significant differences in levels of protein carbonyls in the liver or kidneys of animals across all the groups.

3.9 Measurement of Creatinine Clearance and Associated Parameters

Creatinine clearance is the volume of blood plasma cleared of creatinine per unit time and is used in determining renal function status (Shahbaz and Gupta, 2021). Creatinine clearance is calculated using the formula: $Clcr = \text{urine creatine (mg/dL)} \times \text{urine flow rate (mL/min)} / \text{serum creatinine (mg/dL)}$, provided by Bazzano *et al.* (2015). Therefore, urine

creatinine, serum creatinine, and urine flow rate of control and treated animals were measured (n = 33; n = 8 for control, Na-DMDTC, and ZnCl₂; n = 9 for ZM). Urine and serum creatinine were measured using colorimetric assay kits from Cayman Chemical (Ann Arbor, MI, USA). In order to calculate urine flow rate, animals were placed in metabolism cages the night prior to euthanasia for 14 hours in order to collect the urine. Urine flow rate was calculated by dividing the 14 hours of urine volume by 840, which equates to the number of minutes in 14 hours. In the process of measuring urine flow rate, the total water consumption and total urine production of control and treated animals were assessed.

3.9.1 Urine Creatinine

The result of this assay is summarized in Figure 13. A significant decrease in urine creatinine was seen in animals treated with ZM (35.01 mg/dL, SEM: 6.04) when compared to control (81.57 mg/dL, SEM: 9.81) and the ZnCl₂ (77.84 mg/dL, SEM: 10.28) treated animals.

3.9.2 Serum Creatinine

The result of this assay is summarized in Figure 14. There were no significant differences in serum creatinine levels in animals across all the groups.

3.9.3 Urine Flow Rate

The result of this calculation is summarized in Figure 15. A significant increase in urine flow rate was seen in animals treated with ZM (0.042 mL/min, SEM: 0.008) when compared to control (0.017 mL/min, SEM: 0.002) and the ZnCl₂ (0.016 mL/min, SEM: 0.002) treated animals.

3.9.4 Total Water Consumption

The result of this measurement is summarized in Figure 16. A significant increase in total water consumption was seen in animals treated with ZM (30.11 mL, SEM: 7.39) when compared to control (6.63 mL, SEM: 1.95) and the ZnCl₂ (6.75 mL, SEM: 1.99) treated animals.

3.9.5 Total Urine Production

The result of this measurement is summarized in Figure 17. A significant increase in total urine production was seen in animals treated with ZM (35.46 mL, SEM: 6.93) when compared to control (13.99 mL, SEM: 1.90) and the ZnCl₂ (13.84 mL, SEM: 1.96) treated animals.

3.9.6 Creatinine Clearance

The result of this calculation is summarized in Figure 18. There were no significant differences in creatinine clearance in animals across all the groups.

3.10 Immunohistochemical Detection of KIM-1 and NGAL

Immunohistochemistry is a technique that combines histological, immunological, and biochemical techniques to visualize specific components in tissue by using appropriate antibodies that bind specifically to their target antigen on the tissue section. In this study, renal sections were subjected to heat-activated antigen retrieval and a primary antibody was used to detect the antigen of interest. A secondary antibody labeled with horseradish peroxidase, incubated with the substrate DAB (3,3'-diaminobenzidine), was used for chromogenic detection at the antigen localization site. Incubation with DAB leads to precipitation of an insoluble, brown colored precipitate at the antigen localization site. The two markers of interest in this study were kidney injury marker-1 (KIM-1) and neutrophil

gelatinase-associated lipocalin (NGAL), as these two molecules are novel biomarkers used in the detection of renal injury.

3.10.1 *KIM-1*

Immunohistochemical staining for KIM-1 on kidney sections for control or treated animals are seen in Figure 19. Figure 19 is separated into 4 panels (Panel A, B, C, D), with each panel representing control and treatment (ZM, Na-DMDTC, and ZnCl₂) groups in the study. All of the images in Figure 19 were captured with an objective magnification of 40X.

Panel A shows a representative micrograph of the kidneys of control animals. The panel shows glomeruli and tubules with basal level of KIM-1 immunoreactivity. The glomeruli are characterized by a circular mass of cells and capillaries surrounded by empty space known as the Bowman's space, all of which is encapsulated by a layer of simple squamous epithelial cells known as the Bowman's capsule. The glomeruli are surrounded by the renal tubules which are a single layer of simple cuboidal epithelium. Panel B and C are representative micrographs of animals treated with ZM or Na-DMDTC, respectively. In both of these micrographs, increased immunoreactivity with KIM-1, as indicated by the development of a dark brown staining, is seen in the tubular regions of the kidney tissue. Panel D shows a representative micrograph of kidney sections of animals treated with ZnCl₂. In this micrograph, immunoreactivity with KIM-1 is comparable to that of control animals.

3.10.2 *NGAL*

Immunohistochemical staining for NGAL on kidney sections for control and treated animals are seen in Figure 20. Figure 20 is separated into 4 panels (Panel A, B, C,

D), with each panel representing control and treatment (ZM, Na-DMDTC, and ZnCl₂) groups in the study. All of the images in Figure 20 were captured with an objective magnification of 40X.

Panel A shows a representative micrograph of the kidneys of control animals. The panel shows glomeruli and tubules with basal level of NGAL immunoreactivity. The glomeruli are characterized by a circular mass of cells and capillaries surrounded by empty space known as the Bowman's space, all of which is encapsulated by a layer of simple squamous epithelial cells known as the Bowman's capsule. The glomeruli are surrounded by the renal tubules which are a single layer of simple cuboidal epithelium. Panels B, C, and D are representative micrographs of kidneys of animals treated with ZM, Na-DMDTC, and ZnCl₂ respectively. In all of these micrographs, immunoreactivity with NGAL is comparable to that of control animals.

3.11 Light Microscopy – Hematoxylin and Eosin Staining

Hematoxylin and eosin staining is a basic screening technique used for histopathology. In this study, this technique is used to visualize gross morphological alterations in hepatic and renal tissue in animals treated with ZM, Na-DMDTC, or ZnCl₂, when compared to the control animal.

3.11.1 Liver – H&E

Liver sections stained with hematoxylin and eosin are seen in Figure 21. Figure 21 is separated into 4 panels (Panel A, B, C, D), with each panel representing control and treatment (ZM, Na-DMDTC, and ZnCl₂) groups in the study. All of the images in Figure 21 were captured with an objective magnification of 40X.

Panel A shows a representative micrograph of the liver of control animals. In this micrograph, sheets of polygonal hepatocytes are seen and interspersed between the hepatocytes are spaces for the transport of blood cells, known as the sinusoids. In this image, the central vein is present and is well defined. Panel B is a representative micrograph of the liver of animals treated with ZM. In this micrograph, the presence of infiltration, cellular debris, and vacuolization is seen in the hepatocytes surrounding the central vein. Panel C and D are representative micrographs of the liver of animals treated with Na-DMDTC and ZnCl₂, respectively. In these micrographs, the cells appear unremarkable, with no obvious alterations and comparable to that of control animals.

3.11.2 Kidney – H&E

Kidney sections stained with hematoxylin and eosin are seen in Figure 22. Figure 22 is separated into 4 panels (Panel A, B, C, D), with each panel representing control and treatment (ZM, Na-DMDTC, and ZnCl₂) groups in the study. All of the images in Figure 22 were captured with an objective magnification of 40X.

Panel A shows a representative micrograph of the kidneys of control animals. The panel shows the presence of well-defined glomeruli and tubules. The glomeruli are characterized by a circular mass of cells and capillaries surrounded by empty space known as the Bowman's space, all of which is encapsulated by a layer of simple squamous epithelial cells known as the Bowman's capsule. The glomeruli are surrounded by the renal tubules which are a single layer of simple cuboidal epithelium. Panel B and C are representative micrographs of the kidneys of animals treated with ZM or Na-DMDTC, respectively. In both of these treatment groups, the presence of protein aggregation and sloughing of tubular cells are seen. Panel D shows a representative micrograph of kidney

sections of animals treated with ZnCl₂. In this micrograph, the cells appear unremarkable, with no obvious alterations and comparable to that of control animals.

3.12 Light Microscopy – Masson’s Trichrome Staining

Masson’s trichrome staining is a technique used for detection of extracellular matrix deposition. In this study, hepatic and renal sections were stained with Masson’s trichrome in order to determine if treatment with ZM, Na-DMDTC, or ZnCl₂, would result in the accumulation of collagenous connective tissue fibers.

3.12.1 Liver – Masson’s Trichrome Staining

Liver sections stained with Masson’s Trichrome are seen in Figure 23. Figure 23 is separated into 4 panels (Panel A, B, C, D), with each panel representing control and treatment (ZM, Na-DMDTC, and ZnCl₂) groups in the study. All of the images in Figure 23 were captured with an objective magnification of 40X.

Panel A shows a representative micrograph of the liver of control animals. In this micrograph, sheets of polygonal hepatocytes are seen and interspersed between the hepatocytes are spaces for the transport of blood cells, known as the sinusoids. In this image, the central vein is present and is well defined. Panels B and C are representative micrographs of the liver of animals treated with ZM and Na-DMDTC, respectively. In both micrographs, the presence of infiltration near the central veins are seen. Panel D is a representative micrograph of animals treated with ZnCl₂ respectively. In this micrograph, the cells appear unremarkable, with no obvious alterations and comparable to that of control animals. Extracellular matrix accumulation in all treatment groups are unremarkable and comparable to that of the control.

3.12.2 Kidney – Masson’s Trichrome Staining

Kidney sections stained with Masson’s Trichrome are seen in Figure 24. Figure 24 is separated into 4 panels (Panel A, B, C, D), with each panel representing control and treatment (ZM, Na-DMDTC, and ZnCl₂) groups in the study. All of the images in Figure 24 were captured with an objective magnification of 40X.

Panel A shows a representative micrograph of the kidneys of control animals. The panel shows the presence of well-defined glomeruli and tubules. The glomeruli are characterized by a circular mass of cells and capillaries surrounded by empty space known as the Bowman’s space, all of which is encapsulated by a layer of simple squamous epithelial cells known as the Bowman’s capsule. The glomeruli are surrounded by the renal tubules which are a single layer of simple cuboidal epithelium. Panels B, C, and D, are representative micrographs of the kidney of animals treated with ZM, Na-DMDTC, and ZnCl₂ respectively. Extracellular matrix accumulation in all treatment groups are unremarkable and comparable to that of the control.

3.13 Light Microscopy – Periodic Acid-Schiff Staining with and without Diastase

Digestion

Periodic acid-Schiff (P.A.S) staining is a technique used to detect the presence of carbohydrates such as polysaccharides, mucin, and glycogen. In the liver sections stained with H&E, animals treated with ZM or Na-DMDTC exhibited the presence of vacuolization. The origin of these vacuoles can be attributed to disruption of glycogen storage or through another mechanism, such as oxidative stress. To rule out the possibility of glycogen storage disruption, liver sections were digested with diastase (α -amylase) prior to staining with P.A.S.

Kidney sections did not undergo diastase digestion and were stained with P.A.S following standard procedure as outlined in section 2.19.3. P.A.S staining of kidney tissue was conducted due to the clarity and improved definition the stain provides to the basement membrane, Bowman's capsule, and the glomerular capillaries.

3.13.1 Liver – P.A.S Staining with Diastase Digestion

Liver sections digested with diastase and stained with P.A.S are seen in Figure 25. Figure 25 is separated into 4 panels (Panel A, B, C, D), with each panel representing control and treatment (ZM, Na-DMDTC, and ZnCl₂) groups in the study. All of the images in Figure 25 were captured with an objective magnification of 40X.

Panel A shows a representative micrograph of the liver of control animals. In this micrograph, sheets of polygonal hepatocytes are seen and interspersed between the hepatocytes are spaces for the transport of blood cells, known as the sinusoids. In this image, the central vein is present and is well defined. Panel B and C are representative micrographs of liver of animals treated with ZM and Na-DMDTC, respectively. In both of these treatment groups, vacuolization of hepatocytes near the central vein are seen, indicating that the vacuoles are not due to disruptions of glycogen storage. Panel D shows a representative micrograph of liver sections of animals treated with ZnCl₂. In this micrograph, the cells appear unremarkable, with no obvious alterations and are comparable to that of control animals.

3.13.2 Kidney – P.A.S Staining without Diastase Digestion

Kidney sections stained with P.A.S without diastase digestion are seen in Figure 26. Figure 26 is separated into 4 panels (Panel A, B, C, D), with each panel representing

control and treatment (ZM, Na-DMDTC, and ZnCl₂) groups in the study. All of the images in Figure 26 were captured with an objective magnification of 40X.

Panel A shows a representative micrograph of the kidneys of control animals. The panel shows the presence of well-defined glomeruli and tubules. The glomeruli are characterized by a circular mass of cells and capillaries surrounded by empty space known as the Bowman's space, all of which is encapsulated by a layer of simple squamous epithelial cells known as the Bowman's capsule. The glomeruli are surrounded by the renal tubules which are a single layer of simple cuboidal epithelium. Panel B and C are representative micrographs of the kidneys of animals treated with ZM and Na-DMDTC, respectively. In these two treatment groups, thickening of the Bowman's capsules are seen. Panel D shows a representative micrograph of kidney sections of animals treated with ZnCl₂. In this micrograph, the cells appear unremarkable, with no obvious alterations and comparable to that of control animals.

3.14 Transmission Electron Microscopy

Transmission electron microscopy (TEM) is a microscopy technique that uses a particle beam of electrons to visualize specimens and generate a highly magnified image. Transmission electron microscopy is employed to visualize ultrastructural changes in cellular morphology of hepatic and renal tissue after treatment with ZM, Na-DMDTC, or ZnCl₂. In order to visualize the samples under a transmission electron microscope, liver and kidney tissues were embedded in plastic and sectioned on an ultramicrotome to produce ultra-thin sections. Sections were then stained with uranyl acetate and lead citrate to provide contrast to the images.

3.14.1 Liver – TEM

Liver sections of control animals demonstrate unremarkable hepatocytes, with the presence of red blood cells and Kupffer cells in the sinusoids (Panel A, Figure 27). Higher magnification electron micrographs of the cell demonstrate well defined cellular features such as a nucleus with a nuclear envelope, mitochondria with cristae, and the presence of smooth and rough endoplasmic reticulum (Panel B, Figure 27). Low and high magnification micrographs of liver sections of ZM treated animals show the presence of lipid deposition and cellular edema (Panel A and B, Figure 28). Low and high magnification micrographs of liver sections of Na-DMDTC treated animals show the presence of vacuolization and swelling of the endoplasmic reticulum (Panel A and B, Figure 29). Panel A and B in Figure 30 are representative low and high magnification electron micrographs of animals treated with ZnCl₂. The hepatocytes appear unremarkable and comparable to that of control animals.

3.14.2 Kidney – TEM of Glomeruli

Transmission electron micrographs of kidney sections of control animals demonstrate unremarkable glomerular structure, with the presence of mesangial cells, podocytes, capillary loops, and epithelial cell of the Bowman's capsule (Panel A, Figure 31). Higher magnification electron micrographs of the glomeruli demonstrate an unremarkable capillary loop structure, with the presence of podocytes, and individual podocyte foot processes encompassing the capillary loop (Panel B, Figure 31). Low and high magnification electron micrographs of animals treated with ZM (Panel A and B, Figure 32) and Na-DMDTC (Panel A and B, Figure 33) demonstrate fusion of podocytes, accompanied by a thickening of the basement membrane. Panel A and B in Figure 34 are

representative low and high magnification electron micrographs of animals treated with $ZnCl_2$. The glomeruli and the structures within it appear unremarkable and comparable to that of the control animal.

3.14.3 Kidney – TEM of Tubular Cells

Low and high magnification transmission electron micrographs of kidney sections of control animals demonstrate unremarkable tubular structure, with the presence of undisturbed nuclei and a distinct lumen (Panel A and B, Figure 35). Low and high magnification electron micrographs of animals treated with ZM (Panel A and B, Figure 36) and Na-DMDTC (Panel A and B, Figure 37) demonstrate the presence of vacuolization and disruption of mitochondria in the tubular cells. Panel A and B in Figure 38 are representative low and high magnification electron micrographs of animals treated with $ZnCl_2$. The tubular structure appears unremarkable and comparable to that of the control animal.

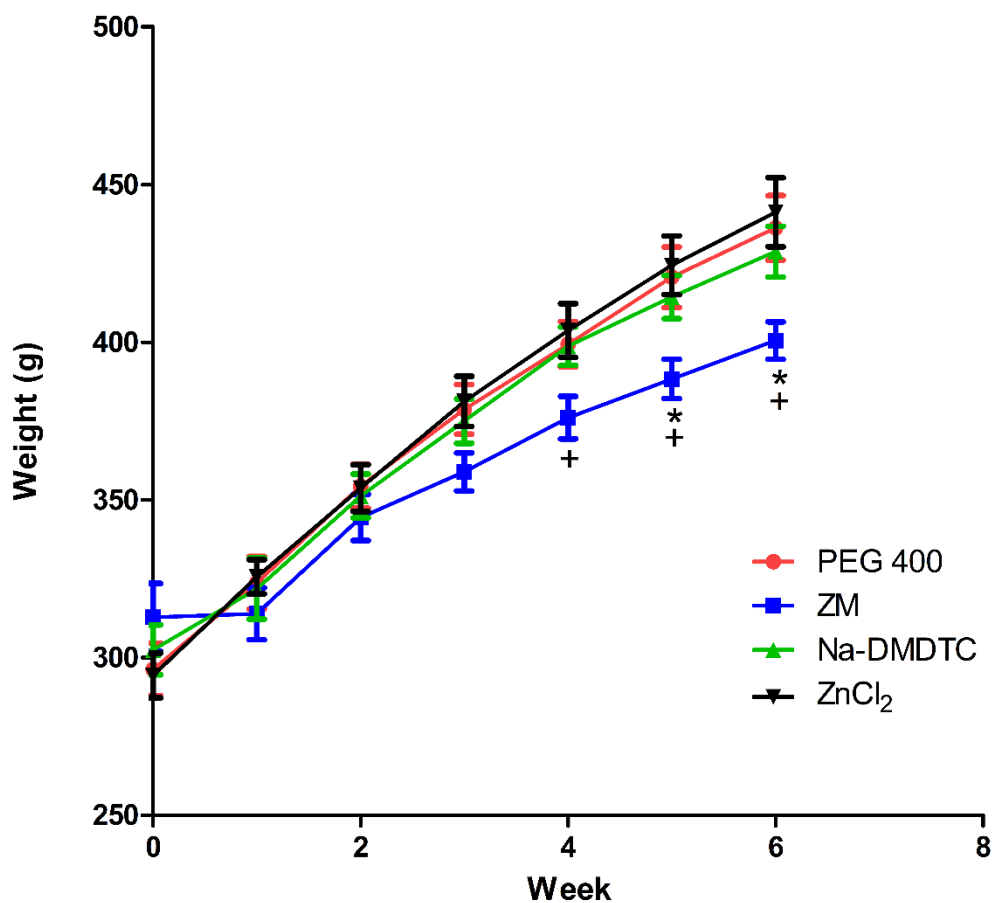


Figure 2. Animal Weights (g)

Animal weights throughout the 6-week study. Animals were orally dosed daily with either 50% PEG400 (Vehicle Control), 100 mg/kg ziram (ZM), 94 mg/kg sodium dimethyldithiocarbamate (Na-DMDTC), or 45 mg/kg ZnCl₂ (n=9 for ZM, n=8 for all other groups). Animal weights are expressed in grams (g). Values represent mean \pm SEM and were analyzed using a one-way ANOVA followed by Tukey's Multiple Comparison post-hoc test. Significant decreases in total animal weights in the ZM treatment group were seen as compared to the ZnCl₂ treatment group in week 4. Significant decreases in total animal weights in the ZM treatment were seen as compared to the control and ZnCl₂ treatment group in weeks 5 and 6. *: $p < 0.05$ (compared to vehicle control); +: $p < 0.05$ (compared to ZnCl₂)

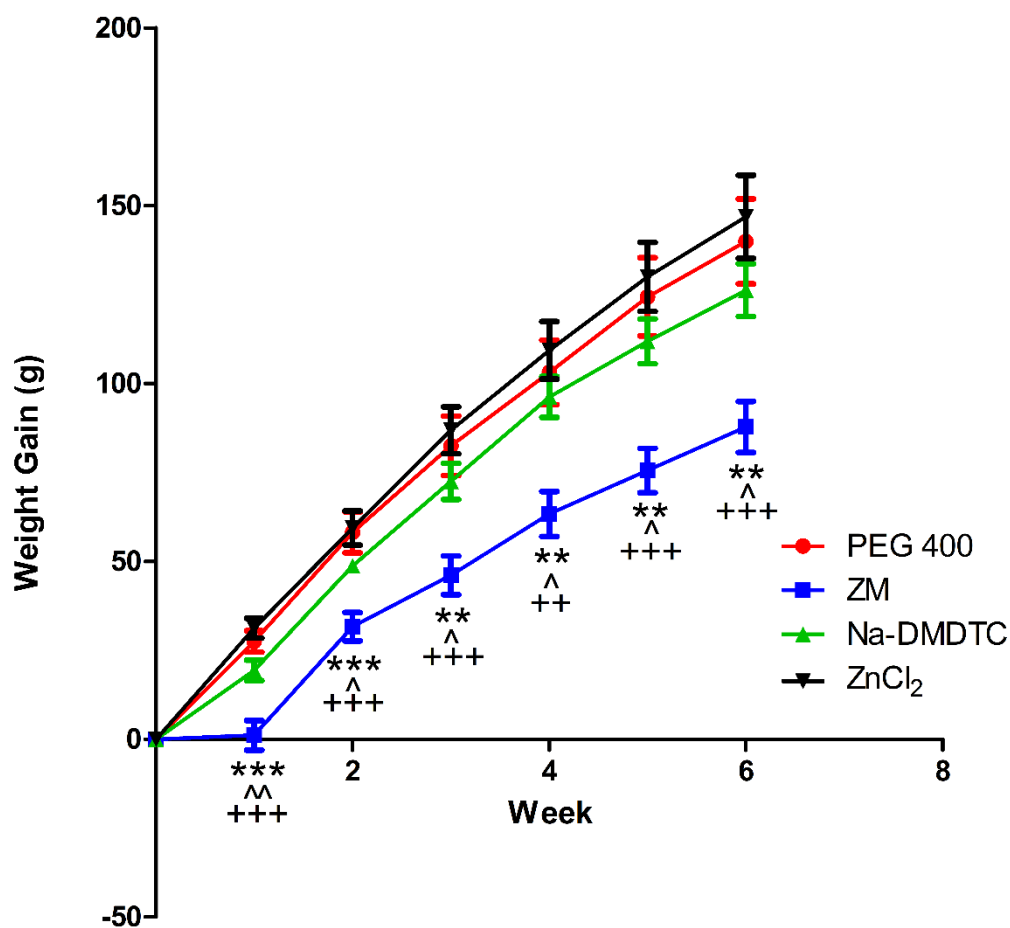


Figure 3. Animal Weight Gain (g)

Animal weight gain throughout the 6-week study. Animals were orally dosed daily with either 50% PEG400 (Vehicle Control), 100 mg/kg ziram (ZM), 94 mg/kg sodium dimethyldithiocarbamate (Na-DMDTC), or 45 mg/kg ZnCl₂ (n=9 for ZM, n=8 for all other groups). Animal weight gain was expressed in grams (g). Values represent mean \pm SEM and were analyzed using a one-way ANOVA followed by Tukey's Multiple Comparison post-hoc test. Significant decreases in weight gain in the ZM treatment group were seen starting in week 1 and remained significant throughout the course of the study as compared to all other groups. **: $p < 0.01$, ***: $p < 0.001$ (compared to vehicle control); ^: $p < 0.05$, ^^: $p < 0.01$ (compared to Na-DMDTC); +++: $p < 0.001$ (compared to ZnCl₂).

ANALYTE	PEG-400	ZM	Na-DMDTC	ZnCl ₂	UNITS
Alanine Aminotransferase	32.6±1.64	25.1±1.09 *	31.0±2.31	26.0±1.86	U/L
Aspartate Aminotransferase	104±16.4	83.3±3.75	92.1±6.78	84.5±1.79	U/L
Alkaline Phosphatase	106±8.38	110±6.36	111±7.82	131±7.32	U/L
Albumin	4.91±0.06	4.77±0.06	4.89±0.08	4.65±0.10	g/L
Total Protein	5.78±0.07	5.66±0.07	5.81±0.04	5.56±0.14	mg/mL
Blood Urea Nitrogen	16.3±0.65	16.4±0.50	16.5±0.50	17.5±0.78	mg/dL
Total Bilirubin	0.275±0.02	0.288±0.02	0.275±0.03	0.300±0.000	mg/dL
Glucose	203±8.13	170±7.42 *	210±8.50	224±9.19	mg/dL
Sodium	146±0.69	146±0.87	145±0.69	144±0.65	mmol/L
Potassium	5.41±0.12	5.33±0.13	5.34±0.09	5.51±0.11	mmol/L
Calcium	10.8±0.10	10.6±0.14	10.8±0.10	10.7±0.13	mg/dL
Globulin	0.863±0.03	0.900±0.03	0.938±0.07	0.888±0.07	g/dL
Thyroxine	3.13±0.21	2.87±0.21	2.89±0.26	2.93±0.26	µg/dL
Cholesterol	77.50±2.63	82.78±2.05	77.50±4.24	73.75±3.18	mg/dL

Table 2. Serum Parameters: Preventive Care Profile Plus and T4 Rotor

Analysis of serum chemistry parameters following 6-week oral treatment to either 50% PEG400 (Vehicle Control), 100 mg/kg ziram (ZM), 94 mg/kg sodium dimethyldithiocarbamate (Na-DMDTC), or 45 mg/kg ZnCl₂ (n=9 for ZM, n=8 for all other groups). Fresh serum samples following euthanasia were loaded onto the Preventive Care Profile Plus or T4/Cholesterol Rotor and analyzed on the Abaxis VetScan V2. Values represent mean ± SEM and were analyzed using a one-way ANOVA followed by Tukey's Multiple Comparison post-hoc test. Animals treated with ZM had significantly lower alanine aminotransferase levels and glucose levels as compared to the control. *: p < 0.05 (compared to vehicle control).

SAMPLE	PEG-400	ZM	Na-DMDTC	ZnCl ₂
Liver	26.33±0.60	64.03±3.17 ***,^^^,+++	28.86±0.94	29.22±1.29
Kidney	22.10±0.84	41.37±2.37 ***,^^^,+++	21.56±0.33	24.91±0.89
Serum	2.46±0.19	11.91±1.11 ***,^^^,+++	2.42±0.22	3.59±0.32
Urine	1.59±0.33	14.12±3.58 **,^	1.34±0.42	4.08±0.86
Feces	31.93±2.54	264.80±28.09 ***,^^^	30.75±2.19	258.60±25.80 ***,^^^

Table 3. ICP-OES Elemental Analysis: Zinc (ppm)/Dry Weight (g)

Measurement of zinc levels in the liver, kidney, serum, urine, and feces of rats after 6 weeks of oral treatment with either vehicle control (PEG 400), 100 mg/kg ZM, 94 mg/kg Na-DMDTC, or 45 mg/kg ZnCl₂. (Liver: n ≥ 7 for all groups; Kidney: n ≥ 7 for all groups; Serum: n ≥ 7 for all groups; Urine: n ≥ 3 for all groups; Feces: n ≥ 7 for all groups). Concentration (ppm) was normalized by dry sample weight after lyophilization. Values represent mean ± SEM and were analyzed using a one-way ANOVA followed by Tukey's Multiple Comparison post-hoc test. Significant increases in zinc levels were observed in the liver, kidney, serum, and urine of animals treated with ZM as compared to the control. Significant increases in feces zinc levels were observed in the ZM and ZnCl₂ as compared to control and Na-DMDTC group. **: p < 0.01, ***: p < 0.001 (compared to vehicle control); ^: p < 0.05, ^^: p < 0.001 (compared to Na-DMDTC); +++: p < 0.001 (compared to ZnCl₂).

SAMPLE	PEG-400	ZM	Na-DMDTC	ZnCl ₂
Liver	3.85±0.06	5.22±0.16 ***,^^^,+++	4.01±0.07	3.84±0.03
Kidney	9.64±1.90	6.61±0.36	7.82±0.81	8.59±0.93
Serum	4.95±0.18	4.46±0.08 *	4.69±0.07	4.64±0.09
Urine	5.15±1.11	5.07±0.53	3.73±0.47	6.33±0.41
Feces	6.15±0.41	7.08±0.35	5.75±0.37	6.53±0.36

Table 4. ICP-OES Elemental Analysis: Copper (ppm)/Dry Weight (g)

Measurement of copper levels in the liver, kidney, serum, urine, and feces of rats after 6 weeks of oral treatment with either vehicle control (PEG 400), 100 mg/kg ZM, 94 mg/kg Na-DMDTC, or 45 mg/kg ZnCl₂. (Liver: n ≥ 7 for all groups; Kidney: n ≥ 7 for all groups; Serum: n ≥ 7 for all groups; Urine: n ≥ 3 for all groups; Feces: n ≥ 7 for all groups). Concentration (ppm) was normalized by dry sample weight after lyophilization. Values represent mean ± SEM and were analyzed using a one-way ANOVA followed by Tukey's Multiple Comparison post-hoc test. Significant increases in liver copper levels were observed in the ZM treatment group as compared to all other groups. Significant decreases were observed in serum copper levels in the ZM treatment group when compared to vehicle control. No significant changes were observed in kidney, urine, or feces copper levels in treatment groups when compared to vehicle control. *: $p < 0.05$, ***: $p < 0.001$ (compared to vehicle control); ^^: $p < 0.001$ (compared to Na-DMDTC); +++: $p < 0.001$ (compared to ZnCl₂).

SAMPLE	PEG-400	ZM	Na-DMDTC	ZnCl ₂
Liver	93.09±4.90	82.99±3.58	87.49±3.69	62.13±5.32 ***,^^,#
Kidney	56.73±3.12	52.28±1.21	56.12±4.57	47.86±1.77
Serum	4.67±0.33	3.74±0.32	3.61±0.23	4.26±0.51
Urine	7.29±2.19	12.79±2.23	6.42±0.60	10.89±3.93
Feces	85.55±9.86	96.92±7.53	75.61±5.74	79.62±6.34

Table 5. ICP-OES Elemental Analysis: Iron (ppm)/Dry Weight (g)

Measurement of iron levels in the liver, kidney, serum, urine, and feces of rats after 6 weeks of oral treatment with either vehicle control (PEG 400), 100 mg/kg ZM, 94 mg/kg Na-DMDTC, or 45 mg/kg ZnCl₂. (Liver: n ≥ 7 for all groups; Kidney: n ≥ 7 for all groups; Serum: n ≥ 7 for all groups; Urine: n ≥ 3 for all groups; Feces: n ≥ 7 for all groups). Concentration (ppm) was normalized by dry sample weight after lyophilization. Values represent mean ± SEM and were analyzed using a one-way ANOVA followed by Tukey's Multiple Comparison post-hoc test. Significant decreases were observed in liver iron levels in the ZnCl₂ treatment group as compared to all other groups. No significant changes in iron levels were observed in the kidney, serum, urine, and feces of animals across the groups. ***: $p < 0.001$ (compared to vehicle control); ^^: $p < 0.01$ (compared to Na-DMDTC); #: $p < 0.05$ (compared to ZM).

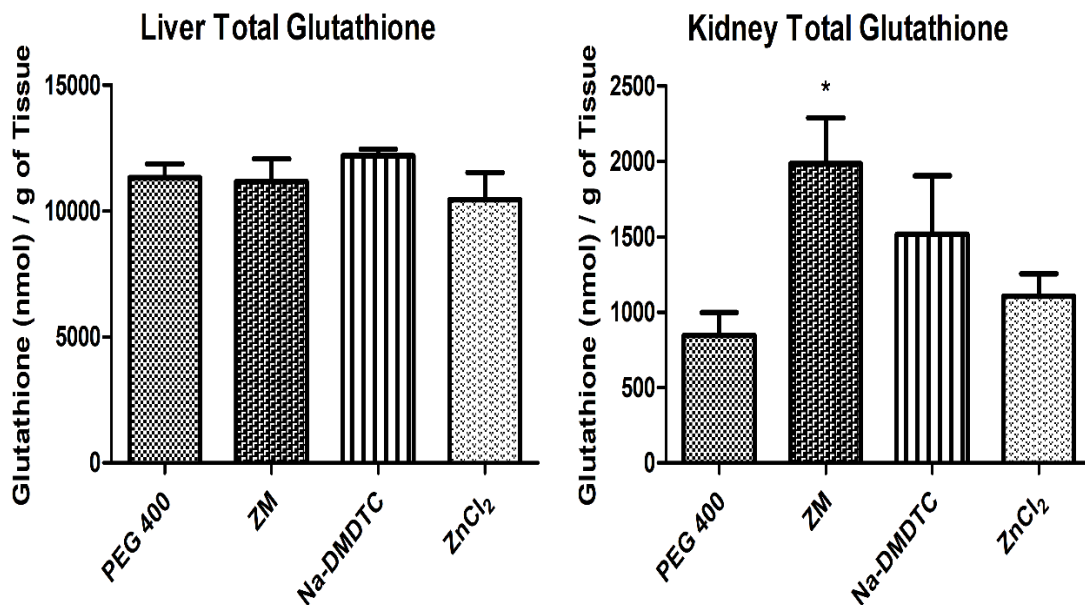


Figure 4. Total Glutathione Levels (nmol)/Tissue Weight (g)

Total glutathione levels (reduced glutathione and oxidized form) in the liver and kidney after 6 weeks of oral treatment with either vehicle control (PEG 400), 100 mg/kg ZM, 94 mg/kg Na-DMDTC, or 45 mg/kg ZnCl₂ (Liver n = 5 per group; Kidney n = 8 per group). The levels of total glutathione were interpolated from a glutathione disulfide standard curve and normalized to tissue weight prior to homogenization in 5% (w/v) metaphosphoric acid. Values represent mean ± SEM and were analyzed using a one-way ANOVA followed by Tukey's Multiple Comparison post-hoc test. No significant changes were seen in total glutathione levels in the liver across all treatment groups. Significantly increased total glutathione levels were observed in the kidneys of animals treated with ZM as compared to control. *: $p < 0.05$ (compared to vehicle control)

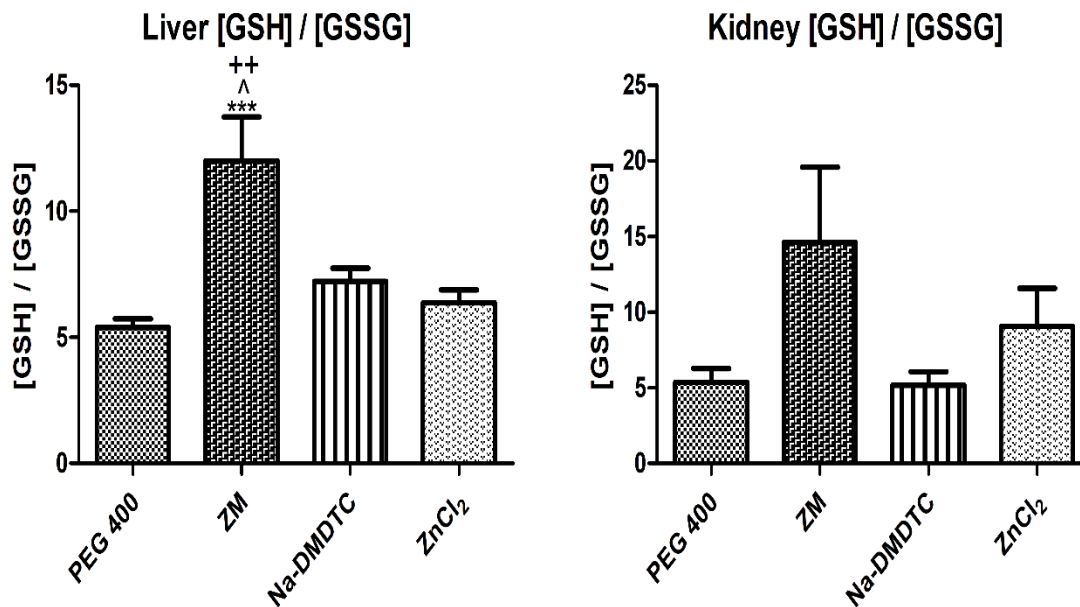


Figure 5. [GSH]/[GSSG]

The ratio of reduced to oxidized glutathione in the liver and kidney after 6 weeks of oral treatment with either vehicle control (PEG 400), 100 mg/kg ZM, 94 mg/kg Na-DMDTC, or 45 mg/kg ZnCl₂ (Liver n = 5 per group; Kidney n = 8 per group). Glutathione ratios were calculated by subtracting the concentration of total glutathione by the concentration oxidized glutathione to determine the concentration of reduced glutathione. Thereafter, the concentration of reduced glutathione is divided by the concentration of oxidized glutathione to determine the ratio. Values represent mean ± SEM and were analyzed using a one-way ANOVA followed by Tukey's Multiple Comparison post-hoc test. Significantly increased GSH to GSSG ratios were observed in the liver of animals treated with ZM as compared to all other groups. No significant changes in the GSH to GSSG ratio were seen in the kidneys across all the groups. ***: $p < 0.001$ (compared to vehicle control); ^: $p < 0.05$ (compared to Na-DMDTC); ++: $p < 0.01$ (compared to ZnCl₂).

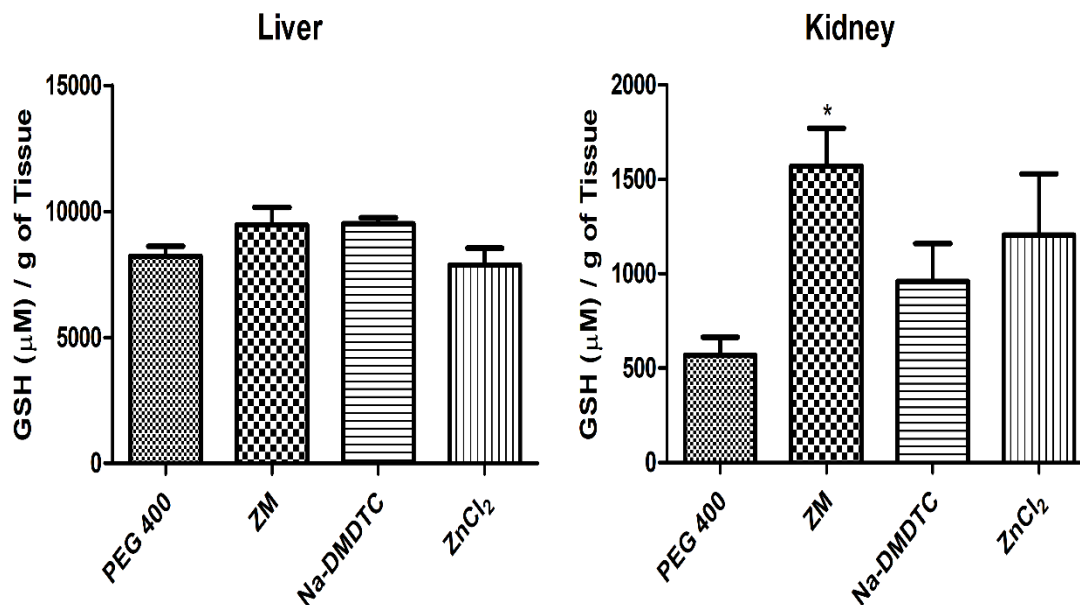


Figure 6. Reduced Glutathione (GSH) (μM)/Tissue Weight (g)

The concentration of reduced glutathione in the liver and kidney after 6 weeks of oral treatment with either vehicle control (PEG 400), 100 mg/kg ZM, 94 mg/kg Na-DMDTC, or 45 mg/kg ZnCl₂ (Liver n = 5 per group; Kidney n = 8 per group). Reduced glutathione levels were calculated by subtracting the concentration of total glutathione by the concentration oxidized glutathione and normalized to tissue weight prior to homogenization in 5% (w/v) metaphosphoric acid. Values represent mean \pm SEM and were analyzed using a one-way ANOVA followed by Tukey's Multiple Comparison post-hoc test. No significant changes in the reduced glutathione levels were observed in the liver of animals across all groups. Significantly increased GSH levels were observed in the kidneys of animals treated with ZM as compared to the control. *: $p < 0.05$ (compared to vehicle control)

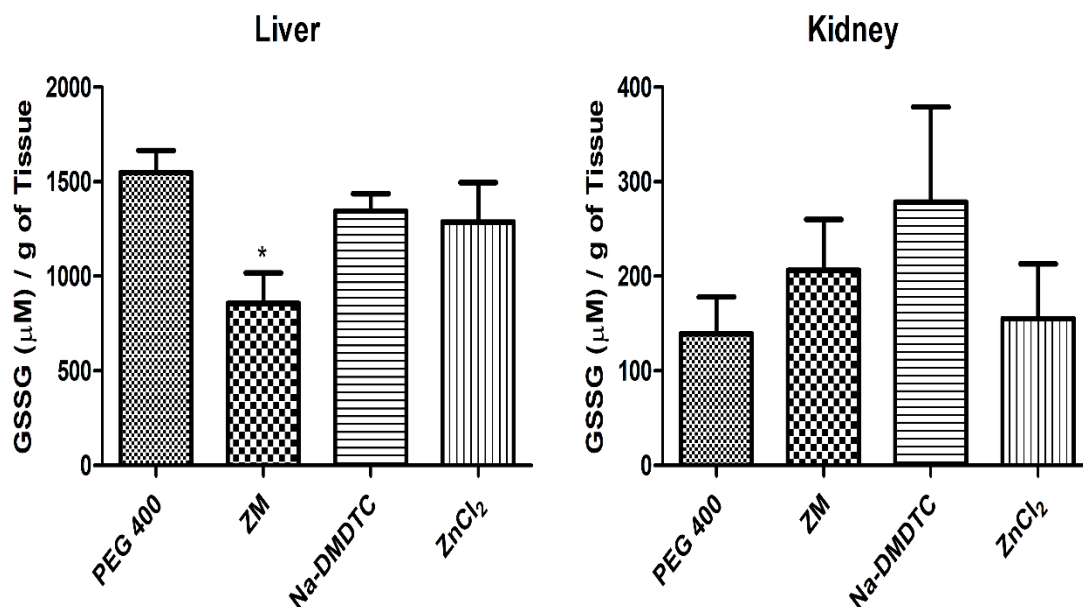


Figure 7. Oxidized Glutathione (GSSG) (μM)/Tissue Weight (g)

The concentration of oxidized glutathione in the liver and kidney after 6 weeks of oral treatment with either vehicle control (PEG 400), 100 mg/kg ZM, 94 mg/kg Na-DMDTC, or 45 mg/kg ZnCl_2 (Liver $n = 5$ per group; Kidney $n = 8$ per group). The levels of oxidized glutathione were interpolated from a glutathione disulfide standard curve and normalized to tissue weight prior to homogenization in 5% (w/v) metaphosphoric acid. Values represent mean \pm SEM and were analyzed using a one-way ANOVA followed by Tukey's Multiple Comparison post-hoc test. Significant decreases in the oxidized glutathione levels were observed in the liver of animals treated with ZM when compared to the control. No significant changes in oxidized glutathione levels were seen in the kidneys of animals across the treatment groups. *: $p < 0.05$ (compared to vehicle control)

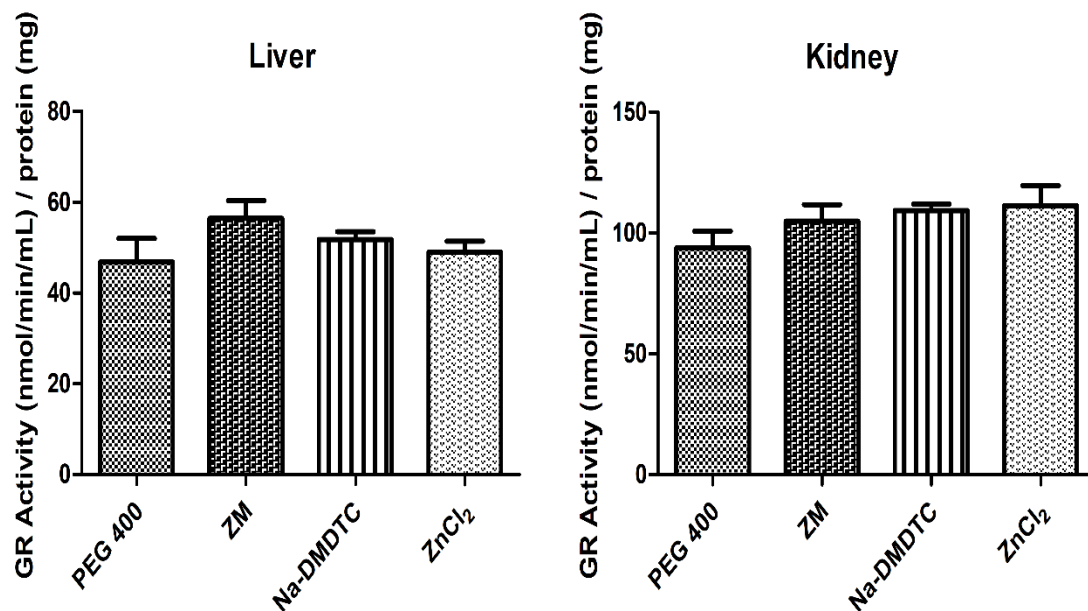


Figure 8. Glutathione Reductase Activity (nmol/min/mL)/Protein (mg)

The glutathione reductase activity in the liver and kidney after 6 weeks of oral treatment with either vehicle control (PEG 400), 100 mg/kg ZM, 94 mg/kg Na-DMDTC, or 45 mg/kg ZnCl₂ (n = 6 per group). Glutathione reductase activity was determined by measuring the decrease in absorption at 340 nm due to the oxidation of NADPH to NADP⁺ which was directly proportional to the GR activity in the samples. GR activity was then normalized to the protein concentration of the sample. Values represent mean ± SEM and were analyzed using a one-way ANOVA followed by Tukey's Multiple Comparison post-hoc test. No significant changes were seen in the glutathione reductase activity in either liver or kidney of the animals across the groups.

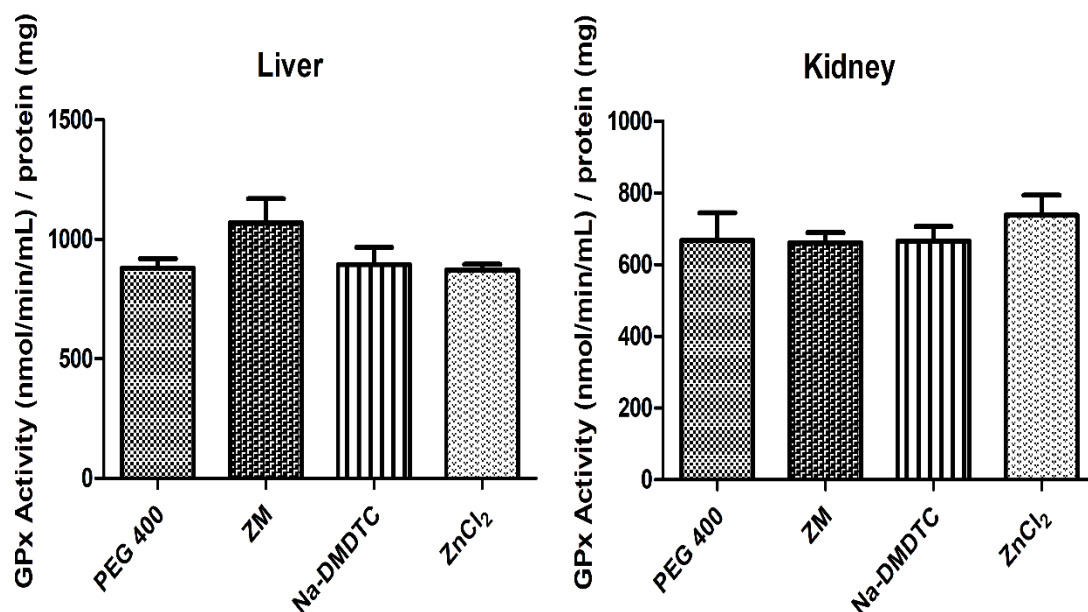


Figure 9. Glutathione Peroxidase Activity (nmol/min/mL)/Protein (mg)

The glutathione peroxidase activity in the liver and kidney after 6 weeks of oral treatment with either vehicle control (PEG 400), 100 mg/kg ZM, 94 mg/kg Na-DMDTC, or 45 mg/kg ZnCl₂ (n = 6 per group). Glutathione peroxidase activity is determined by measuring the decrease in absorption at 340 nm due to the oxidation of NADPH to NADP⁺ facilitated by glutathione reductase. The decrease in absorbance is directly proportional to the GPx activity in the samples when GPx is the rate limiting enzyme. GPx activity was then normalized to the protein concentration of the sample. Values represent mean ± SEM and were analyzed using a one-way ANOVA followed by Tukey's Multiple Comparison post-hoc test. No significant changes were seen in the glutathione peroxidase activity in either liver or kidney of the animals across the groups.

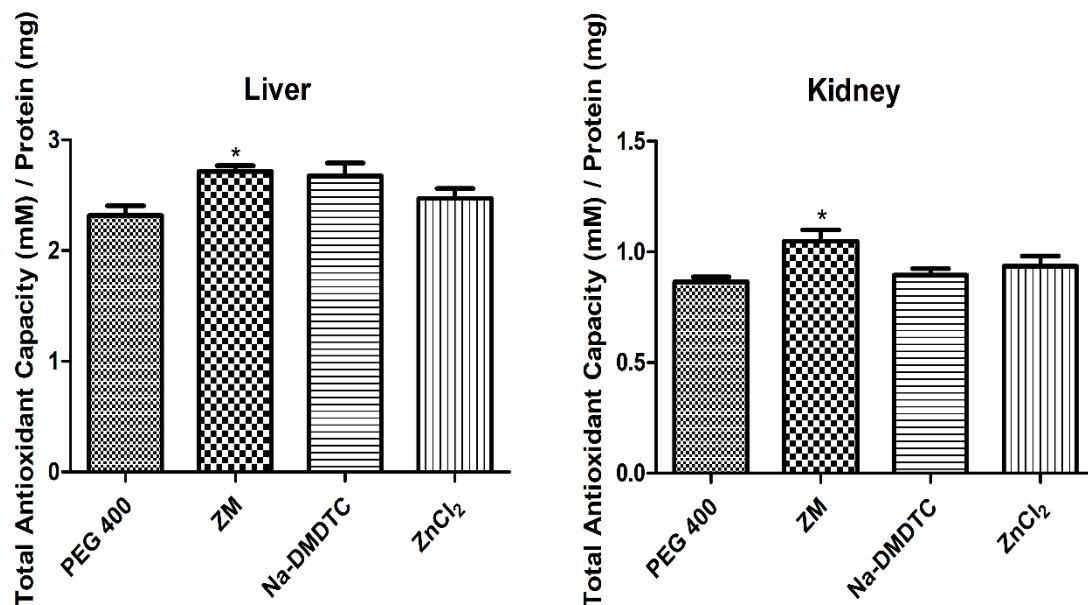


Figure 10. Total Antioxidant Levels (mM)/Protein (mg)

The total antioxidant levels in the liver and kidney after 6 weeks of oral treatment with either vehicle control (PEG 400), 100 mg/kg ZM, 94 mg/kg Na-DMDTC, or 45 mg/kg ZnCl₂ (n = 6 per group). The total antioxidant levels were determined by measuring the production of ABTS^{®+•}, which is inversely proportional to the total antioxidant levels in the sample, as a higher level of antioxidants will suppress the production of ABTS^{®+•}. The total antioxidant levels were quantified as mM Trolox equivalents normalized by the protein content in the sample. Values represent mean ± SEM and were analyzed using a one-way ANOVA followed by Tukey's Multiple Comparison post-hoc test. A significant increase in total antioxidant levels were seen in the animals treated with ZM in both the liver and the kidneys as compared to the control. *: $p < 0.05$ (compared to vehicle control)

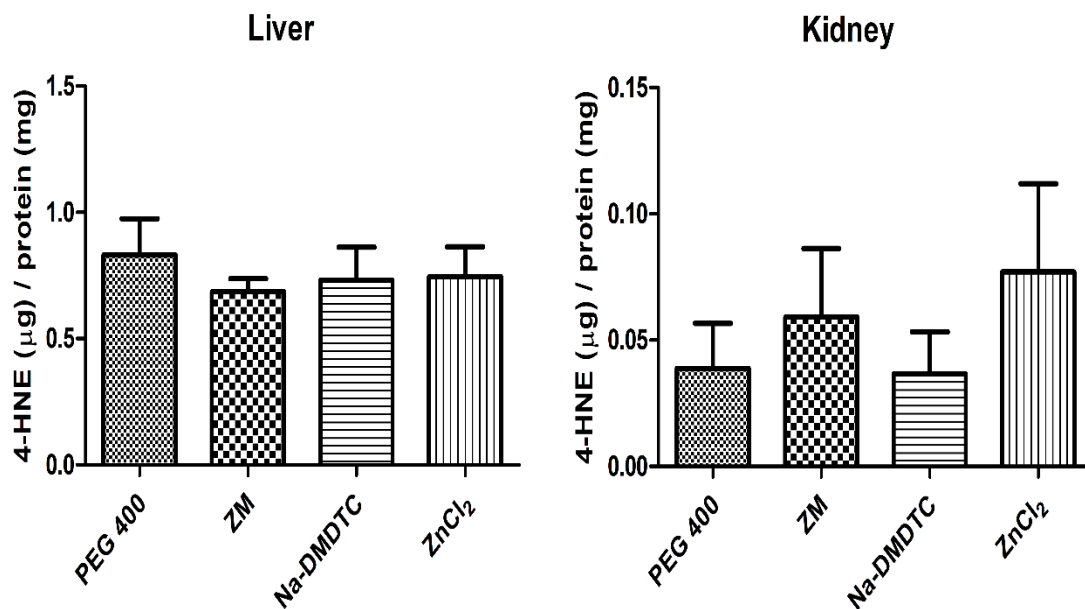


Figure 11. 4-Hydroxynonenol (4-HNE) (μg)/Protein (mg)

The 4-HNE levels in the liver and kidney after 6 weeks of oral treatment with either vehicle control (PEG 400), 100 mg/kg ZM, 94 mg/kg Na-DMDTC, or 45 mg/kg ZnCl₂ (n = 6 per group). The 4-HNE levels were measured using an ELISA detection kit. 4-HNE levels were normalized by the protein content in the sample. Values represent mean ± SEM and were analyzed using a one-way ANOVA followed by Tukey's Multiple Comparison post-hoc test. No significant changes were seen in the 4-HNE levels in either liver or kidney of the animals across the groups.

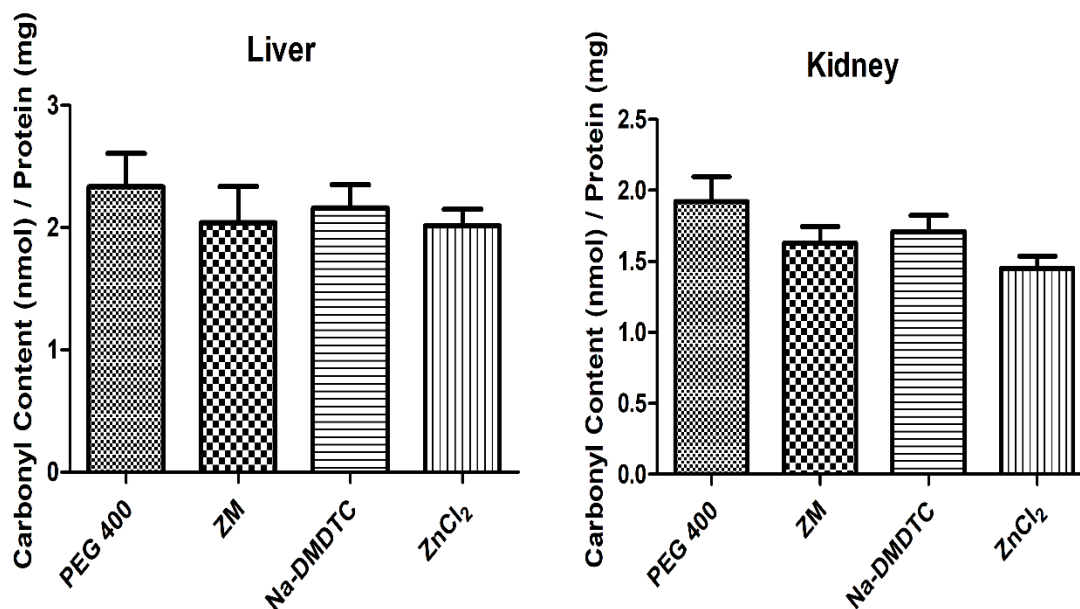


Figure 12. Protein Carbonyls (nmol)/Protein (mg)

The protein carbonyls content in the liver and kidney after 6 weeks of oral treatment with either vehicle control (PEG 400), 100 mg/kg ZM, 94 mg/kg Na-DMDTC, or 45 mg/kg ZnCl₂ (n = 6 per group). Protein carbonyl content was measured at 370 nm and normalized by the protein content in the sample. Values represent mean \pm SEM and were analyzed using a one-way ANOVA followed by Tukey's Multiple Comparison post-hoc test. No significant changes were seen in the protein carbonyl content in either liver or kidney of the animals across the groups.

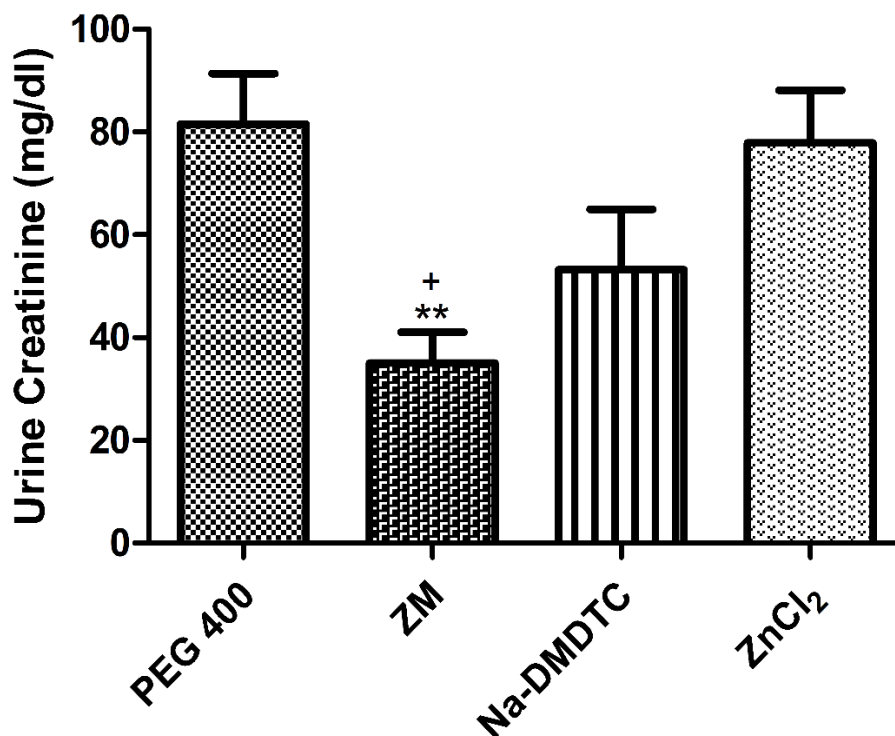


Figure 13. Urine Creatinine (mg/dL)

The urine creatinine levels of animals after 6 weeks of oral treatment with either vehicle control (PEG 400), 100 mg/kg ZM, 94 mg/kg Na-DMDTC, or 45 mg/kg ZnCl₂ (n=9 for ZM, n=8 for all other groups). Urine creatinine was measured utilizing the Jaffe's reaction and read at 490 nm. Values represent mean ± SEM and were analyzed using a one-way ANOVA followed by Tukey's Multiple Comparison post-hoc test. Significantly decreased levels of urine creatinine were seen in the ZM treatment group as compared to control and ZnCl₂ treatment group. **: $p < 0.01$ (compared to vehicle control); +: $p < 0.05$ (compared to ZnCl₂).

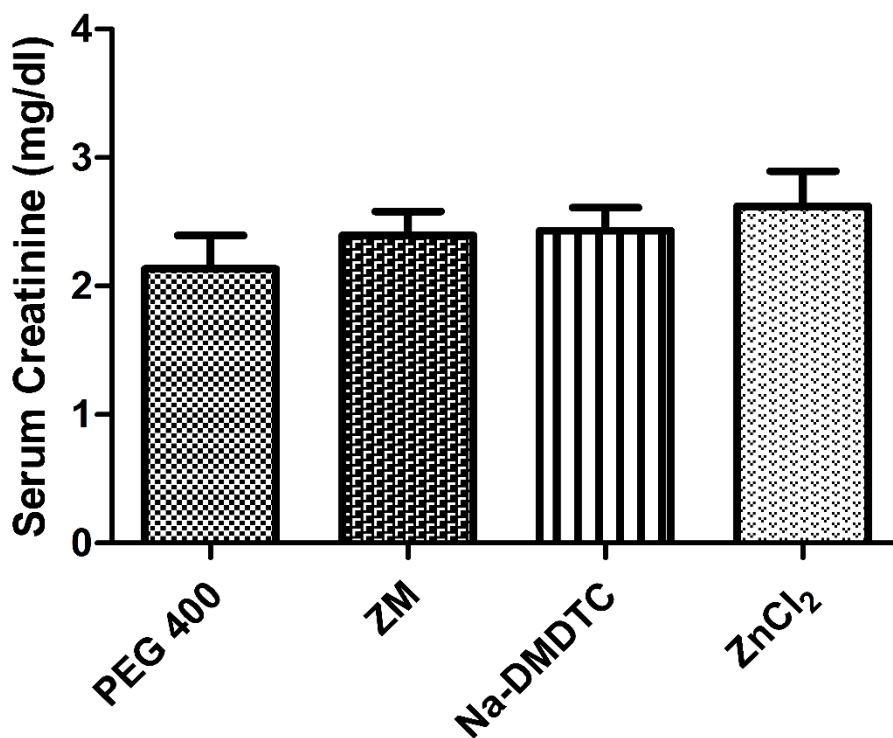


Figure 14. Serum Creatinine (mg/dL)

The serum creatinine levels of animals after 6 weeks of oral treatment with either vehicle control (PEG 400), 100 mg/kg ZM, 94 mg/kg Na-DMDTC, or 45 mg/kg ZnCl₂ (n=9 for ZM, n=8 for all other groups). Serum creatinine was measured utilizing the Jaffe's reaction and read at 490 nm. Values represent mean \pm SEM and were analyzed using a one-way ANOVA followed by Tukey's Multiple Comparison post-hoc test. No significant changes were seen in the serum creatinine levels in the animals across the groups.

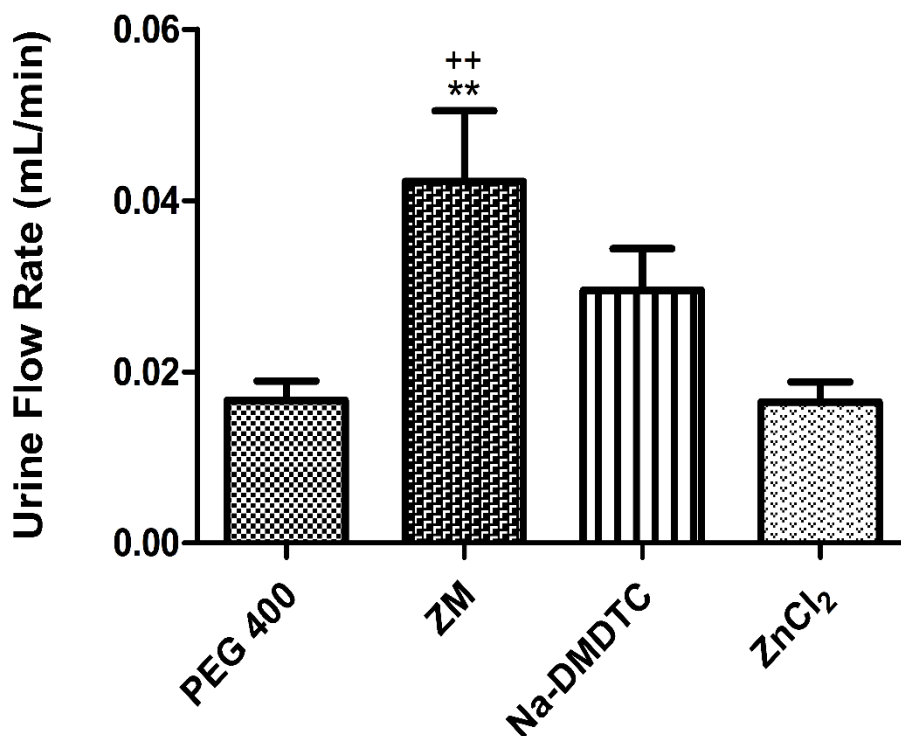


Figure 15. Urine Flow Rate (mL/min)

The urine flow rate of animals after 6 weeks of oral treatment with either vehicle control (PEG 400), 100 mg/kg ZM, 94 mg/kg Na-DMDTC, or 45 mg/kg ZnCl₂ (n=9 for ZM, n=8 for all other groups). Urine flow rates were calculated by dividing the 14 hours of urine volume by 840, which equates to the number of minutes in 14 hours (14 hours x 60 min = 840). Urine flow rate (mL/min) = value of urine volume (mL in 24h)/840. Values represent mean \pm SEM and were analyzed using a one-way ANOVA followed by Tukey's Multiple Comparison post-hoc test. A significant increase in urine flow rate was seen in the ZM treatment group as compared to control and ZnCl₂ treatment group. **: $p < 0.01$ (compared to vehicle control); ++: $p < 0.01$ (compared to ZnCl₂).

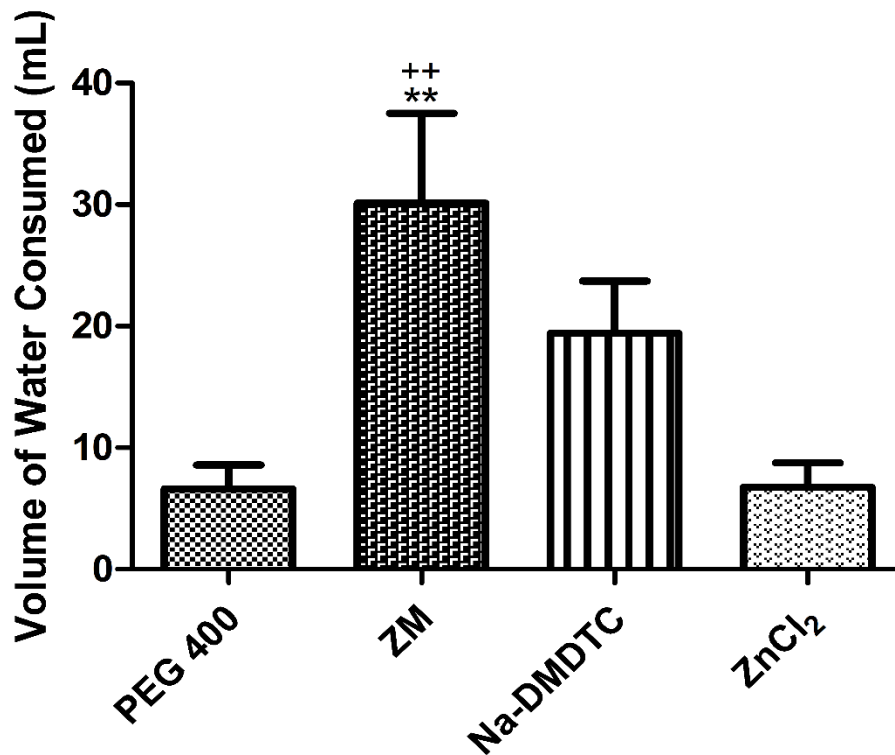


Figure 16. Total Water Consumption in 14 Hours (mL)

The total water consumption over 14 hours of animals after 6 weeks of oral treatment with either vehicle control (PEG 400), 100 mg/kg ZM, 94 mg/kg Na-DMDTC, or 45 mg/kg ZnCl₂ (n=9 for ZM, n=8 for all other groups). Total water consumption of animals was measured by placing animals in metabolism cages for 14 hours, provided with 100 mL of water. After the 14 hours, the remaining amount of water was subtracted from 100 mL of water to find the amount of water consumed. Values represent mean \pm SEM and were analyzed using a one-way ANOVA followed by Tukey's Multiple Comparison post-hoc test. A significant increase in total water consumption was seen in the ZM treatment group as compared to control and ZnCl₂ treatment group. **: $p < 0.01$ (compared to vehicle control); ++: $p < 0.01$ (compared to ZnCl₂).

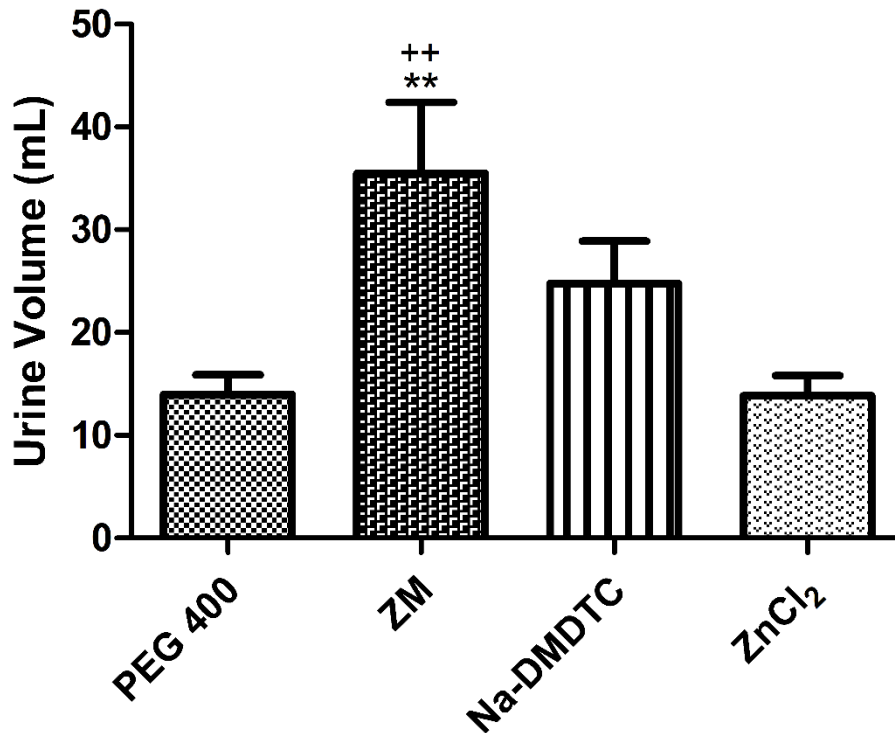


Figure 17. Urine Volume Production in 14 Hours

The urine production in 14 hours of animals after 6 weeks of oral treatment with either vehicle control (PEG 400), 100 mg/kg ZM, 94 mg/kg Na-DMDTC, or 45 mg/kg ZnCl₂ (n=9 for ZM, n=8 for all other groups). The urine volume production of animals was measured by placing animals in metabolism cages for 14 hours and collecting the urine in a 50 mL tube. After 14 hours, the volume of urine was measured. Values represent mean ± SEM and were analyzed using a one-way ANOVA followed by Tukey's Multiple Comparison post-hoc test. A significant increase in urine volume was seen in the ZM treatment group as compared to control and ZnCl₂ treatment group. **: $p < 0.01$ (compared to vehicle control); ++: $p < 0.01$ (compared to ZnCl₂).

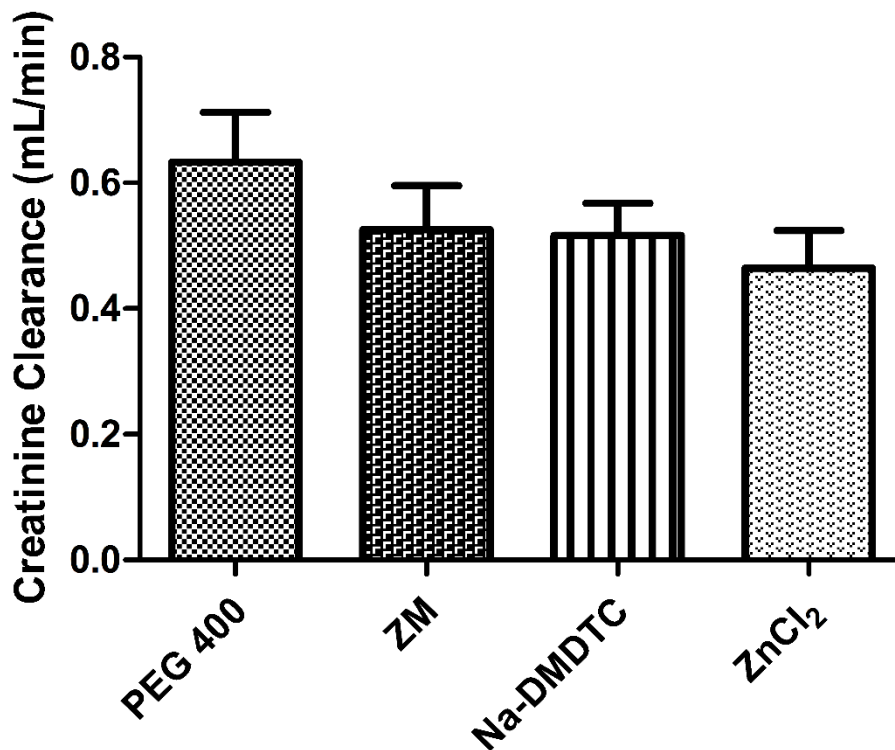


Figure 18. Creatinine Clearance (mL/min)

The creatinine clearance of animals after 6 weeks of oral treatment with either vehicle control (PEG 400), 100 mg/kg ZM, 94 mg/kg Na-DMDTC, or 45 mg/kg ZnCl₂ (n=9 for ZM, n=8 for all other groups). Creatinine clearance was calculated using the formula: $\text{Clcr} = \text{urine creatine (mg/dL)} \times \text{urine flow rate (mL/min)} / \text{serum creatinine (mg/dL)}$. Values represent mean \pm SEM and were analyzed using a one-way ANOVA followed by Tukey's Multiple Comparison post-hoc test. No significant changes were seen in the creatinine clearance rates in the animals across the groups.

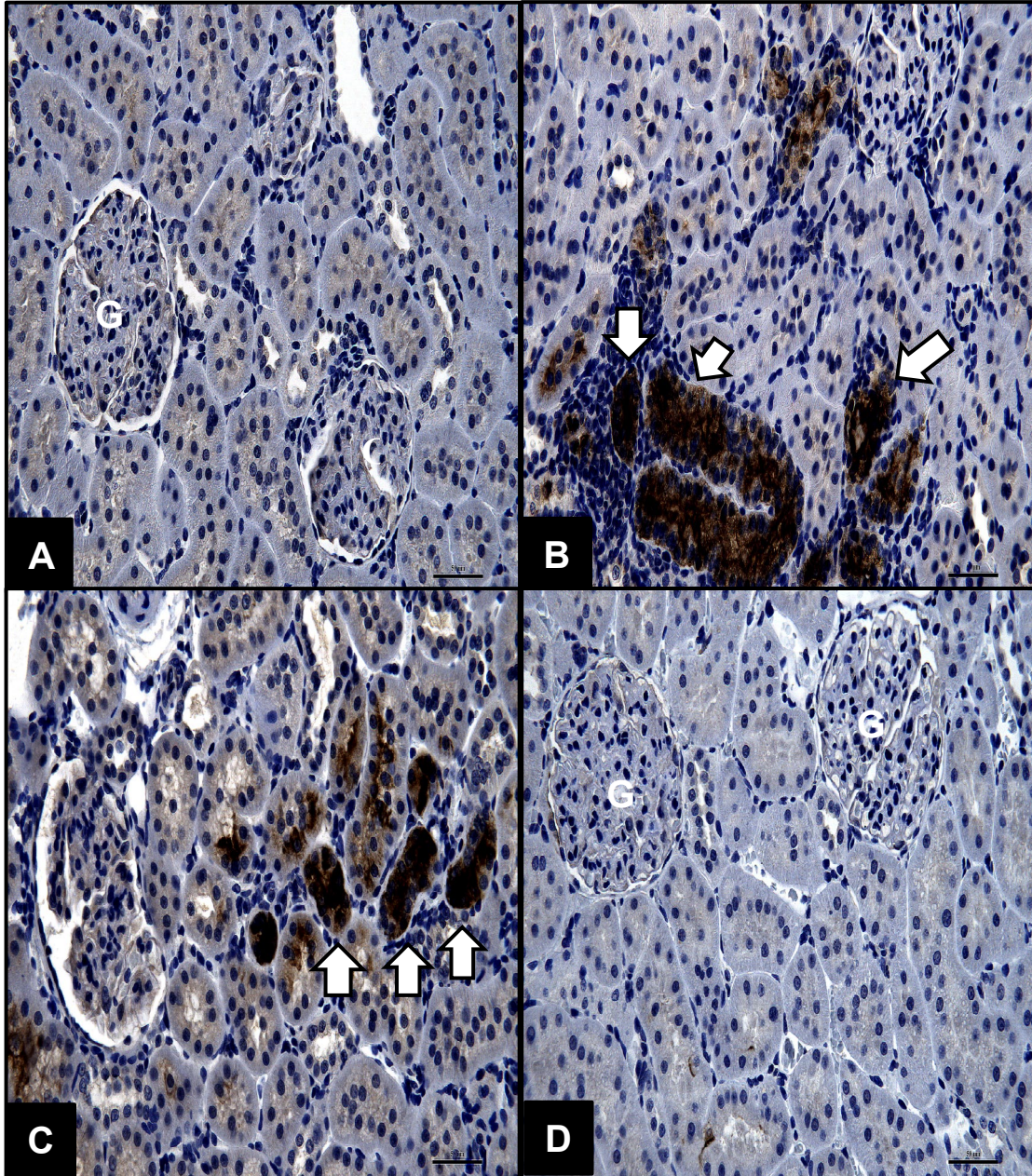


Figure 19. Immunohistochemical Staining for KIM-1, Objective x40

Light micrographs of kidney sections immunohistochemically stained for KIM-1 (Objective magnification x40) after 6 weeks of oral treatment with either vehicle control (PEG 400) (A), 100 mg/kg ZM (B), 94 mg/kg Na-DMDTC (C), or 45 mg/kg ZnCl₂ (D). Unremarkable glomeruli and undisrupted tubule cells, exhibiting basal levels of KIM-1 immunoreactivity are present in the control (A). Increased presence of KIM-1 immunoreactivity in the tubular region of animals treated with ZM (B) and Na-DMDTC (C) are seen and indicated by the white arrows. Immunoreactivity of KIM-1 in animals treated with ZnCl₂ (D) is comparable to that of control. The glomeruli are denoted with the letter (G). Scale bar = 50 μm

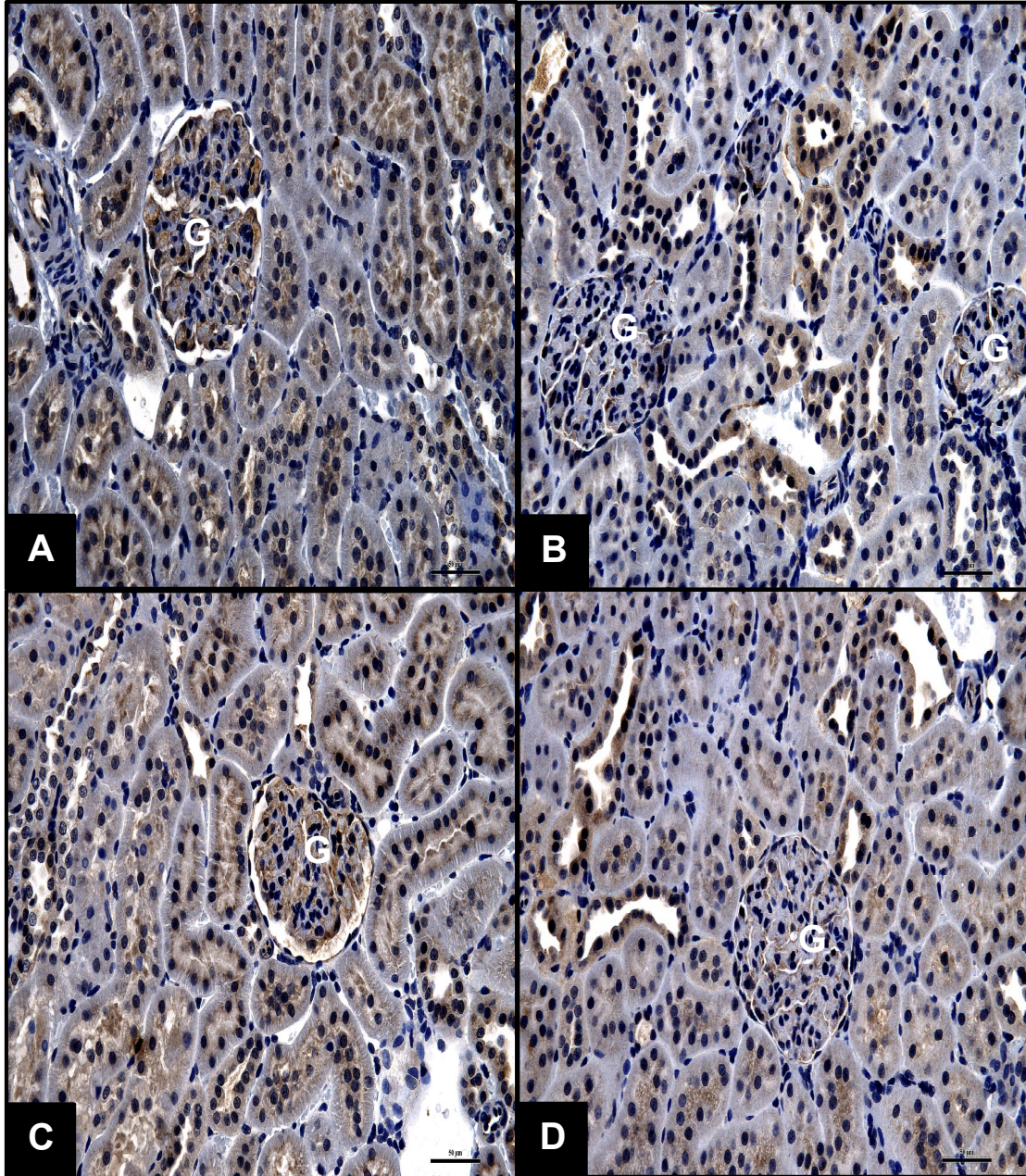


Figure 20. Immunohistochemical Staining for NGAL, Objective x40

Light micrographs of kidney sections immunohistochemically stained for NGAL (Objective magnification x40) after 6 weeks of oral treatment with either vehicle control (PEG 400) (A), 100 mg/kg ZM (B), 94 mg/kg Na-DMDTC (C), or 45 mg/kg ZnCl₂ (D). Unremarkable glomeruli and undisrupted tubule cells, exhibiting basal levels of NGAL immunoreactivity are present in the control (A). Basal levels of NGAL immunoreactivity comparable to that of control are seen in all treatment groups (B, C, &D). The glomeruli are denoted with the letter (G). Scale bar = 50 μ m.

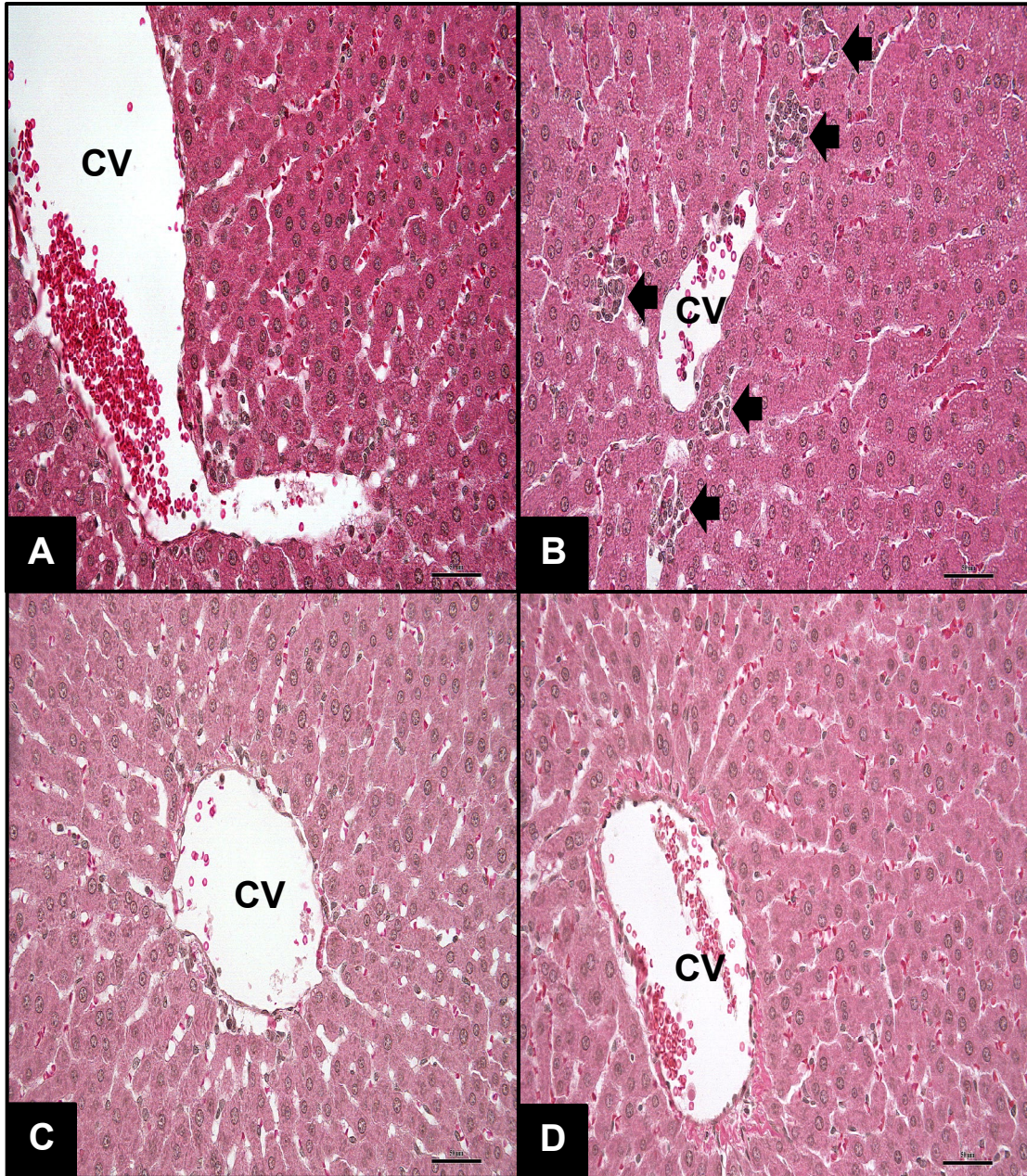


Figure 21. Liver Histology: Hematoxylin and Eosin Staining

Light micrographs of liver sections stained with hematoxylin and eosin (Objective magnification x40) after 6 weeks of oral treatment with either vehicle control (PEG 400) (A), 100 mg/kg ZM (B), 94 mg/kg Na-DMDTC (C), or 45 mg/kg ZnCl₂ (D). Regular arrangements of hepatocytes and sinusoids are seen, and cells appear to maintain their normal morphology with no obvious alterations in the control (A), Na-DMDTC (C), and ZnCl₂ (D) treatment group. Increased presence of infiltration near the central veins in the ZM (B) treatment group are noted and are indicated by the black arrows. Central veins (CV) are labelled in the figures. Scale bar = 50 µm.

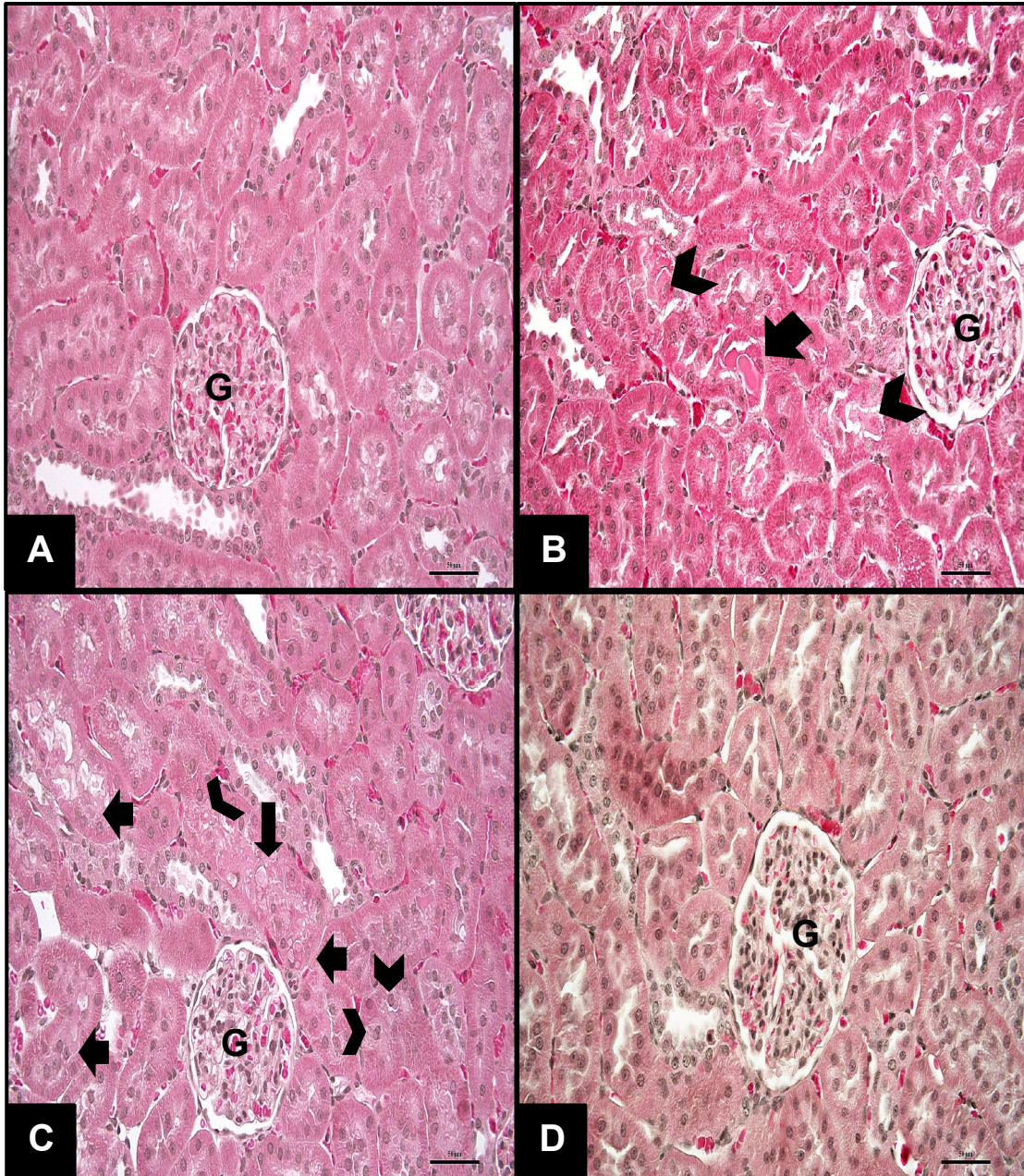


Figure 22. Kidney Histology: Hematoxylin and Eosin Staining

Light micrographs of kidney sections stained with hematoxylin and eosin (Objective magnification x40) after 6 weeks of oral treatment with either vehicle control (PEG 400) (A), 100 mg/kg ZM (B), 94 mg/kg Na-DMDTC (C), or 45 mg/kg ZnCl₂ (D). Unremarkable glomeruli and undisrupted tubule cells are present in the control (A) and ZnCl₂ (D) treatment group. The presence of protein aggregation (arrow) and sloughing of tubular cells (arrowhead) are noted in the ZM (B) and Na-DMDTC (C) treatment groups. Glomeruli (G) are labelled in the figures. Scale bar = 50 μm.

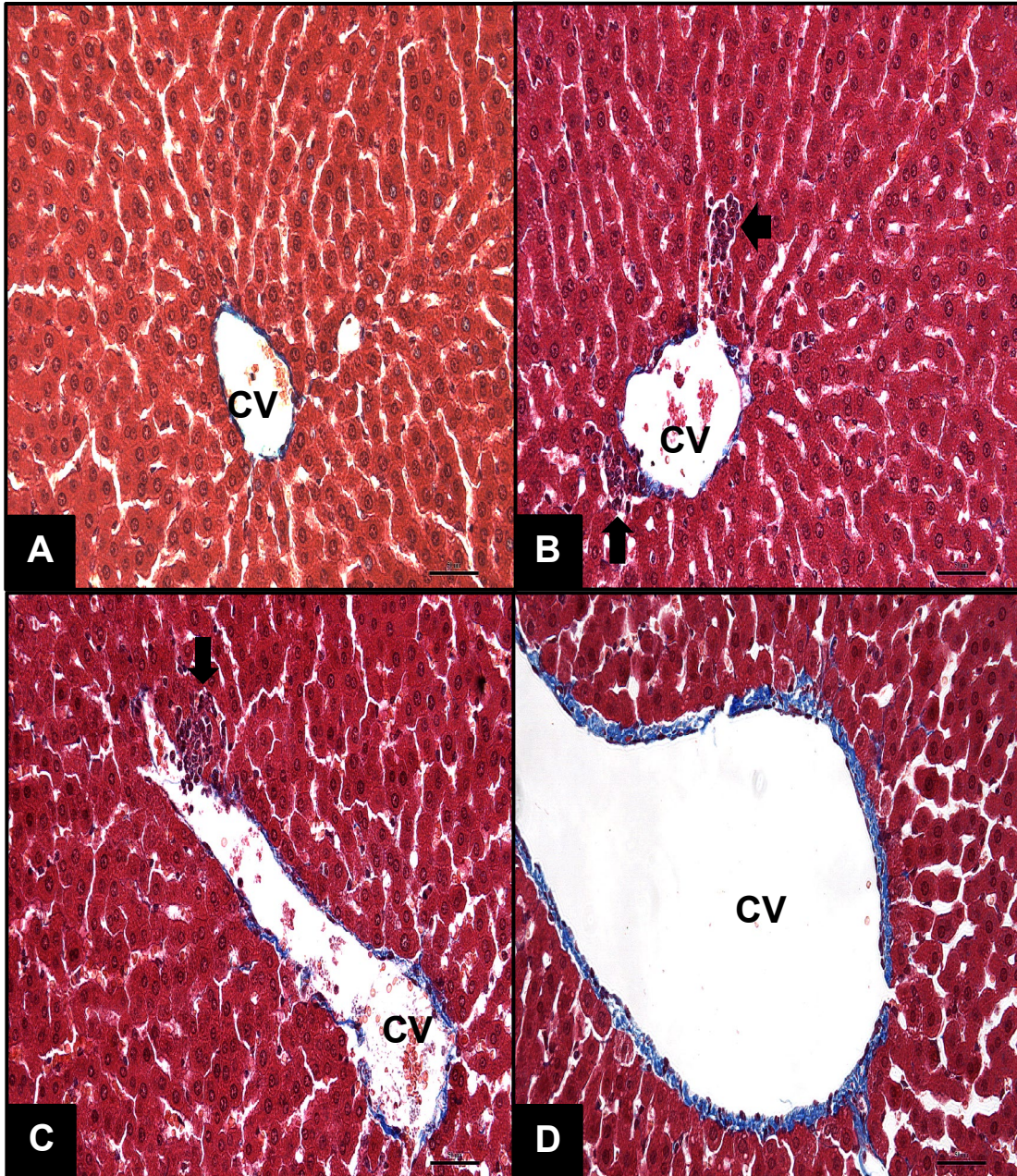


Figure 23. Liver Histology: Masson's Trichrome Staining

Light micrographs of liver sections stained with Masson's Trichrome (Objective magnification x40) after 6 weeks of oral treatment with either vehicle control (PEG 400) (A), 100 mg/kg ZM (B), 94 mg/kg Na-DMDTC (C), or 45 mg/kg ZnCl₂ (D). Regular arrangements of hepatocytes and sinusoids are seen, and cells appear to maintain their normal morphology with no obvious alterations in the control (A) and ZnCl₂ (D) treatment group. Increased presence of infiltration near the central veins in the ZM (B) and Na-DMDTC (C) treatment groups are noted and are indicated by the black arrows, however, extracellular matrix deposition across the treatment groups appears unremarkable and comparable to that of control animals. Central veins (CV) are labelled in the figures. Scale bar = 50 μm.

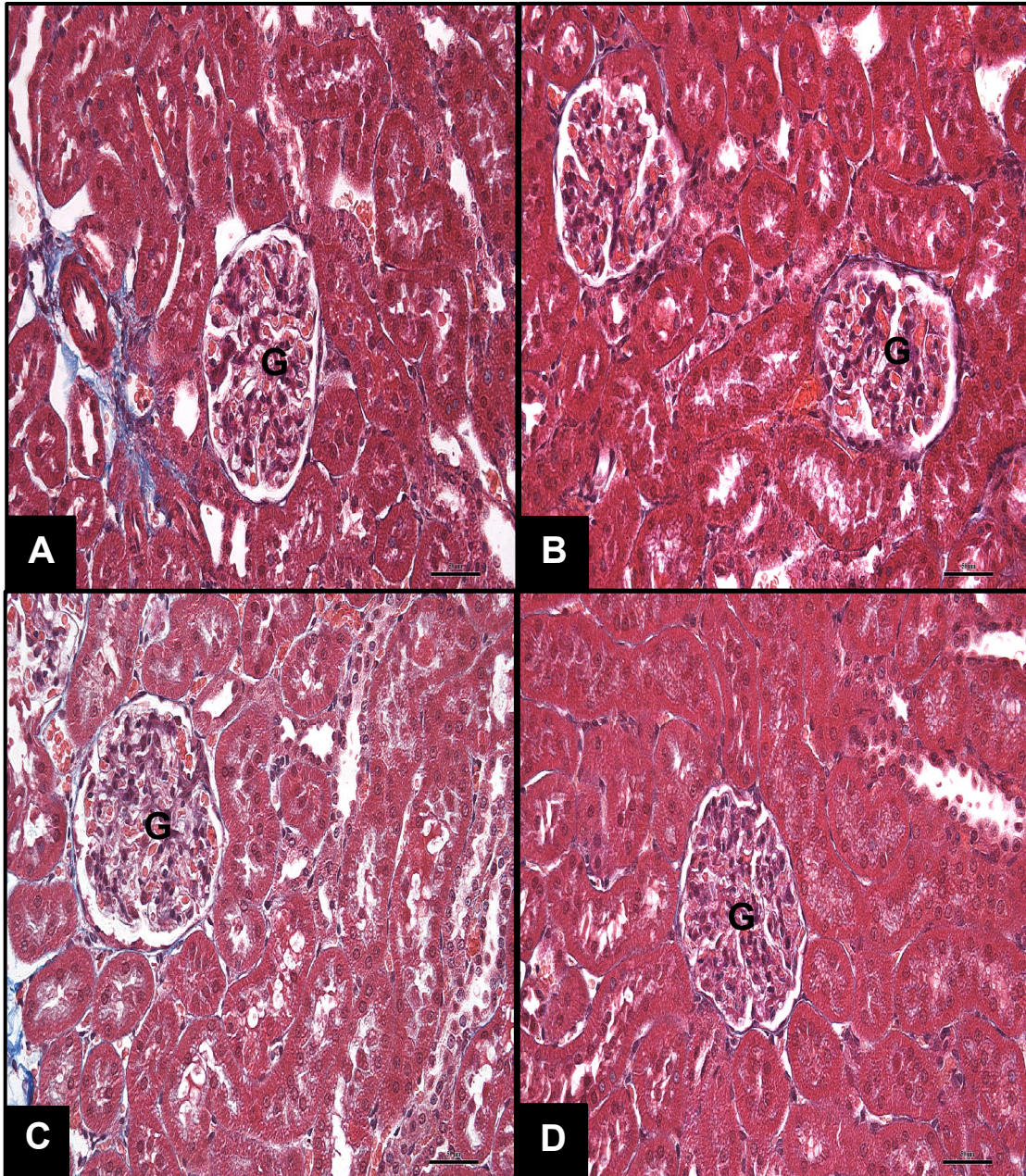


Figure 24. Kidney Histology: Masson's Trichrome Staining

Light micrographs of kidney sections stained with Masson's Trichrome (Objective magnification x40) after 6 weeks of oral treatment with either vehicle control (PEG 400) (A), 100 mg/kg ZM (B), 94 mg/kg Na-DMDTC (C), or 45 mg/kg ZnCl₂ (D). Unremarkable glomeruli and undisrupted tubule cells are present in the control with unremarkable levels of extracellular matrix deposition (A). Extracellular matrix deposition across the treatment groups (B, C, & D) appears unremarkable and comparable to that of control animals. Glomeruli (G) are labelled in the figures. Scale bar = 50 µm.

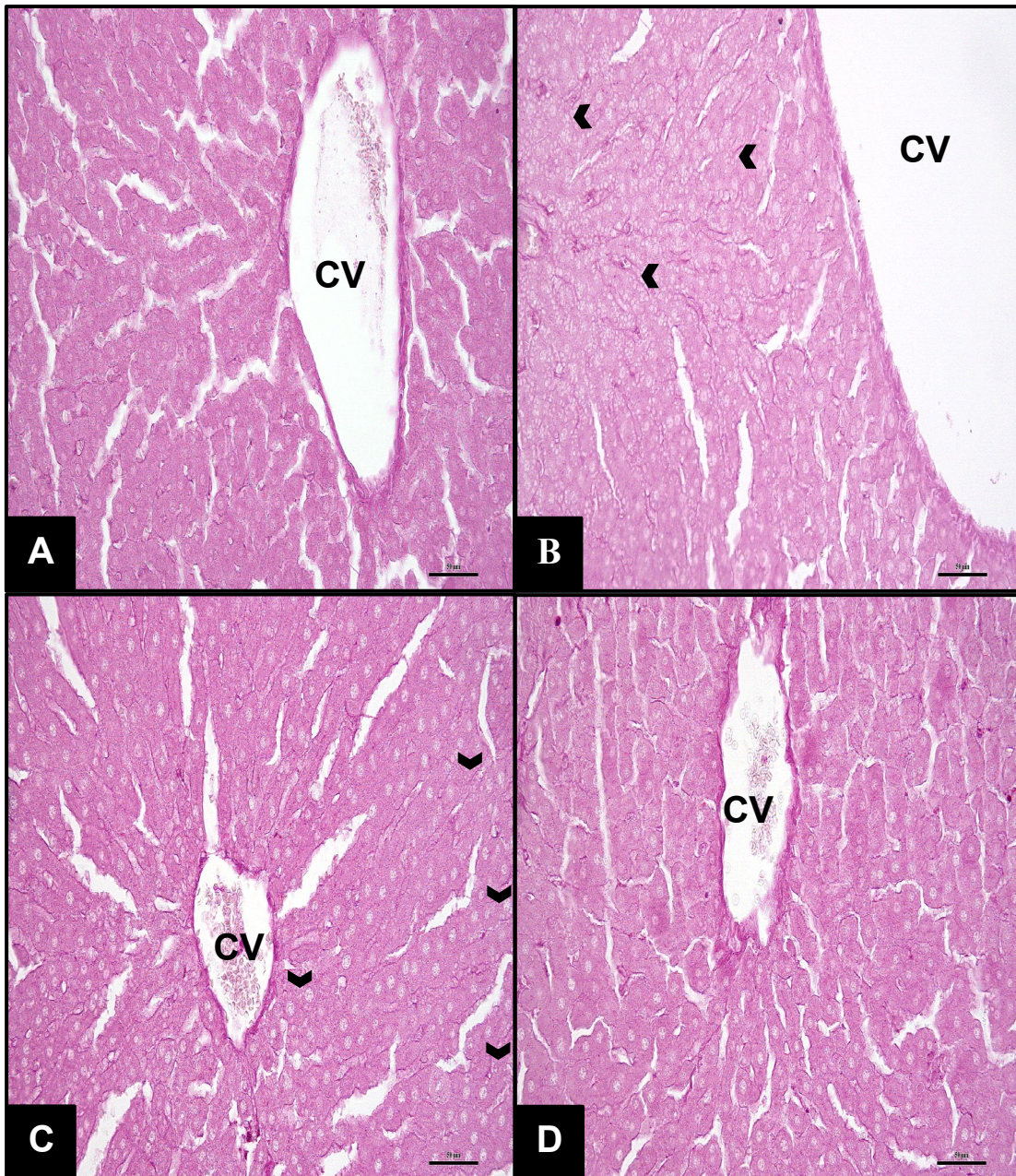


Figure 25. Liver Histology: P.A.S Staining with Diastase Digestion

Light micrographs of liver sections digested with diastase and stained with P.A.S staining (Objective magnification x40) after 6 weeks of oral treatment with either vehicle control (PEG 400) (A), 100 mg/kg ZM (B), 94 mg/kg Na-DMDTC (C), or 45 mg/kg ZnCl₂ (D). Regular arrangements of hepatocytes and sinusoids are seen, and cells appear to maintain their normal morphology with no obvious alterations in the control (A) and ZnCl₂ (D) treatment groups. The presence of vacuolation in hepatocytes are seen in the ZM (B) and Na-DMDTC (C) treated animals and are indicated by the arrowheads. Central veins (CV) are labelled in the figures. Scale bar = 50 µm.

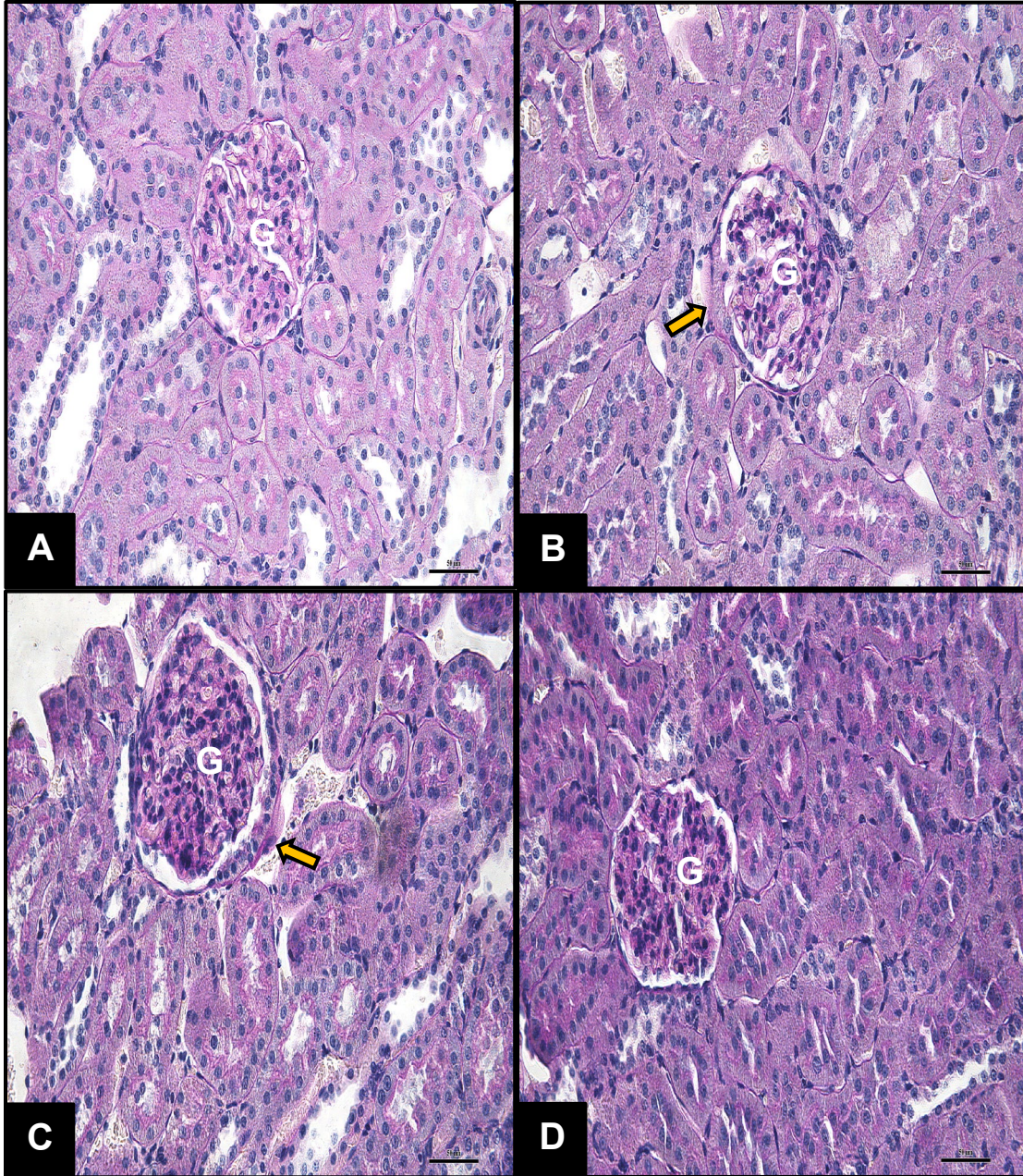


Figure 26. Kidney Histology: P.A.S Staining without Diastase Digestion

Light micrographs of kidney sections stained with P.A.S Staining (Objective magnification x40) after 6 weeks of oral treatment with either vehicle control (PEG 400) (A), 100 mg/kg ZM (B), 94 mg/kg Na-DMDTC (C), or 45 mg/kg ZnCl₂ (D). Unremarkable glomeruli and undisrupted tubule cells are present in the control (A) and ZnCl₂ (D) treatment groups. Thickening of the Bowman's Capsule is seen in the ZM (B) and Na-DMDTC (C) treatment group and are indicated by the orange arrows. Glomeruli (G) are labelled in the figures. Scale bar = 50 µm.

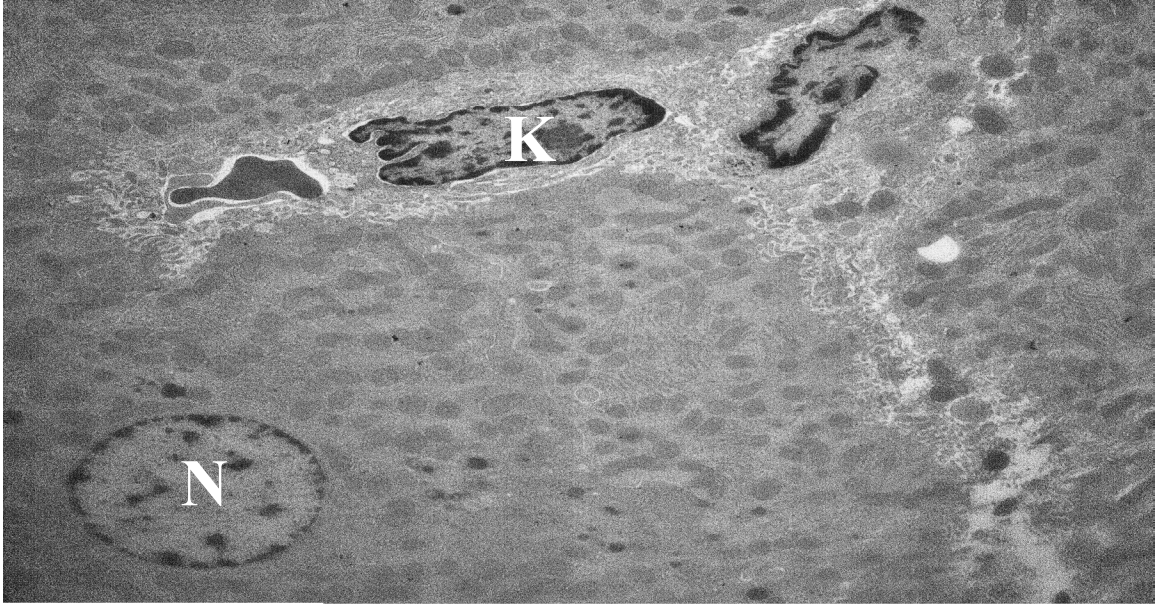


Fig 27. Panel A

2 μ m
Direct Mag: 5000x

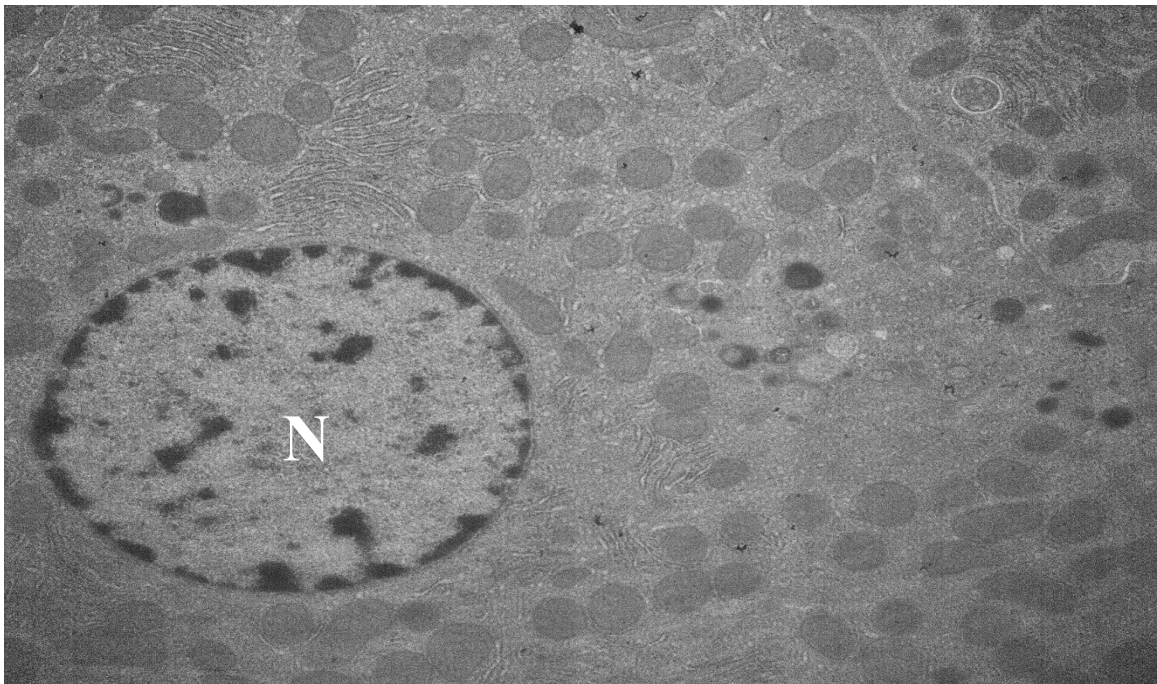


Fig 27. Panel B

500 nm
Direct Mag: 10000x

Figure 27. Liver TEM – Control

Transmission electron micrographs of liver sections after 6 weeks of oral treatment with vehicle control (PEG 400) (Panel A&B). Low magnification image (A) = 5000X. High magnification image (B) = 10,000X. Nuclei (N) and Kupffer (K) are labelled in the figures if present. Liver sections of control animals (A&B) demonstrate unremarkable hepatocytes, with the presence of Kupffer cells in the sinusoids and defined cellular features such as a nucleus with a nuclear envelope, and mitochondria with cristae.

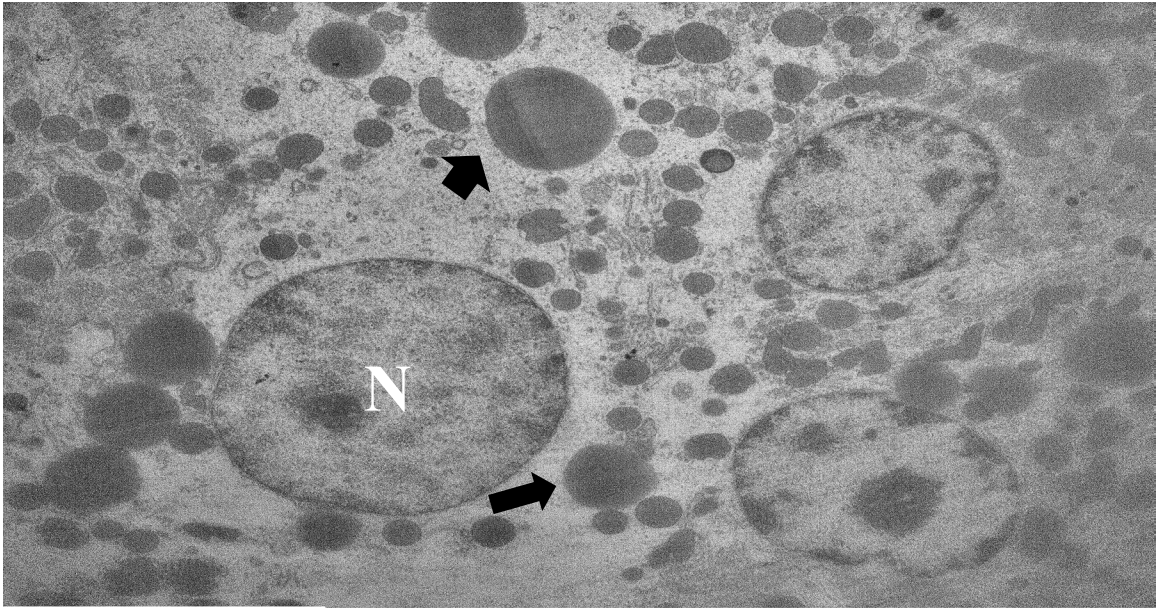


Fig 28. Panel A

2 μ m
Direct Mag: 5000x

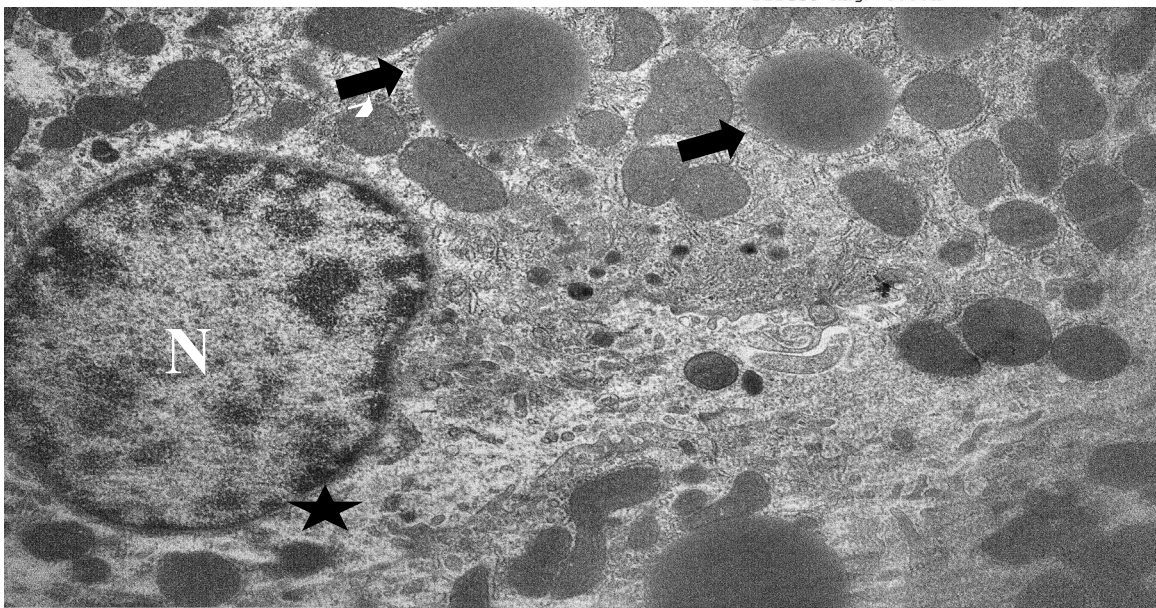


Fig 28. Panel B

500 nm
Direct Mag: 10000x

Figure 28. Liver TEM – ZM

Transmission electron micrographs of liver sections after 6 weeks of oral treatment with 100 mg/kg ZM (Panel A&B). Low magnification image (A) = 5000X. High magnification image (B) = 10,000X. Liver sections of ZM treated animals show the presence of lipid deposition (arrow) and cellular edema (star),

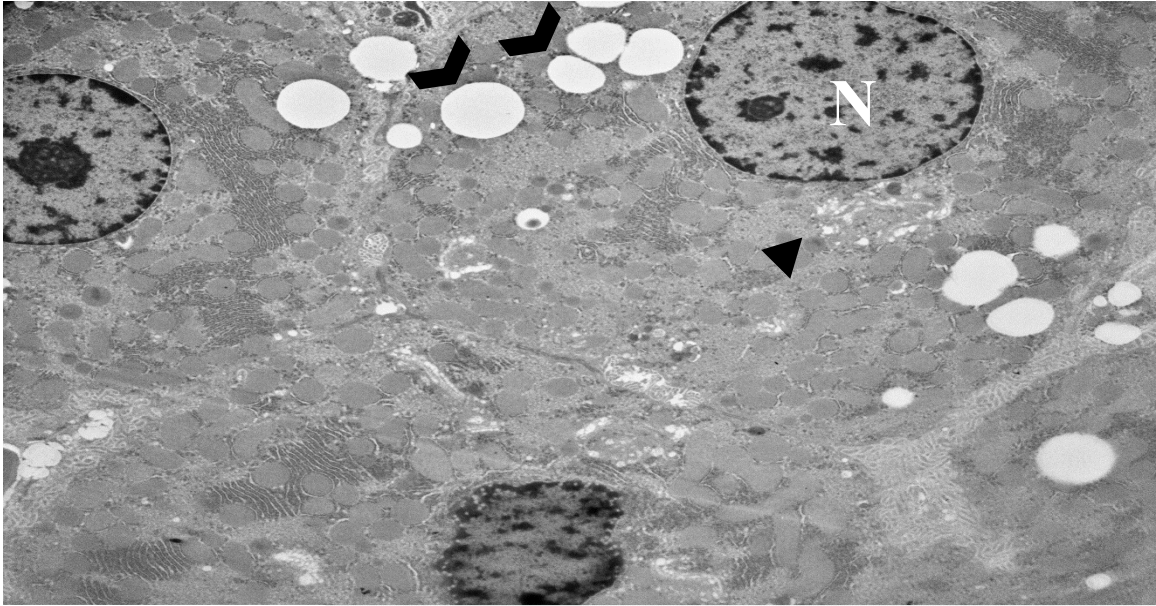


Fig 29. Panel A

2 μ m
Direct Mag: 5000x

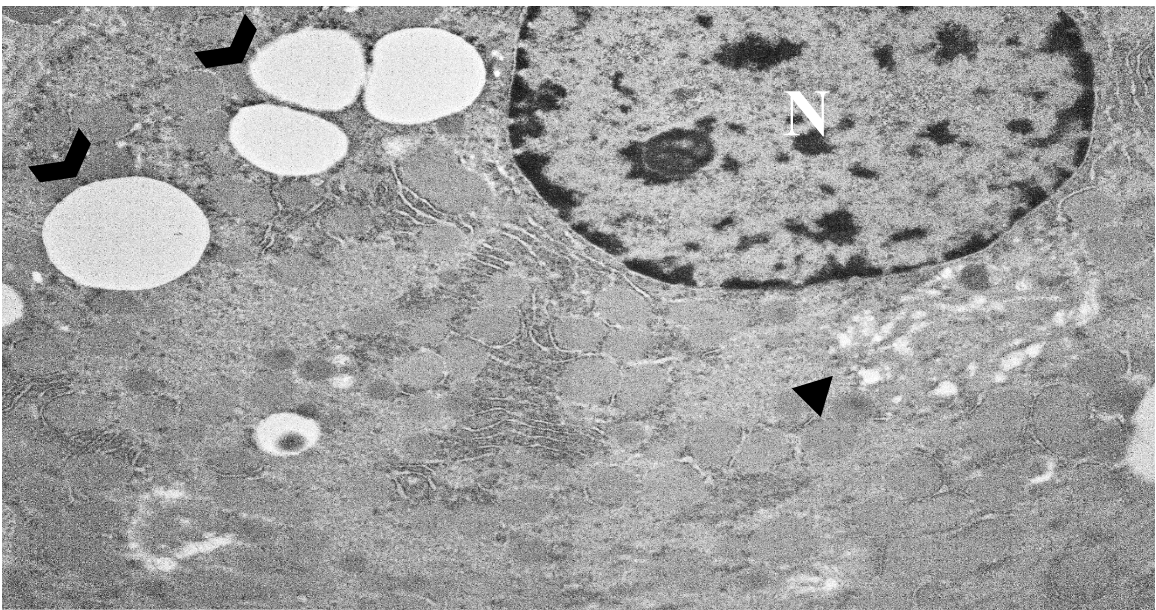


Fig 29. Panel B

500 nm
Direct Mag: 10000x

Figure 29. Liver TEM – Na-DMDTC

Transmission electron micrographs of liver sections after 6 weeks of oral treatment with 94 mg/kg Na-DMDTC (Panel A&B). Low magnification image (A) = 5000X. High magnification image (B) = 10,000X. Liver sections of Na-DMDTC treated animals show the presence of vacuolization (arrowhead) and swelling of the endoplasmic reticulum (black triangle).

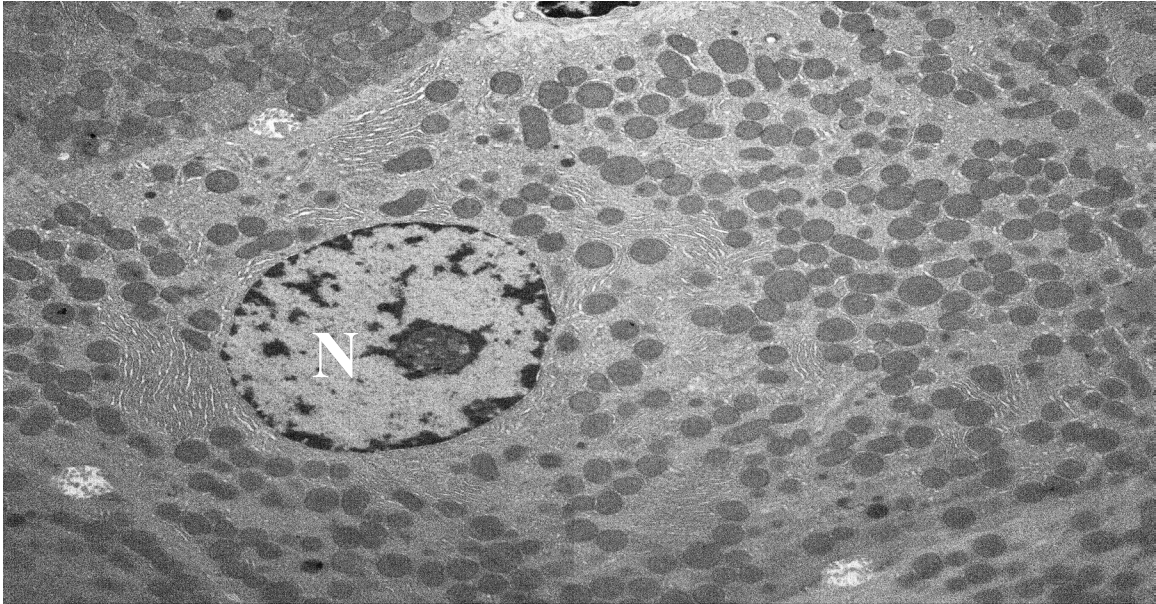


Fig 30. Panel A

2 μ m
Direct Mag: 5000x

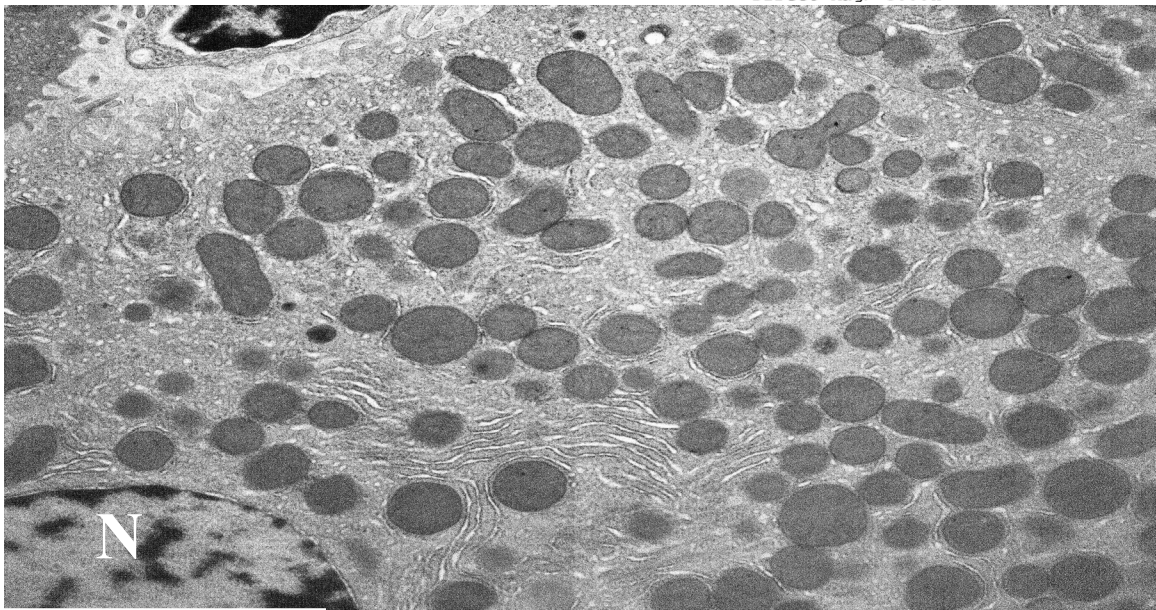


Fig 30. Panel B

500 nm
Direct Mag: 10000x

Figure 30. Liver TEM – ZnCl₂

Transmission electron micrographs of liver sections after 6 weeks of oral treatment with 94 mg/kg Na-DMDTC (Panel A&B). Low magnification image (A) = 5000X. High magnification image (B) = 10,000X. Hepatocytes of animals treated with ZnCl₂ appear unremarkable and comparable to that of control animals.

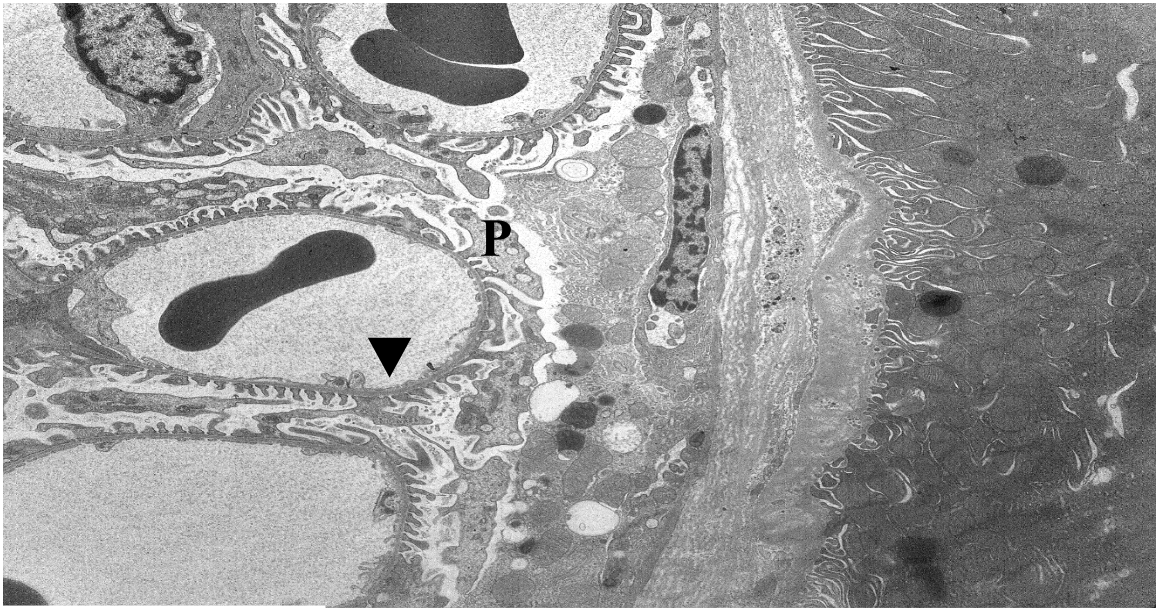


Fig 31. Panel A

2 μ m
Direct Mag: 5000x

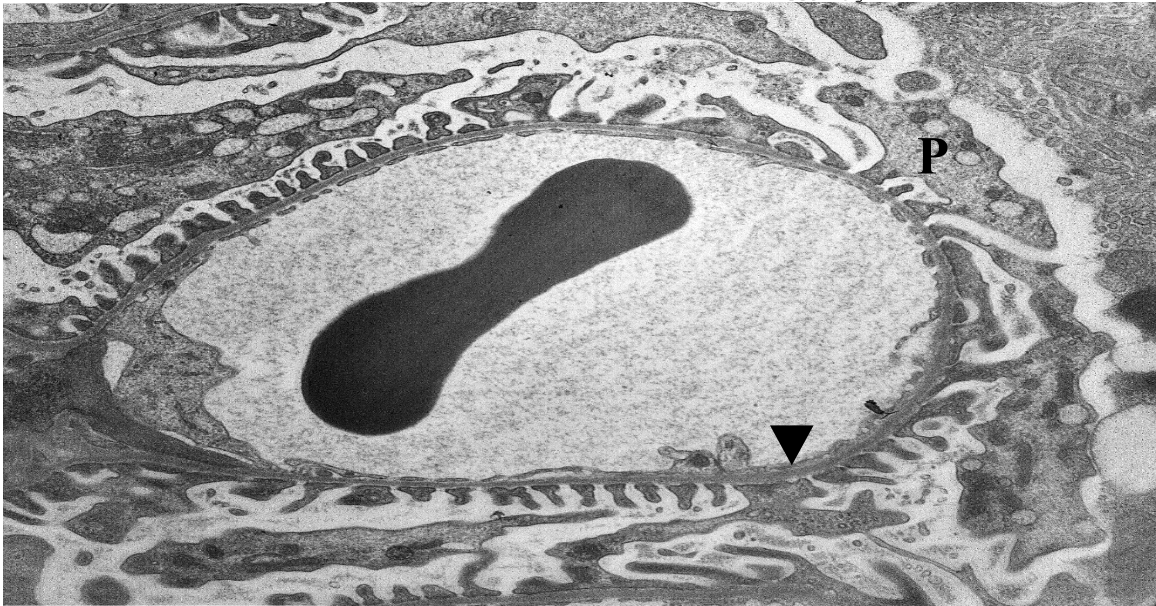


Fig 31. Panel B

500 nm
Direct Mag: 10000x

Figure 31. Kidney TEM - Glomerulus - Control

Transmission electron micrographs of kidney sections, specifically the glomerulus, after 6 weeks of oral treatment with vehicle control (PEG 400) (Panel A&B), Low magnification images (A) = 5000X. High magnification images (B) = 10,000X. Kidney sections of control animals demonstrate unremarkable glomerular structure, with the presence of podocytes (P), podocyte foot processes, and capillary loops (black triangle).

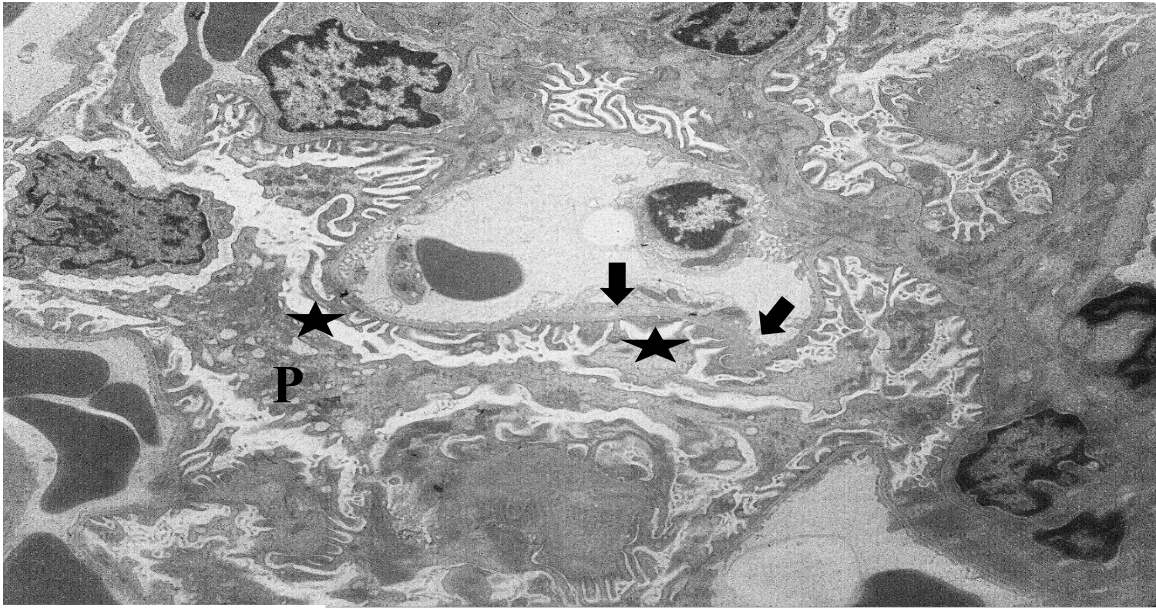


Fig 32. Panel A

2 μ m
Direct Mag: 5000x



Fig 32. Panel B

500 nm
Direct Mag: 10000x

Figure 32. Kidney TEM - Glomerulus - ZM

Transmission electron micrographs of kidney sections, specifically the glomerulus, after 6 weeks of oral treatment with 100 mg/kg ZM (Panel A&B), Low magnification images (A) = 5000X. High magnification images (B) = 10,000X. Animals treated with ZM demonstrate fusion of podocytes (star), accompanied by a thickening of the basement membrane (arrow).

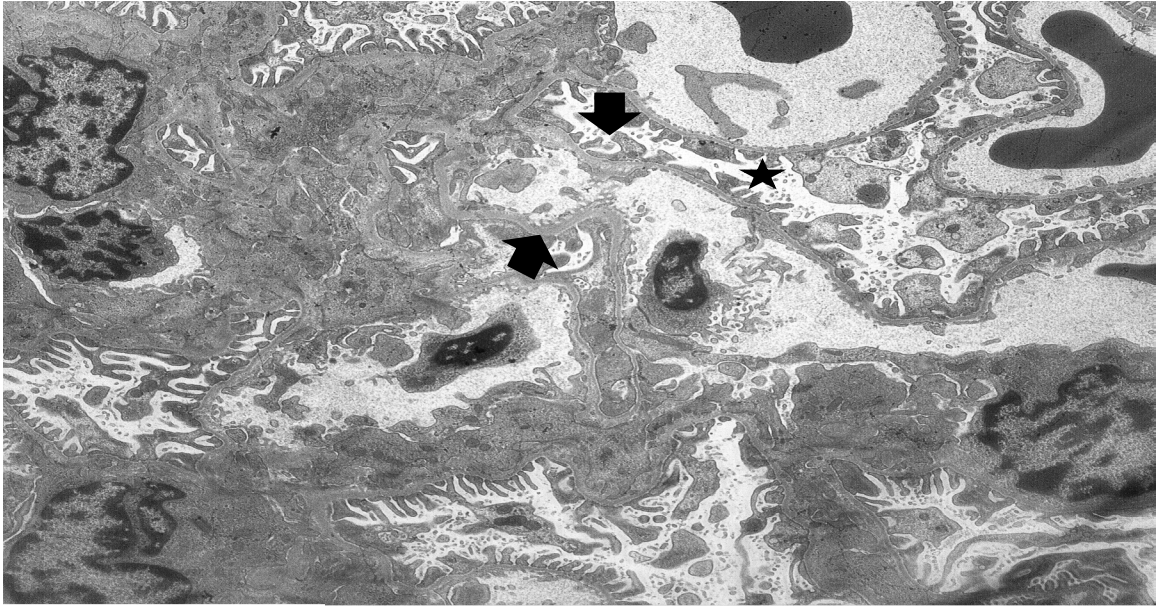


Fig 33. Panel A

2 μ m
Direct Mag: 5000x

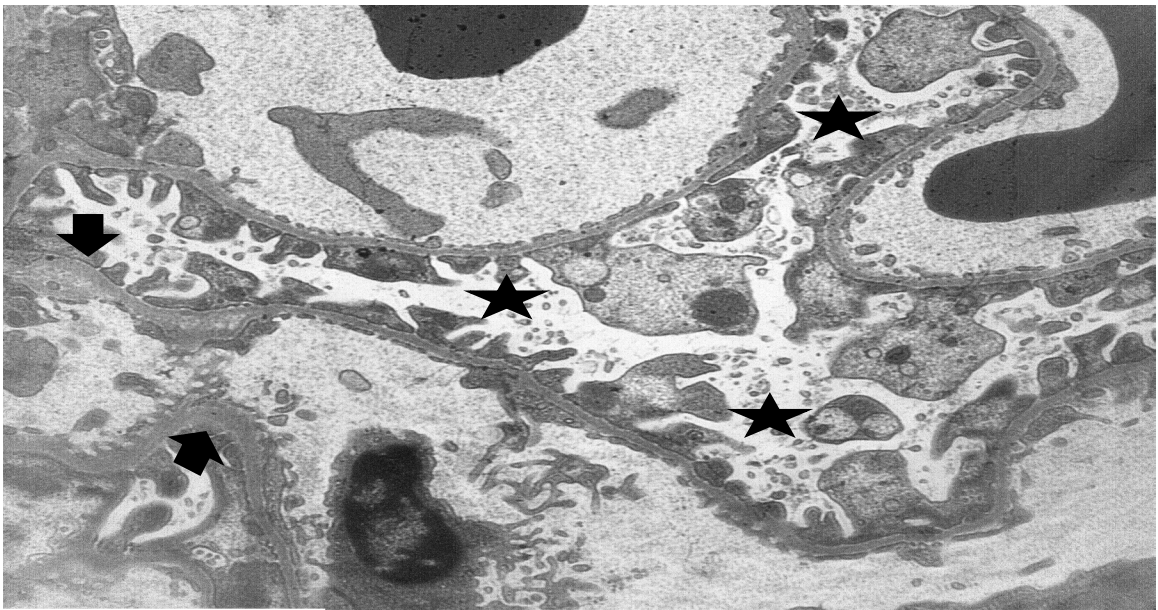


Fig 33. Panel B

500 nm
Direct Mag: 10000x

Figure 33. Kidney TEM - Glomerulus – Na-DMDTC

Transmission electron micrographs of kidney sections, specifically the glomerulus, after 6 weeks of oral treatment with 94 mg/kg Na-DMDTC (Panel A&B), Low magnification images (A) = 5000X. High magnification images (B) = 10,000X. Animals treated with ZM demonstrate fusion of podocytes (star), accompanied by a thickening of the basement membrane (arrow).

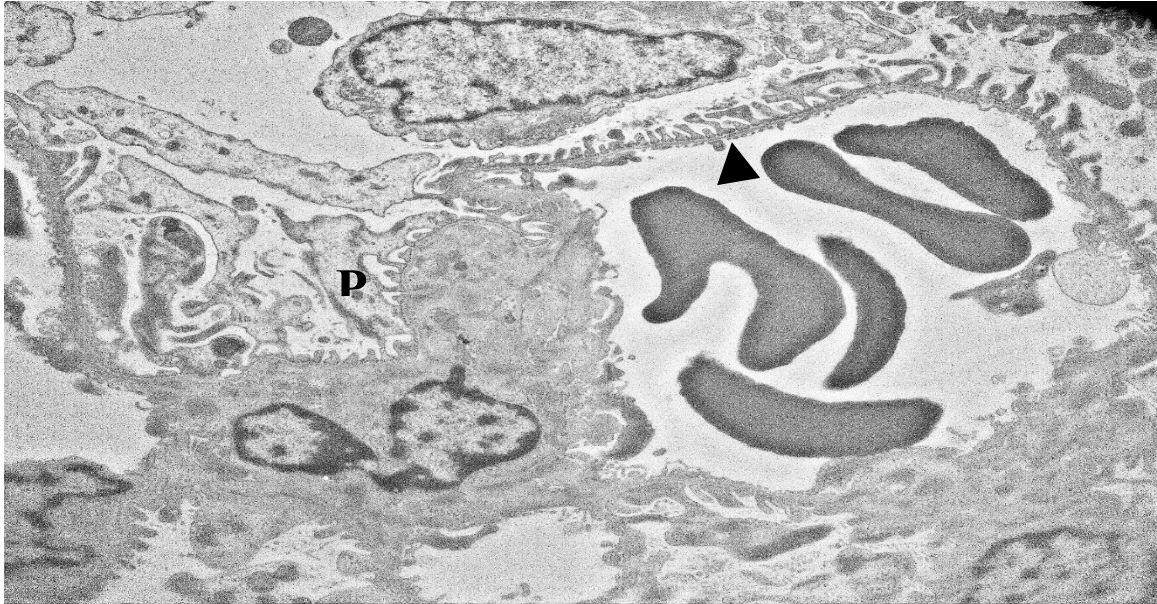


Fig 34. Panel A

2 μ m
Direct Mag: 6000x

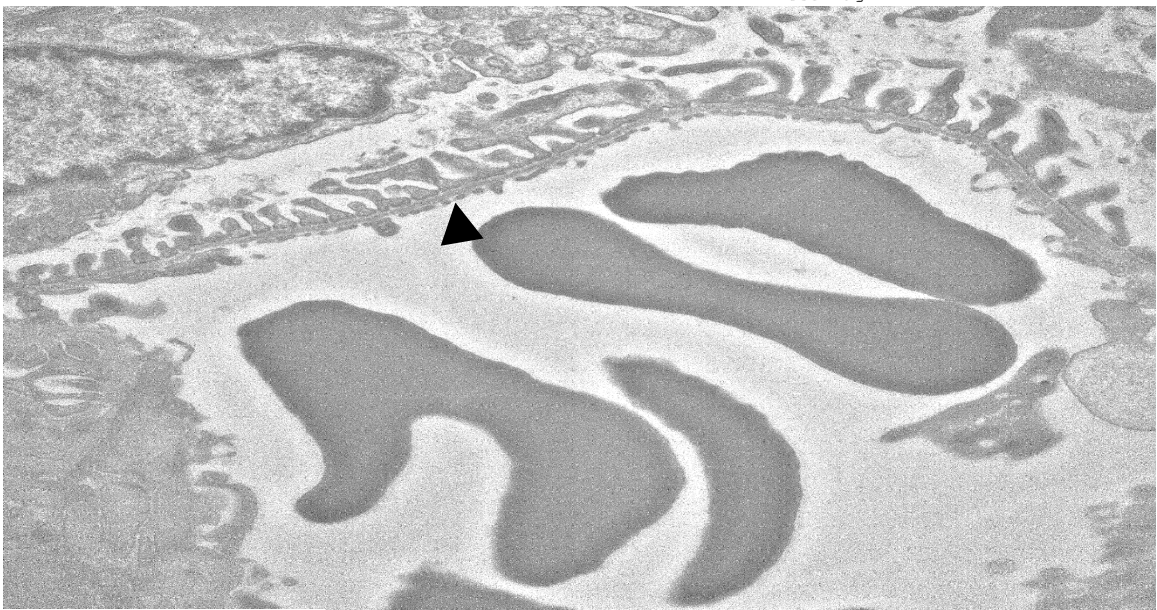


Fig 34. Panel B

500 nm
Direct Mag: 10000x

Figure 34. Kidney TEM - Glomerulus – ZnCl₂

Transmission electron micrographs of kidney sections, specifically the glomerulus, after 6 weeks of oral treatment with 45 mg/kg ZnCl₂ (Panel A&B), Low magnification images (A) = 6000X. High magnification images (B) = 10,000X. The glomerular structure of animals treated with ZnCl₂ appears unremarkable and comparable to that of control animals.

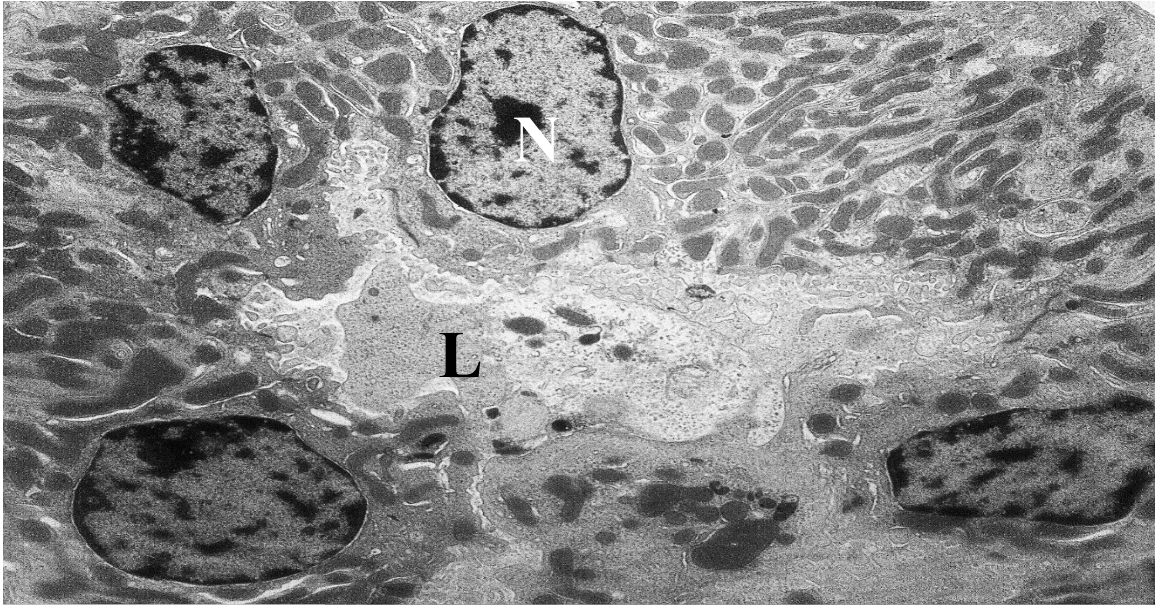


Fig 35. Panel A

2 μ m
Direct Mag: 5000x

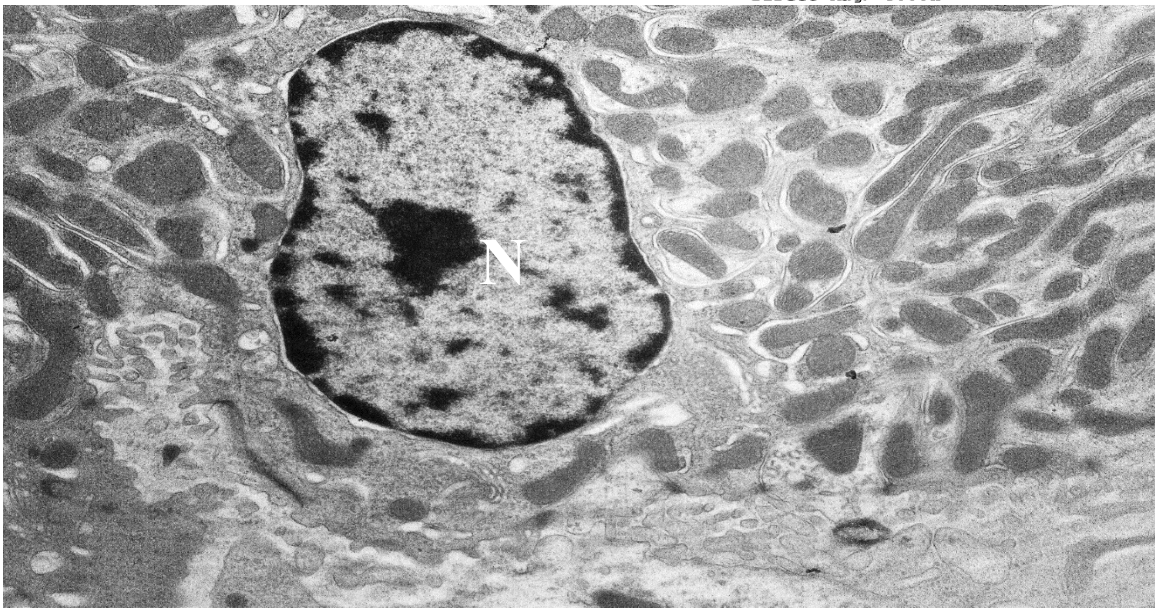


Fig 35. Panel B

500 nm
Direct Mag: 10000x

Figure 35. Kidney TEM – Tubular Cells – Control

Transmission electron micrographs of kidney sections, specifically the tubular region, after 6 weeks of oral treatment with vehicle control (PEG 400) (A&B Low magnification images (A) = 5000X. High magnification images (B) = 10,000X. Nuclei (N) and Lumen (K) are labelled in the figures if present. Kidney sections of control animals (A&B) demonstrate unremarkable tubular structure, with the presence of undisturbed nuclei and a distinct lumen.

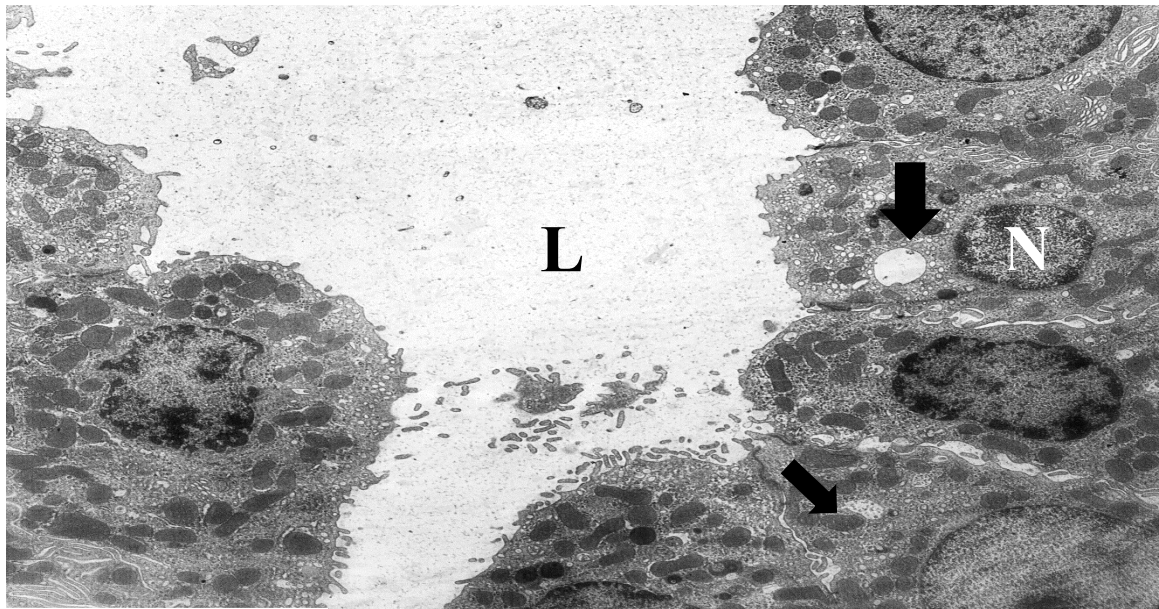


Fig 36. Panel A

2 μ m
Direct Mag: 5000x

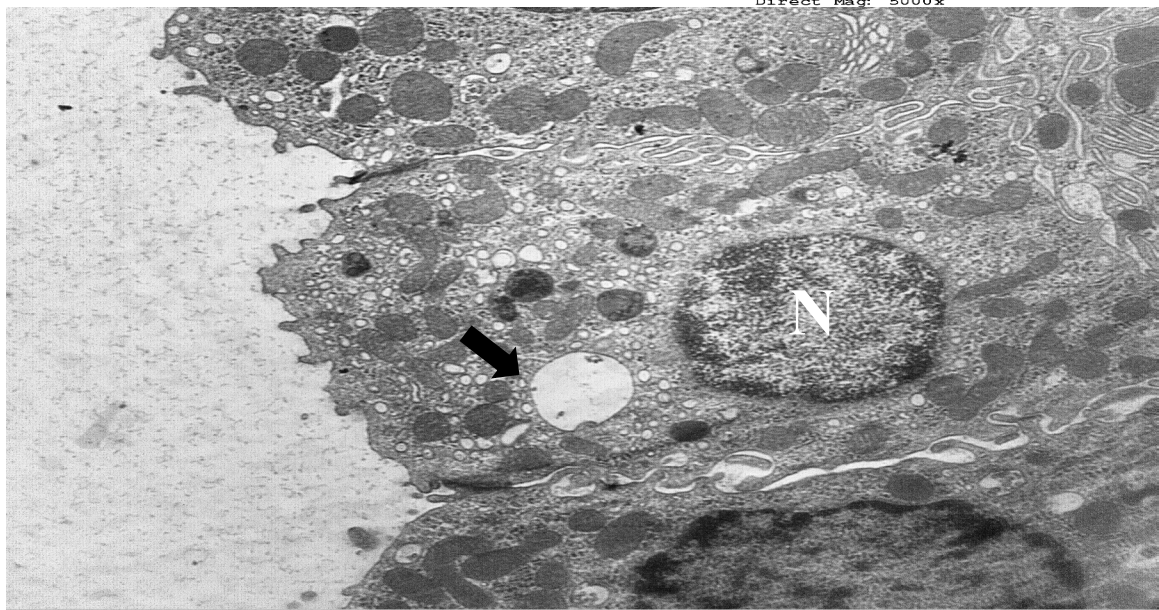


Fig 36. Panel B

500 nm
Direct Mag: 10000x

Figure 36. Kidney TEM – Tubular Cells – ZM

Transmission electron micrographs of kidney sections, specifically the tubular region, after 6 weeks of oral treatment with 100 mg/kg ZM (Panel A&B), Low magnification images (A) = 5000X. High magnification images (B) = 10,000X. Animals treated with ZM demonstrate the presence of vacuolization (arrow) in tubular cells.

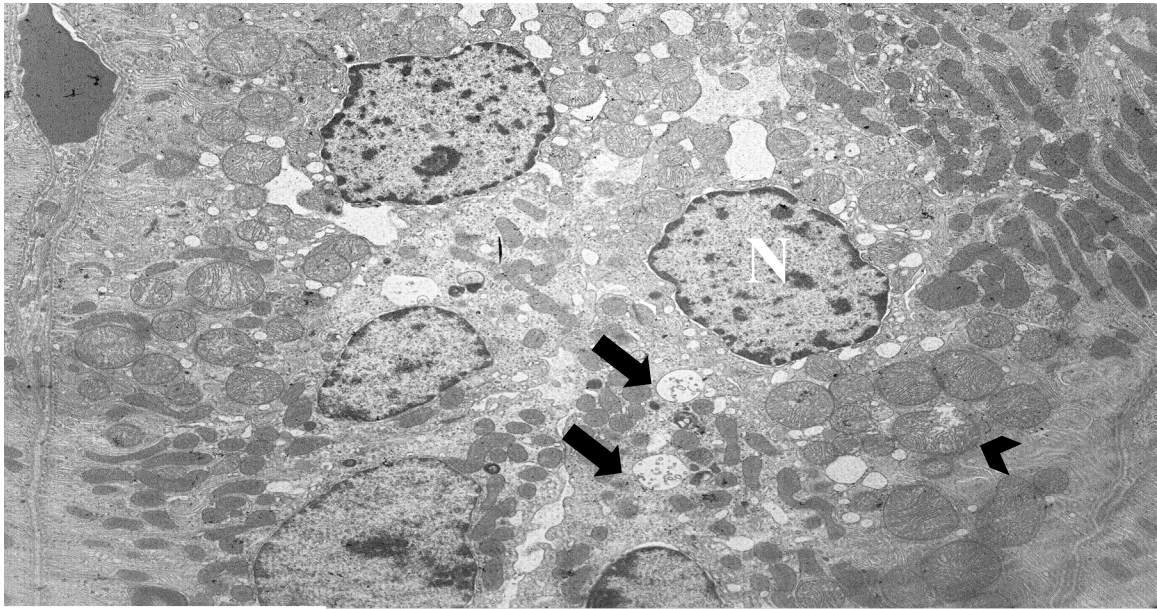


Fig 37. Panel A

2 μ m
Direct Mag: 5000x

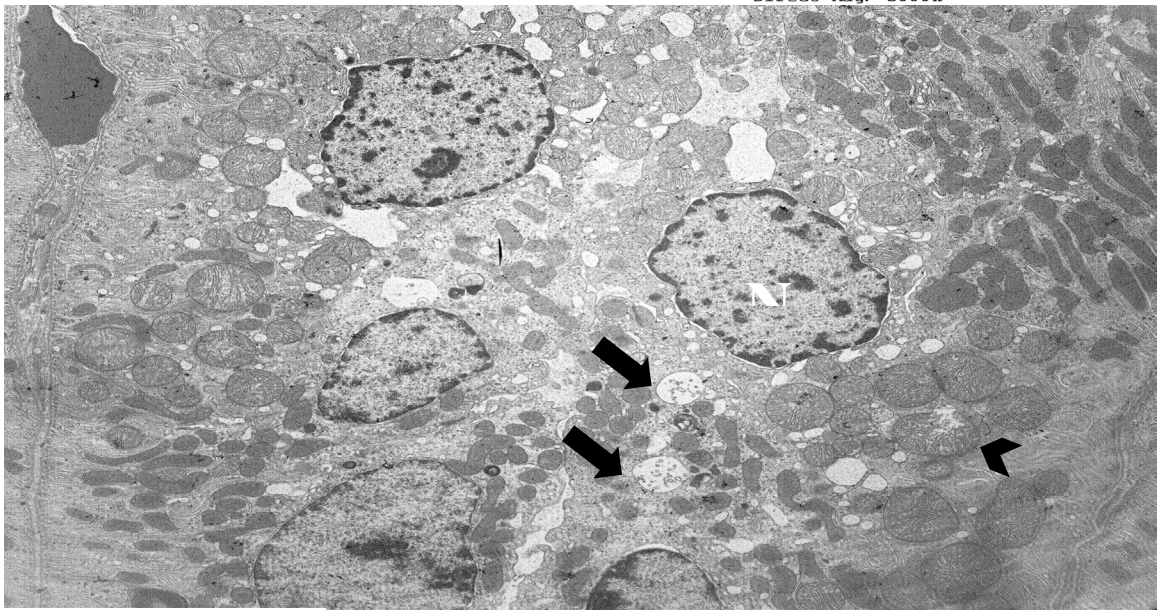


Fig 37. Panel B

2 μ m
Direct Mag: 5000x

Figure 37. Kidney TEM – Tubular Cells – Na-DMDTC

Transmission electron micrographs of kidney sections, specifically the tubular region, after 6 weeks of oral treatment with 94 mg/kg Na-DMDTC (Panel A&B), Low magnification images (A) = 5000X. High magnification images (B) = 10,000X. Animals treated with Na-DMDTC demonstrate the presence of vacuolization (arrow) and disruption of mitochondria (arrowhead) in the tubular cells.

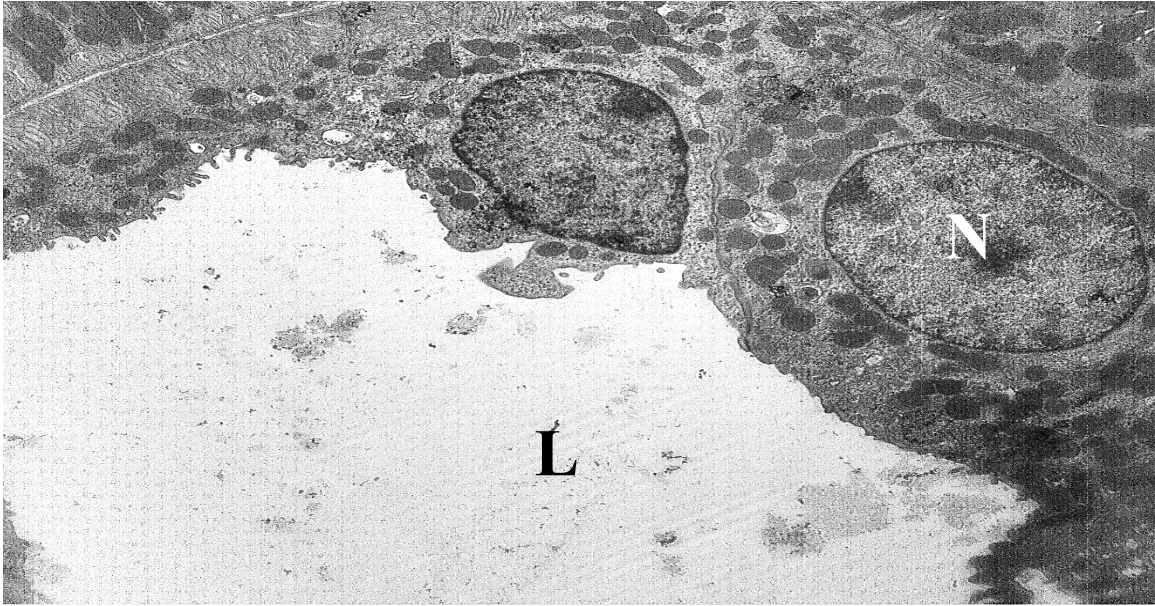


Fig 38. Panel A

2 μ m
Direct Mag: 5000x

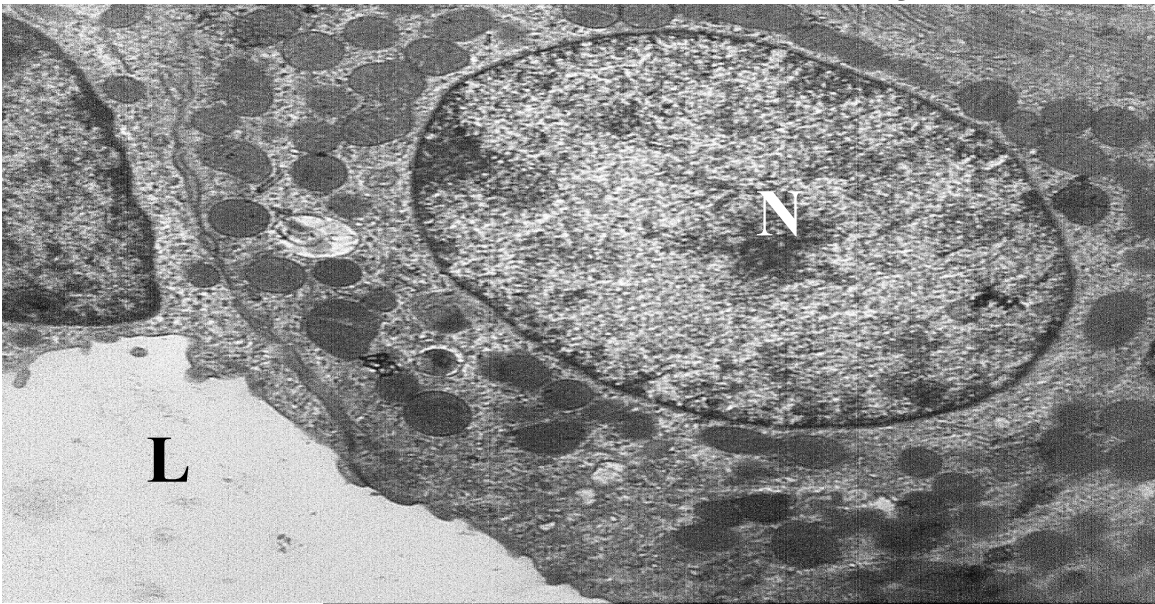


Fig 38. Panel B

500 nm
Direct Mag: 10000x

Figure 38. Kidney TEM – Tubular Cells – ZnCl₂

Transmission electron micrographs of kidney sections, specifically the tubular region, after 6 weeks of oral treatment with 45 mg/kg ZnCl₂ (Panel A&B), Low magnification images (A) = 5000X. High magnification images (B) = 10,000X. Animals treated with ZnCl₂ are unremarkable and comparable to control (G&H).

CHAPTER 4. DISCUSSION

There is no doubt that the use of pesticides may be justified as a necessary evil due to their ability to increase the quality and quantity of our food supply, however rampant use, and lack of specificity to target organisms is cause for serious concern. In 2012, U.S. pesticide usage totaled over 1.1 billion pounds, with the U.S. being responsible for nearly 23% of the worldwide pesticide usage between 2008 and 2012 (Atwood and Paisley-Jones, 2017). Ziram is a fungicide that is widely used in the U.S., with an annual usage of roughly 1.9 million pounds of active ingredient prior to its ban in 2021. Ziram has been shown to display a wide array of toxicological effects, with the main target organs being the thyroid, liver, and nervous system (EPA, RED 2003). Epidemiology studies have shown that ZM, in combination with various other pesticides, is associated with a 1 to 3-fold increase in risk for developing Parkinson's Disease (Wang et al., 2011). Ziram has also been shown to preferentially damage tyrosine hydroxylase positive neurons, along with disrupting the ubiquitin protease system, a biological system implicated in the etiology of PD (Chou et al., 2008). Various studies conducted by the EPA have established that ZM is a hepatotoxin, with various subchronic and chronic studies demonstrating liver histopathology after exposure. Ziram is also an endocrine disruptor due to its toxicity on the thyroid gland.

Due to its demonstrated toxicity and the paucity of human data with exposure to this pesticide, it was chosen for investigation in the current study. In the present study, hepatic and renal toxicological effects of the fungicide, ziram, were assessed in Long-Evan rats following daily oral treatment for 6-weeks. Following treatment with ZM, the liver and kidneys were extracted to assess for alterations in metal homeostasis, antioxidant defenses, oxidative damage, and changes in tissue morphology. It is unknown whether the

toxicological effects seen with exposure to ZM, and related compounds, are owed to its organic backbone or to the metal moiety complexed to the backbone. Therefore, treatment groups of sodium dimethyldithiocarbamate and ZnCl_2 were included to investigate the individual effects of either the dimethyldithiocarbamate backbone or the zinc metal moiety.

Throughout the entire course of the study, animals were weighed prior to oral treatment with either PEG-400 (vehicle control), ZM, Na-DMDTC, or ZnCl_2 . Animal weights are a widely accepted indicator of toxicity, as a decrease in animal weights can be a sign of distress, reduced appetite, metabolic alterations, increased energy expenditure, or malabsorption (Talbot et al., 2020). In the present work, significant decreases in total raw weight were seen in animals treated with ZM as compared to the ZnCl_2 treatment group starting in week 4 and were significant when compared to the control starting in week 5. The difference in weight remained significant for the remainder of the study. In addition to decreases in total raw weight, a significant decrease in total weight gain was seen in the ZM treatment group as compared to all other groups starting at week 1 and remained significant for the entire duration of the study. The work of Enomoto et al., (1989) is in agreement with the current study, showing significant decreases in total raw weight in rats after treatment with 2000 ppm of ZM in feed, after 13 weeks, 26 weeks, 52 weeks, 78 weeks, and 104 weeks. Although similar effects on total weight and weight gain were not seen in this study in the Na-DMDTC treated animals, a study conducted by the European Chemicals Agency (ECHA), demonstrated significant decreases in total weight and weight gain in dogs, after oral treatment with 185 and 500 ppm of Na-DMDTC for 52 weeks (ECHA, 1993). This may be attributed to the shorter time span of the current work as compared to the ECHA study.

Weight loss in animals could be owed to a variety of reasons such as distress, loss of appetite, or metabolic alterations (Talbot et al., 2020). In this study, distress or loss of appetite may play a role in the decrease of total weight and weight gain, however, it is most likely not the main contributor as treated animals, although not recorded, were observed frequently consuming food. During the study, animals did not show any signs of lethargy or distress as animals were observed playing with cage-mates, along with frequent grooming. Ruling out the other two factors leaves the option of metabolic alterations. Dithiocarbamate compounds are known endocrine disruptors and possess the ability to specifically target the thyroid gland. The thyroid gland, with the production of thyroxine (T4) and triiodothyronine (T3), is a vital organ involved in the process of growth and development (Tarim, 2011).

The presumed mechanism of thyroid toxicity is owed to the metabolite ethylenethiourea (ETU), a compound which is able to inhibit the synthesis of thyroid hormones, such as thyroxine (T4) and triiodothyronine (T3). Inhibition of these two thyroid hormones leads to elevated levels of thyroid stimulating hormone due to feedback stimulation of the hypothalamus and the pituitary, ultimately leading to hypertrophy and hyperplasia of thyroid cells in rats and mice (Costa and Aschner., 2014). Although the mechanism involves inhibition of T4 and T3 levels, serum analysis of T4 levels were not significantly altered following treatment. In addition, the general mechanism of DTC degradation to ETU is only applicable to certain DTC subclasses, such as the ethylene-bis-dithiocarbamates. Pharmacokinetic studies demonstrate that 24 hours following ZM exposure, water-soluble metabolites are found in the blood, spleen, liver, kidney, and thyroid (IARC, 1991). Metabolism studies of ZM suggest that upon exposure, ZM is not

metabolized to ETU, but rather into dimethyldithiocarbamate anions which are then subsequently metabolized to carbon disulfide and dimethylamine (EPA OPP, 2021). Although ETU is not a degradation product of ZM and T4 levels were not changed, ZM is a known toxicant to the thyroid gland as it is able to disrupt metabolic activity and lead to hyperplasia and tumor formation (Pandey and Dikshith, 1990; EPA RED, 2003). The lack of alteration in serum T4 levels may be attributed to the short duration of study, as the studies referenced above were life-long studies. ZM may also be able to disrupt thyroid functions via a different mechanism such as disrupting T3 or other molecules in the hypothalamic-pituitary-thyroid axis. Despite the lack of changes in T4, various studies collaborate the finding that ZM induces a decrease in body weight and weight gain. A 90-day oral rat toxicity study conducted by the EPA, demonstrated decreases in body weight and weight gain at doses as low as 7.4 mg/kg. In two separate developmental studies, one conducted on rats, and another conducted on rabbits, decreases in maternal body weight and weight gain were seen at doses of 4 and 3 mg/kg, respectively (EPA RED, 2003). Whether ZM disrupts growth through alterations of thyroid function, or another mechanism is unknown and warrants further investigation.

Measurement of blood parameters is another strategy for investigation of toxicity upon exposure to potentially toxic agents in *in vivo* studies. Therefore, prior to euthanasia, blood was withdrawn from the animals through cardiac puncture for investigation. A significant decrease was seen in both ALT and glucose levels in the ZM treatment group when compared to control. Although statistically significant, the decrease seen in ALT was perplexing, as only an increase in ALT has been associated with toxicity. Plasma glucose levels are affected by glucose entry and removal from the circulation. The significant

decrease seen in glucose levels in the ZM treatment group can be owed to disruptions of the thyroid gland as thyroid disorders and glucose metabolism are closely related (Eom et al., 2022). Thyroid hormones affect glucose uptake through different pathways in the gastrointestinal tract, liver, and skeletal pathways. In the gastrointestinal tract, thyroid hormones increase glucose absorption by increasing gastrointestinal motility, and in the liver, thyroid hormones can stimulate gluconeogenesis and glycogenolysis (Park et al., 1995; Nishi, 2018). As a thyroid toxicant, ZM-related thyroid dysfunction may cause disturbances in any of these pathways leading to alterations in glucose homeostasis.

One of the main mechanisms of toxicity of DTC compounds is its ability to alter metal homeostasis due to its metal moiety, by introducing excess metal, or through the effects of transchelation, a process by which the compound is able to bind to and redistribute essential metals from one part of the body to another. The levels of essential metals in the body are kept in a delicate equilibrium and fluctuations in their levels will lead to disease states or toxicity. The metal altering and chelating effects of various DTC compounds are well studied and documented in the literature, with effects including accumulation of metals such as manganese and zinc, and chelation of copper (Delmaestro and Trombetta, 1995; Hoffman and Hardej, 2016; Kisting and Hardej, 2022; Stephenson and Trombetta, 2020; Viquez et al., 2008). However, the metal altering effects of ZM have not been well studied and documented *in vivo*. Therefore, the current work utilized ICP-OES to measure the levels of zinc, copper, and iron in various organs after treatment with ZM, Na-DMDTC, or ZnCl₂ for 6 weeks.

The levels of zinc, copper, and iron were measured in the liver, kidney, serum, urine, and feces. Starting with zinc, a significant increase in zinc levels is seen in the liver, kidney,

serum, and urine in animals treated with ZM as compared to all other groups. This result is not unexpected as zinc is the main metal moiety attached to ZM. *In vitro* studies documented in the literature have also demonstrated accumulation of zinc in cells after treatment with ZM (Dennis and Valentine, 2015; Kanemoto-Kataoka et al., 2017). This result was also mirrored in my master's thesis, where zinc accumulation was seen in rat hippocampal astrocytes after treatment with ZM. In the feces, zinc was significantly increased in the ZM and ZnCl₂ treated animals when compared to control and Na-DMDTC treatment group. The amount of zinc found in the feces between both groups were similar (ZM = 264.80±28.09 ppm/g, ZnCl₂ = 258.60±25.80 ppm/g). The dose of ZnCl₂ given was an equal molar concentration of the ZM dose and it is believed that upon ingestion of ZM, zinc is dissociated from the dimethyldithiocarbamate backbone, therefore, it would be expected that a similar amount of zinc is being excreted into the feces. Although similar concentrations of zinc are found in the feces between the ZM group and the ZnCl₂, a similar pattern of zinc accumulation is not seen in the rest of the organs. This suggests that the backbone may play a significant role in sequestering and movement of zinc in the body.

With regards to copper levels, a significant increase was seen in the liver, accompanied by a significant decrease in the serum of animals treated with ZM when compared to the control. These results demonstrate that ZM is also able to participate in the transchelating effect known to DTCs. Similar findings were observed in *in vitro* studies where HEK293 cells showed significant increases in copper levels following treatment with ZM (Dennis and Valentine, 2015). This result was also mirrored in my master's thesis, where copper accumulation was also demonstrated in rat hippocampal astrocytes after treatment with ZM (unpublished data). The source of copper accumulation in the liver is

believed to be attributed to three factors: the serum, kidneys, and rodent chow. Metal analysis demonstrated that a significant decrease in serum copper was seen in the ZM treatment animals accompanied by a decrease, although non-significant, in the kidneys. In the initial pilot study of this dissertation study, animals treated for 4 weeks with ZM exhibited similar results, with significant increases in liver copper levels but with significant decreases seen in the kidneys. It is believed that with the extension of the treatment period from 4 to 6 weeks, copper homeostasis was slowly being reestablished in the kidneys. Rodent chow is another source of copper, however there were no significant changes of copper levels in the feces. Due to this finding, it is believed that small amounts of copper were being redistributed over the course of the treatment period.

As previously discussed, the ability of DTC to chelate copper is a well-known phenomenon. Sodium diethyldithiocarbamate exposure has been shown to cause accumulation in the liver and brain of rats (Tonkin et al., 2004; Viquez et al., 2008). Mancozeb exposure caused copper accumulation in the kidneys of rats, while disulfiram caused copper accumulation in the heart of rats (Kistingner and Hardej, 2022; Stephenson and Trombetta, 2020). These findings suggest that each dithiocarbamate subclass may have its own unique target organ for transchelation. In the present study, we believe that we are the first to report accumulation of copper in the liver of animals treated with ZM.

For iron levels, no significant changes were seen across the various samples in animals treated with either ZM or Na-DMDTC. For animals treated with $ZnCl_2$, a significant decrease in iron levels were seen in the liver when compared to the control. This effect can be attributed to zinc's influence on the absorption of iron as gastrointestinal

absorption of iron is directly inhibited by high doses of zinc (Solomons, 1986), however, this was not seen in animals treated with ZM.

The investigation of disturbed metal homeostasis after exposure to DTC is a critical topic because it directly relates to its main presumed mechanism of toxicity, oxidative stress. Previous studies have shown that dithiocarbamates exert their toxicity through production of oxidative stress, with their metal components or the transchelation of other essential metals, playing a key role in this process via Fenton reactions (Dennis and Valentine, 2015; Fitsanakis et al., 2002; Grosicka-Maciag et al., 2012; Kanemoto-Kataoka et al., 2017). In Fenton reactions, transition metals such as copper, can react with hydrogen peroxide producing the highly toxic hydroxyl radical which can then cause a cascade of toxicology effects. In the present study, the antioxidant status of both hepatic and renal tissue was assessed along with biomarkers of lipid peroxidation and protein oxidation.

In order to investigate the antioxidant status of treated animals, the glutathione defense system and the total antioxidant capacity of both liver and kidney tissue were assessed. The glutathione defense system includes total glutathione, GSH/GSSG ratio, glutathione reductase, and glutathione peroxidase. Total glutathione involves measurement of both the reduced and oxidized forms together. In an event of oxidative stress, the increase or decrease of total glutathione can be indicative of different scenarios. An increase in total glutathione may indicate the activation of the defense system in response to oxidative insult whereas a decrease in total glutathione may indicate depletion of the antioxidant or disruption in its synthesis. For the ratio of glutathione-to-glutathione disulfide ratio, a decrease is indicative of oxidative stress as GSH reserves are being depleted, leading to a

decrease in the ratio. An increase in the ratio can indicate activation of the defense system, as more GSSG is being converted to GSH to counteract oxidative stress.

When assessing levels of total glutathione, a significant increase in the kidneys were seen in animals treated with ZM as compared to control. There were no changes in total glutathione levels in the liver across the various treated groups, however, a significant increase in the GSH/GSSG ratio is seen in the livers of animals treated with ZM when compared to control. The ratio of GSH/GSSG was unaffected in the kidneys. Examining the individual concentrations of GSH and GSSG, demonstrates a significant increase in the GSH levels in the kidneys of animals treated with ZM when compared to control, and a significant decrease in GSSG levels in the liver of animals treated with ZM when compared to the control. No alterations were seen in either glutathione reductase activity or glutathione peroxidase activity across the treatment groups. Although there was a lack of alterations in the activities of glutathione reductase and peroxidase, assessment of the total antioxidant levels in the organs demonstrated significant increases in both, the liver and kidneys, of animals treated with ZM when compared to control.

The two markers of oxidative damage that were assessed in this study are 4-hydroxynonenol (4-HNE), a product of lipid peroxidation, and protein carbonyls, a product of protein oxidation. No significant increases in either 4-HNE or protein carbonyls were seen in either liver or kidney across the treated groups. These results were aligned with the serum data as there were no significant increases in any of the liver injury markers such as ALT, ALP, or AST. In addition, these findings are in line with the results of the antioxidant data as we believe that currently, the antioxidant defense systems are not overwhelmed, but rather activated to counteract the current oxidative insult. Similar findings were seen in the

study of Kistingner and Hardej (2022), where rats treated for 4 weeks with the ethylene-bis-dithiocarbamate mancozeb, saw increases in the glutathione defense system but a lack of changes in oxidative damage markers in the liver and the kidney.

The increases seen in the glutathione defense system and total antioxidant levels in the organs implies that at the current dose and timepoint, the system was not overwhelmed, but rather a compensatory or adaptive mechanism was active before the onset of overt toxicity. The glutathione defense system is controlled and regulated by the nuclear factor erythroid 2-related factor 2 (Nrf2). In response to oxidative stress, the transcription factor Nrf2 binds to antioxidant response elements (ARE) in the promoter region of genes that are responsible for coding for antioxidants such as glutathione (Vomhof-DeKrey and Picklo, 2012). Numerous studies in the literature have demonstrated that dithiocarbamates are able to activate the Nrf2 system, leading to upregulation in antioxidants. Copper diethyldithiocarbamate was found to accumulate within vascular endothelial cells, leading to nuclear translocation of Nrf2, and upregulation of antioxidants without cytotoxic effects (Fujie et al., 2016). Similar events were seen in astrocytes, where treatment with pyrrolidine dithiocarbamate led to induction of the Nrf2 signaling pathway (Liddell et al., 2016). A similar event could be occurring in this study, where oxidative insult from treatment, leads to activation of the Nrf2 signaling pathway, causing an upregulation of antioxidants, thereby counteracting oxidative damage, and preventing an increase in oxidative damage markers. Interestingly, the changes seen in the ZM treated animals were not mirrored by either the backbone or ZnCl₂, implying that perhaps the alterations in antioxidant parameters are mediated by an intrinsic property of ZM as opposed to any singular part in its structure.

One of the initial findings in the pilot study were morphological alterations in renal tissue, characterized by cast formation and degeneration of the tubules, in the rats treated with ZM. Due to these findings, evaluation of creatinine clearance (Clcr) was conducted to assess if there were physiological changes associated with ZM treatment. In addition, assessment of renal injury markers, kidney injury marker-1 (KIM-1) and neutrophil gelatinase-associated lipocalin (NGAL), were also conducted. Creatinine clearance is defined as the volume of blood plasma cleared of creatinine per unit time and is a routine endpoint to assess renal function status (Shahbaz and Gupta, 2021). Creatinine clearance is calculated by using the formula: $Clcr = \frac{\text{urine creatinine} \left(\frac{mg}{dl}\right) \times \text{urine flow rate} \left(\frac{mL}{min}\right)}{\text{serum creatinine} \left(\frac{mg}{dl}\right)}$ (Bazzano *et al.*, 2015). Animals treated with ZM had significant decreases in urine creatinine when compared to control. No changes were seen in serum creatinine levels across the groups. Urine flow rate is the amount of urine produced per minute and a significant increase in urine flow rate was seen in animals treated with ZM as compared to control. Accompanying the increase in urine flow rate, was a significant increase in water consumption and urine volume production in the animals treated with ZM as compared to the control. Factoring in urine creatinine, serum creatinine, and urine flow rate into the creatinine clearance equation, creatinine clearance can be calculated and there were no significant alterations seen across the groups. The significant increase in urine flow rate balanced the significant decrease in urine creatinine, thereby raising the creatinine clearance of ZM treated animals.

In a scenario of overt renal toxicity, a stark raise in serum creatinine would be seen as the organ is unable to eliminate the excess creatinine in the body. In this study, a rise in serum creatinine is not seen, but rather a stark increase in urine flow rate and urine

production. This implies that a compensatory or adaptive mechanism is active, or that these alterations are a result of another disturbance. Kidney alterations as a result of thyroid dysfunction have been documented in the literature (Basu and Mohapatra, 2012). For example, in hyperthyroidism, enhanced activation of the renin-angiotensin-aldosterone system is seen, whereas in hypothyroidism, reduction in glomerular filtration rate is seen (Basu and Mohapatra, 2012). Since ZM is a thyroid toxicant, interplay between thyroid dysfunction and disruptions in the physiological functions of the kidney may be the cause of the changes seen in this study.

Despite the lack of changes in creatinine clearance, immunohistochemical staining for KIM-1 demonstrated an increase in KIM-1 immunoreactivity in kidney tissue of ZM and Na-DMDTC treated animals. Alterations in NGAL immunoreactivity in kidney tissue were not seen across the groups. Both KIM-1 and NGAL are two novel biomarkers that have been proposed to be used as early biomarkers for diagnosing acute kidney injury (Vaidya et al., 2008). During kidney injury, the expressions of both KIM-1 and NGAL are upregulated and subsequently shed from the tubular cells into the urine. Out of the two biomarkers, KIM-1 is the most highly upregulated during kidney injury and is believed to have the highest sensitivity and specificity (Vaidya et al., 2008). Due to the increase presence in KIM-1 immunoreactivity but a lack of changes in creatinine clearance, it is believed that at this timepoint and dose, the renal toxicity seen is not overt enough to cause drastic changes in creatinine clearance.

Histopathological investigation of liver and kidney tissue were evaluated using hematoxylin and eosin (H&E), periodic acid-Schiff (P.A.S), and Masson's trichrome staining along with transmission electron microscopy. Light micrographs of liver tissue

stained with H&E indicate the presence of infiltration near the central veins of animals treated with ZM. The presence of protein aggregation and sloughing of tubular cells are seen in kidney tissue stained with H&E in both the ZM and the Na-DMDTC treated animals. Masson's trichrome staining is a technique used for evaluation of extracellular matrix deposition. Alterations in extracellular matrix deposition were not seen in the liver or kidneys of treated animals and were comparable to that of the control. Examination of liver tissue stained with P.A.S demonstrates the presence of vacuolization in hepatocytes of animals treated with ZM and Na-DMDTC. Kidney tissue stained with P.A.S demonstrated thickening of the Bowman's capsule in both the ZM and the Na-DMDTC treatment group.

The use of the previously discussed staining techniques is valuable in determining gross morphological alterations. However, to evaluate ultrastructure changes in the tissue, transmission electron microscopy was used. Electron micrographs of liver tissue demonstrated hepatotoxicity, in the form of lipid deposition, cellular edema, vacuolization, and swelling of the endoplasmic reticulum in the ZM and Na-DMDTC treated animals. Animals treated with ZM and Na-DMDTC exhibited thickening of the basement membrane and fusion of podocyte foot processes in the glomerulus of the kidneys. Electron micrographs of the tubular cells exhibited vacuolization and disruption of mitochondria in the animals treated with ZM and Na-DMDTC.

One of the established target organs of ZM toxicity is the liver and similar results of liver histopathology have been documented (EPA RED, 2003). Exposure to other dithiocarbamate compounds has resulted in similar morphological changes. Rats treated every day for 6 weeks with 3.8 to 7.6 mg/kg of bipyridine-gold-dithiocarbamate

demonstrated mild hepatic vacuolization and portal inflammation (Badar et al., 2021). Livers of rats treated with 250 ppm of Maneb displayed degeneration and vacuolization of hepatocytes (Deveci et al., 1999). Similarly, rats treated with n-methyldithiocarbamate exhibited centrilobular necrosis (Thompson et al., 2002). It appears, regardless of the subclass, dithiocarbamates are able to cause significant toxic effects to the liver.

One of the main highlights of the histology is the fact that the renal toxic effects of ZM, such as an increase KIM-1 immunoreactivity, the degeneration of the tubules, and thickening of the basement membrane, are also observed in the Na-DMDTC treatment group. In addition to the histological changes, although not significant, changes in the creatinine clearance parameters in the Na-DMDTC treatment group, mirrored those seen in the ZM treatment group. These results suggest that the renal toxic effects of ZM are perhaps mediated by the dimethyldithiocarbamate backbone structure. Renal injury has not been generally associated with dithiocarbamate exposure, therefore, these results demonstrating renal specific toxicity of ZM, are a novel finding.

CHAPTER 5. CONCLUSION

In the present study, Long-Evan rats were treated every day, orally, for 6 weeks with the dimethyldithiocarbamate fungicide, Ziram, the sodium salt of its organic backbone, sodium dimethyldithiocarbamate, and its metal moiety, $ZnCl_2$. The present study sought to elucidate the mechanism by which Ziram exerts its toxicity and which component was responsible for its effect. In this study, we demonstrated that Ziram possesses the ability to alter metal homeostasis and the antioxidant status of the liver and kidney of treated animals, whereas these changes were not seen in the other treatment groups. Alterations in creatinine clearance parameters along with histopathological changes in both the liver and kidney were seen in animals treated with ZM and Na-DMDTC. These results demonstrate that the organic backbone plays a much greater role in the toxicity of ZM than its metal moiety.

The novel findings of this study are that the kidney is in fact, also a target organ of ZM toxicity and that although the organic backbone did play some part in the toxicity of ZM, the overall toxicological profile of ZM may be due to an intrinsic property of ZM itself, rather than being owed to any specific part of its structure.

REFERENCES

- Aruoma, O. I. (1998). Free radicals, oxidative stress, and antioxidants in human health and disease. *Journal of the American Oil Chemists' Society*, 75(2), 199–212. <https://doi.org/10.1007/s11746-998-0032-9>
- ATSDR. (1996). *TOXICOLOGICAL PROFILE FOR CARBON DISULFIDE*.
- Atwood, D., & Paisley-Jones, C. (2008). *US EPA - Pesticides Industry Sales and Usage 2008 - 2012*.
- Ayala, A., Muñoz, M. F., & Argüelles, S. (2014). Lipid peroxidation: Production, metabolism, and signaling mechanisms of malondialdehyde and 4-hydroxy-2-nonenal. In *Oxidative Medicine and Cellular Longevity* (Vol. 2014). Landes Bioscience. <https://doi.org/10.1155/2014/360438>
- Badar, A., Ahmed, A., Al-Tamimi, D. M., Isab, A. A., Altaf, M., & Ahmed, S. (2021). Histological changes in renal, hepatic and cardiac tissues of wistar rats after 6 weeks treatment with bipyridine gold (III) complex with dithiocarbamate ligands. *Pharmaceutics*, 13(10). <https://doi.org/10.3390/pharmaceutics13101530>
- Basu, G., & Mohapatra, A. (2012). Interactions between thyroid disorders and kidney disease. *Indian Journal of Endocrinology and Metabolism*, 16(2), 204. <https://doi.org/10.4103/2230-8210.93737>
- Bazzano, T., Restel, T. I., Porfirio, L. C., De Souza, A. S., & Silva, I. S. (2015). Renal biomarkers of male and female wistar rats (*Rattus norvegicus*) undergoing renal ischemia and reperfusion. *Acta Cirurgica Brasileira*, 30(4), 277–288. <https://doi.org/10.1590/S0102-865020150040000007>
- Birben, E., Sahiner, U. M., Sackesen, C., Erzurum, S., & Kalayci, O. (2012). Oxidative stress and antioxidant defense. *The World Allergy Organization Journal*, 5(1), 9–19. <https://doi.org/10.1097/WOX.0b013e3182439613>
- Chen, J., Jiang, Y., Shi, H., Peng, Y., Fan, X., & Li, C. (2020). The molecular mechanisms of copper metabolism and its roles in human diseases. In *Pflugers Archiv European Journal of Physiology* (Vol. 472, Issue 10, pp. 1415–1429). Springer. <https://doi.org/10.1007/s00424-020-02412-2>
- Chou, A. P., Maidment, N., Klintonberg, R., Casida, J. E., Li, S., Fitzmaurice, A. G., Fernagut, P. O., Mortazavi, F., Chesselet, M. F., & Bronstein, J. M. (2008). Ziram causes dopaminergic cell damage by inhibiting E1 ligase of the proteasome. *Journal of Biological Chemistry*, 283(50), 34696–34703. <https://doi.org/10.1074/jbc.M802210200>
- Costa, L. G., & Aschner, M. (2014). Toxicology of Pesticides. In *Reference Module in Biomedical Sciences*. Elsevier. <https://doi.org/10.1016/B978-0-12-801238-3.00208-7>

- Delmaestro, E., & Trombetta, L.D. (1995). The effects of disulfiram on the hippocampus and cerebellum of the rat brain: a study on oxidative stress. In *Toxicology letters* (Vol. 75).
- Dennis, K. E., & Valentine, W. M. (2015a). Ziram and sodium N,N -dimethyldithiocarbamate inhibit ubiquitin activation through intracellular metal transport and increased oxidative stress in HEK293 Cells. *Chemical Research in Toxicology*, 28(4), 682–690. <https://doi.org/10.1021/tx500450x>
- Dennis, K. E., & Valentine, W. M. (2015b). Ziram and sodium N,N -dimethyldithiocarbamate inhibit ubiquitin activation through intracellular metal transport and increased oxidative stress in HEK293 Cells. *Chemical Research in Toxicology*, 28(4), 682–690. <https://doi.org/10.1021/tx500450x>
- Deveci, E., Guven, K., Bashan, M., Onen, A., & Pomerai, D. de. (1999). THE ACCUMULATION AND HISTOLOGICAL EFFECTS OF ORGANOMETALLIC FUNGICIDES PROPINEB AND MANEB IN THE LIVERS OF PREGNANT RATS AND THEIR OFFSPRING. *The Journal of Toxicological Sciences*, 24(2), 79–85.
- Enomoto, A., Harada, T., Miata, K., & Shirasu, Y. (1989). EPIPHYSEAL LESIONS OF THE FEMUR AND TIBIA IN RATS FOLLOWING ORAL CHRONIC ADMINISTRATION OF ZINC DIMETHYLDITHIOCARBAMATE (ZIRAM). *Toxicology*, 45–58.
- Eom, Y. S., Wilson, J. R., & Bernet, V. J. (2022). Links between Thyroid Disorders and Glucose Homeostasis. In *Diabetes and Metabolism Journal* (Vol. 46, Issue 2, pp. 239–256). Korean Diabetes Association. <https://doi.org/10.4093/dmj.2022.0013>
- EPA. (2003). *Ziram: Reregistration Eligibility Document (RED)*. www.epa.gov/pesticides/reregistration.
- EPA. (2005). *Toxicology Review of Zinc and Compounds*.
- EPA OPP. (2015). *Ziram: Tier I Review of Human Incidents*.
- European Chemical Agency. (1993). *Sodium dimethyldithiocarbamate - Registration Dossier*. Registration Dossier. <https://echa.europa.eu/registration-dossier/-/registered-dossier/13669/7/6/2>
- Forman, H. J., Zhang, H., & Rinna, A. (2009). Glutathione: Overview of its protective roles, measurement, and biosynthesis. In *Molecular Aspects of Medicine* (Vol. 30, Issues 1–2, pp. 1–12). <https://doi.org/10.1016/j.mam.2008.08.006>
- Fujie, T., Murakami, M., Yoshida, E., Tachinami, T., Shinkai, Y., Fujiwara, Y., Yamamoto, C., Kumagai, Y., Naka, H., & Kaji, T. (2016). Copper diethyldithiocarbamate as an activator of Nrf2 in cultured vascular endothelial cells. *Journal of Biological Inorganic Chemistry*, 21(2), 263–273. <https://doi.org/10.1007/s00775-016-1337-z>
- Hoffman, L., Trombetta, L., & Hardej, D. (2016). Ethylene bisdithiocarbamate pesticides Maneb and Mancozeb cause metal overload in human colon cells. *Environmental Toxicology and Pharmacology*, 41, 78–88. <https://doi.org/10.1016/j.etap.2015.11.002>

- Janz, D. M. (2014). Dithiocarbamates. In *Encyclopedia of Toxicology: Third Edition* (pp. 212–214). Elsevier. <https://doi.org/10.1016/B978-0-12-386454-3.00139-1>
- Jarvisalo, J., Kilpi, J., Euvaara, E., & Vainio, H. (1977). DELETERIOUS EFFECTS OF SUBACUTE CARBON DISULPHIDE EXPOSURE ON MOUSE LIVER. In *Biochemical Pharmacology* (Vol. 26). Pergamon Press.
- Kanemoto-Kataoka, Y., Oyama, T. M., Ishibashi, H., & Oyama, Y. (2017). Zinc is a determinant of the cytotoxicity of Ziram, a dithiocarbamate fungicide, in rat thymic lymphocytes: Possible environmental risks. *Toxicology Research*, 6(4), 499–504. <https://doi.org/10.1039/c7tx00052a>
- Kehrer, J. P. (2000). The Haber-Weiss reaction and mechanisms of toxicity. *Toxicology*, 149(1), 43–50. [https://doi.org/10.1016/s0300-483x\(00\)00231-6](https://doi.org/10.1016/s0300-483x(00)00231-6)
- Kisting, B. R., & Hardej, D. (2022). The ethylene bisdithiocarbamate fungicides mancozeb and nabam alter essential metal levels in liver and kidney and glutathione enzyme activity in liver of Sprague-Dawley rats. *Environmental Toxicology and Pharmacology*, 92. <https://doi.org/10.1016/j.etap.2022.103849>
- Liddell, J. R., Lehtonen, S., Duncan, C., Keksa-Goldsteine, V., Levonen, A. L., Goldsteins, G., Malm, T., White, A. R., Koistinaho, J., & Kanninen, K. M. (2016). Pyrrolidine dithiocarbamate activates the Nrf2 pathway in astrocytes. *Journal of Neuroinflammation*, 13(1). <https://doi.org/10.1186/s12974-016-0515-9>
- Lobo, V., Patil, A., Phatak, A., & Chandra, N. (2010). Free radicals, antioxidants and functional foods: Impact on human health. In *Pharmacognosy Reviews* (Vol. 4, Issue 8, pp. 118–126). <https://doi.org/10.4103/0973-7847.70902>
- Matei, A. M., & Trombetta, L. D. (2016). Exposure of rat hippocampal astrocytes to Ziram increases oxidative stress. *Toxicology and Industrial Health*, 32(4), 579–588. <https://doi.org/10.1177/0748233713504809>
- May, J. M., Qu, Z. C., Neel, D. R., & Li, X. (2003). Recycling of vitamin C from its oxidized forms by human endothelial cells. *Biochimica et Biophysica Acta - Molecular Cell Research*, 1640(2–3), 153–161. [https://doi.org/10.1016/S0167-4889\(03\)00043-0](https://doi.org/10.1016/S0167-4889(03)00043-0)
- Nishi, M. (2018). Diabetes mellitus and thyroid diseases. In *Diabetology International* (Vol. 9, Issue 2, pp. 108–112). Springer Tokyo. <https://doi.org/10.1007/s13340-018-0352-4>
- Pandey, S. P., & Mohanty, B. (2017). Disruption of the hypothalamic-pituitary-thyroid axis on co-exposures to dithiocarbamate and neonicotinoid pesticides: Study in a wildlife bird, *Amandava amandava*. *NeuroToxicology*, 60, 16–22. <https://doi.org/10.1016/j.neuro.2017.02.010>
- Park, E. A., Jerden, D. C., & Bahouth, S. W. (1995). Regulation of phosphoenolpyruvate carboxykinase gene transcription by thyroid hormone involves two distinct binding sites in the promoter. In *Biochem. J* (Vol. 309).

- Pham-Huy, L. A., He, H., & Pham-Huy, C. (2008). Free radicals, antioxidants in disease and health. *International Journal of Biomedical Science : IJBS*, 4(2), 89–96.
- Salam, S., Arif, A., & Mahmood, R. (2020). Thiram-induced cytotoxicity and oxidative stress in human erythrocytes: an in vitro study. *Pesticide Biochemistry and Physiology*, 164, 14–25. <https://doi.org/10.1016/j.pestbp.2019.12.003>
- Salam, S., Iqbal, Z., Khan, A. A., & Mahmood, R. (2021). Oral administration of thiram inhibits brush border membrane enzymes, oxidizes proteins and thiols, impairs redox system and causes histological changes in rat intestine: A dose dependent study. *Pesticide Biochemistry and Physiology*, 178. <https://doi.org/10.1016/j.pestbp.2021.104915>
- Shahbaz, H., & Gupta, M. (2022). *Creatinine Clearance*.
- Stephenson, O. J., & Trombetta, L. D. (2020a). Comparative effects of Mancozeb and Disulfiram-induced striated muscle myopathies in Long-Evans rats. *Environmental Toxicology and Pharmacology*, 74. <https://doi.org/10.1016/j.etap.2019.103300>
- Stephenson, O. J., & Trombetta, L. D. (2020b). Comparative effects of Mancozeb and Disulfiram-induced striated muscle myopathies in Long-Evans rats. *Environmental Toxicology and Pharmacology*, 74. <https://doi.org/10.1016/j.etap.2019.103300>
- Talbot, S. R., Biernot, S., Bleich, A., van Dijk, R. M., Ernst, L., Häger, C., Helgers, S. O. A., Koegel, B., Koska, I., Kuhla, A., Miljanovic, N., Müller-Graff, F. T., Schwabe, K., Tolba, R., Vollmar, B., Weegh, N., Wölk, T., Wolf, F., Wree, A., ... Zechner, D. (2020). Defining body-weight reduction as a humane endpoint: a critical appraisal. *Laboratory Animals*, 54(1), 99–110. <https://doi.org/10.1177/0023677219883319>
- Tanm, Ö. (2011). Thyroid hormones and growth in health and disease. In *JCRPE Journal of Clinical Research in Pediatric Endocrinology* (Vol. 3, Issue 2, pp. 51–55). <https://doi.org/10.4274/jcrpe.v3i2.11>
- Tonkin, E. G., Valentine, H. L., Milatovic, D. M., & Valentine, W. M. (2004). N,N-diethyldithiocarbamate produces copper accumulation, lipid peroxidation, and myelin injury in rat peripheral nerve. *Toxicological Sciences*, 81(1), 160–171. <https://doi.org/10.1093/toxsci/kfh190>
- Vaidya, V. S., Ferguson, M. A., & Bonventre, J. V. (2008). Biomarkers of acute kidney injury. In *Annual Review of Pharmacology and Toxicology* (Vol. 48, pp. 463–493). <https://doi.org/10.1146/annurev.pharmtox.48.113006.094615>
- Viquez, O. M., Valentine, H. L., Amarnath, K., Milatovic, D., & Valentine, W. M. (2008). Copper Accumulation and Lipid Oxidation Precede Inflammation and Myelin Lesions in N,N-Diethyldithiocarbamate Peripheral Myelinopathy. In *Toxicol Appl Pharmacol* (Vol. 229, Issue 1).

- Vomhof-DeKrey, E. E., & Picklo, M. J. (2012). The Nrf2-antioxidant response element pathway: A target for regulating energy metabolism. In *Journal of Nutritional Biochemistry* (Vol. 23, Issue 10, pp. 1201–1206). <https://doi.org/10.1016/j.jnutbio.2012.03.005>
- Wang, A., Costello, S., Cockburn, M., Zhang, X., Bronstein, J., & Ritz, B. (2011). Parkinson's disease risk from ambient exposure to pesticides. *European Journal of Epidemiology*, 26(7), 547–555. <https://doi.org/10.1007/s10654-011-9574-5>
- World Health Organization. (2002). *The world health report 2002 : reducing risks, promoting healthy life*. World Health Organization.
- Wronska-Nofer, T. (1972). The Influence of Low Doses of Nicotinic Acid upon the Development of Lipid Disturbances in Rats Chronically Exposed to Carbon Disulphide. In *Int. Arch. Arbeitsmed* (Vol. 29). Springer-Verlag.
- Zoroddu, M. A., Aaseth, J., Crisponi, G., Medici, S., Peana, M., & Nurchi, V. M. (2019). The essential metals for humans: a brief overview. In *Journal of Inorganic Biochemistry* (Vol. 195, pp. 120–129). Elsevier Inc. <https://doi.org/10.1016/j.jinorgbio.2019.03.013>

VITA

Name	<i>Jeffrey Chen</i>
Baccalaureate Degree	<i>Bachelor of Science/Arts, St. John's University, Queens, NY Major: Toxicology</i>
Date Graduated	<i>May, 2016</i>
Other Degrees and Certificates	<i>Master of Science, St. John's University, Queens, NY Major: Toxicology</i>
Date Graduated	<i>May, 2018</i>